Published in final edited form as:
IEEE Trans Med Imaging. 2013 July ; 32(7): 1153–1190. doi:10.1109/TMI.2013.2265603.

Deformable Medical Image Registration: A Survey

Aristeidis Sotiras [Member, IEEE],
Section of Biomedical Image Analysis, Center for Biomedical Image Computing and Analytics, Department of Radiology, University of Pennsylvania, Philadelphia, PA 19104 USA

Christos Davatzikos [Senior Member, IEEE], and
Section of Biomedical Image Analysis, Center for Biomedical Image Computing and Analytics, Department of Radiology, University of Pennsylvania, Philadelphia, PA 19104 USA

Nikos Paragios [Fellow, IEEE]
Center for Visual Computing, Department of Applied Mathematics, Ecole Centrale de Paris, Chatenay-Malabry, 92 295 FRANCE, the Equipe Galen, INRIA Saclay - Ile-de-France, Orsay, 91893 FRANCE and the Universite Paris-Est, LIGM (UMR CNRS), Center for Visual Computing, Ecole des Ponts ParisTech, Champs-sur-Marne, 77455 FRANCE

Aristeidis Sotiras: aristieidis.sotiras@uphs.upenn.edu; Christos Davatzikos: christos.davatzikos@uphs.upenn.edu

Abstract

Deformable image registration is a fundamental task in medical image processing. Among its most important applications, one may cite: i) multi-modality fusion, where information acquired by different imaging devices or protocols is fused to facilitate diagnosis and treatment planning; ii) longitudinal studies, where temporal structural or anatomical changes are investigated; and iii) population modeling and statistical atlases used to study normal anatomical variability. In this paper, we attempt to give an overview of deformable registration methods, putting emphasis on the most recent advances in the domain. Additional emphasis has been given to techniques applied to medical images. In order to study image registration methods in depth, their main components are identified and studied independently. The most recent techniques are presented in a systematic fashion. The contribution of this paper is to provide an extensive account of registration techniques in a systematic manner.

Index Terms

Deformable registration; medical image analysis; bibliographical review

I. Introduction

Deformable registration [1]–[10] has been, along with organ segmentation, one of the main challenges in modern medical image analysis. The process consists of establishing spatial correspondences between different image acquisitions. The term deformable (as opposed to linear or global) is used to denote the fact that the observed signals are associated through a non-linear dense transformation, or a spatially varying deformation model.

In general, registration can be performed on two or more images. In this paper, we focus on registration methods that involve two images. One is usually referred to as the source or

moving image, while the other is referred to as the target or fixed image. In this paper, the source image is denoted by S, while the target image is denoted by T. The two images are defined in the image domain Ω and are related by a transformation W.

The goal of registration is to estimate the optimal transformation that optimizes an energy of the form:

$$\mathcal{M}(T, S \circ W) + \mathcal{R}(W). \quad (1)$$

The previous objective function (1) comprises two terms. The first term, $\mathcal{M}$, quantifies the level of alignment between a target image T and a source image S. Throughout this paper, we interchangeably refer to this term as matching criterion, (dis)similarity criterion or distance measure. The optimization problem consists of either maximizing or minimizing the objective function depending on how the matching term is chosen.

The images get aligned under the influence of transformation W. The transformation is a mapping function of the domain Ω to itself, that maps point locations to other locations. In general, the transformation is assumed to map homologous locations from the target physiology to the source physiology. The transformation at every position $\mathbf{x} \in \Omega$ is given as the addition of an identity transformation with the displacement field $\mathbf{u}$, or $W(\mathbf{x}) = \mathbf{x} + \mathbf{u}(\mathbf{x})$. The second term, $\mathcal{R}$, regularizes the transformation aiming to favor any specific properties in the solution that the user requires, and seeks to tackle the difficulty associated with the ill-posedness of the problem.

Regularization and deformation models are closely related. Two main aspects of this relation may be distinguished. First, in the case that the transformation is parametrized by a small number of variables $\boldsymbol{\theta}$ and is inherently smooth, regularization may serve to introduce prior knowledge regarding the solution that we seek by imposing task-specific constraints on the transformation. Second, in the case that we seek the displacement of every image element (*i.e.*, non-parametric deformation model), regularization dictates the nature of the transformation.

Thus, an image registration algorithm involves three main components: (i) a deformation model, (ii) an objective function, and (iii) an optimization method. The result of the registration algorithm naturally depends on the deformation model and the objective function. The dependency of the registration result on the optimization strategy follows from the fact that image registration is inherently ill-posed. Devising each component so that the requirements of the registration algorithm are met is a demanding process.

Depending on the deformation model and the input data, the problem may be ill-posed according to Hadamard's definition of well-posed problems [11]. In probably all realistic scenarios, registration is ill-posed. To further elaborate, let us consider some specific cases. In a deformable registration scenario, one seeks to estimate a vector for every position given, in general, scalar information conveyed by image intensity. In this case, the number of unknowns is greater than the number of constraints. In a rigid $2D$ setting, let us consider a consider a scenario where two images of a disk (white background, gray foreground) are registered. Despite the fact that the number of parameters is only 6, the problem is ill-posed. The problem has no unique solution since a translation that aligns the centers of the disks followed by any rotation results in a meaningful solution.

Given non-linear and non-convex objective functions, in general, no closed-form solutions exist to estimate the registration parameters. In this setting, the search methods reach only a local minimum in the parameter space. Moreover, the problem itself has an enormous

number of different facets. The approach that one should take depends on the anatomical properties of the organ (for example, the heart and liver do not adhere to the same degree of deformation), the nature of observations to be registered (same modality versus multimodal fusion), the clinical setting in which registration is to be used (*e.g.*, off-line interpretation versus computer assisted surgery).

An enormous amount of research has been dedicated to deformable registration towards tackling these challenges due to its potential clinical impact. During the past few decades, many innovative ideas regarding the three main algorithmic registration aspects have been proposed. General reviews of the field may be found in [1]–[7], [9]. However due to the rapid progress of the field such reviews are to a certain extent outdated.

The aim of this paper is to provide a thorough overview of the advances of the past decade in deformable registration. Nevertheless, some *classic* papers that have greatly advanced the ideas in the field are mentioned. Even though our primary interest is deformable registration, for the completeness of the presentation, references to linear methods are included as many problems have been treated in this low-degree-of-freedom setting before being extended to the deformable case.

The main scope of this paper is focused on applications that seek to establish spatial correspondences between medical images. Nonetheless, we have extended the scope to cover applications where the interest is to recover the apparent motion of objects between sequences of successive images (optical flow estimation) [12], [13]. Deformable registration and optical flow estimation are closely related problems. Both problems aim to establish correspondences between images. In the deformable registration case, spatial correspondences are sought, while in the optical flow case, spatial correspondences, that are associated with different time points, are looked for. Given data with a good temporal resolution, one may assume that the magnitude of the motion is limited and that image intensity is preserved in time, optical flow estimation can be regarded as a small deformation mono-modal deformable registration problem.

The remainder of the paper is organized by loosely following the structural separation of registration algorithms to three components: 1) deformation model, 2) matching criteria, and 3) optimization method. In Sec. II, different approaches regarding the deformation model are presented. Moreover, we also chose to cover in this section the second term of the objective function, the regularization term. This choice was motivated by the close relation between the two parts. In Sec. III, the first term of the objective function, the matching term, is discussed. The optimization methods are presented in Sec. IV. In every section, particular emphasis was put on further deepening the taxonomy of registration method by grouping the presented methods in a systematic manner. Sec. V concludes the paper.

II. Deformation Models

The choice of deformation model is of great importance for the registration process as it entails an important compromise between computational efficiency and richness of description. It also reflects the class of transformations that are desirable or acceptable, and therefore limits the solution to a large extent. The parameters that registration estimates through the optimization strategy correspond to the degrees of freedom of the deformation model[1]. Their number varies greatly, from 6 in the case of global rigid transformations, to millions when non-parametric dense transformations are considered. Increasing the dimensionality of the state space results in enriching the descriptive power of the model.

[1]Variational approaches in general attempt to determine a function, not just a set of parameters.

This model enrichment may be accompanied by an increase in the model's complexity which, in turns, results in a more challenging and computationally demanding inference. Furthermore, the choice of the deformation model implies an assumption regarding the nature of the deformation to be recovered.

Before continuing, let us clarify an important, from implementation point of view, aspect related to the transformation mapping and the deformation of the source image. In the introduction, we stated that the transformation is assumed to map homologous locations from the target physiology to the source physiology (backward mapping). While from a theoretical point of view, the mapping from the source physiology to the target physiology is possible (forward mapping), from an implementation point of view, this mapping is less advantageous.

In order to better understand the previous statement, let us consider how the direction of the mapping influences the estimation of the deformed image. In both cases, the source image is warped to the target domain through interpolation resulting to a deformed image. When the forward mapping is estimated, every voxel of the source image is pushed forward to its estimated position in the deformed image. On the other hand, when the backward mapping is estimated, the pixel value of a voxel in the deformed image is pulled from the source image.

The difference between the two schemes is in the difficulty of the interpolation problem that has to be solved. In the first case, a scattered data interpolation problem needs to be solved because the voxel locations of the source image are usually mapped to non-voxel locations, and the intensity values of the voxels of the deformed image have to be calculated. In the second case, when voxel locations of the deformed image are mapped to non-voxel locations in the source image, their intensities can be easily calculated by interpolating the intensity values of the neighboring voxels.

The rest of the section is organized by following coarsely and extending the classification of deformation models given by Holden [14]. More emphasis is put on aspects that were not covered by that review.

Geometric transformations can be classified into three main categories (see Fig. 1): i) those that are inspired by physical models, ii) those inspired by interpolation and approximation theory, iii) knowledge-based deformation models that opt to introduce specific prior information regarding the sought deformation, and iv) models that satisfy a task-specific constraint.

Of great importance for biomedical applications are the constraints that may be applied to the transformation such that it exhibits special properties. Such properties include, but are not limited to, inverse consistency, symmetry, topology preservation, diffeomorphism. The value of these properties was made apparent to the research community and were gradually introduced as extra constraints.

Despite common intuition, the majority of the existing registration algorithms are asymmetric. As a consequence, when interchanging the order of input images, the registration algorithm does not estimate the inverse transformation. As a consequence, the statistical analysis that follows registration is biased on the choice of the target domain.

Inverse consistency—Inverse consistent methods aim to tackle this shortcoming by simultaneously estimating both the forward and the backward transformation. The data matching term quantifies how well the images are aligned when one image is deformed by

the forward transformation, and the other image by the backward transformation. Additionally, inverse consistent algorithms constrain the forward and backward transformations to be inverse mappings of one another. This is achieved by introducing terms that penalize the difference between the forward and backward transformations from the respective inverse mappings. Inverse consistent methods can preserve topology but are only asymptotically symmetric. Inverse-consistency can be violated if another term of the objective function is weighted more importantly.

Symmetry—Symmetric algorithms also aim to cope with asymmetry. These methods do not explicitly penalize asymmetry, but instead employ one of the following two strategies. In the first case, they employ objective functions that are by construction symmetric to estimate the transformation from one image to another. In the second case, two transformation functions are estimated by optimizing a standard objective function. Each transformation function map an image to a common domain. The final mapping from one image to another is calculated by inverting one transformation function and composing it with the other.

Topology preservation—The transformation that is estimated by registration algorithms is not always one-to-one and crossings may appear in the deformation field. Topology preserving/homeomorphic algorithms produce a mapping that is continuous, onto, and locally one-to-one and has a continuous inverse. The Jacobian determinant contains information regarding the injectivity of the mapping and is greater than zero for topology preserving mappings. The differentiability of the transformation needs to be ensured in order to calculate the Jacobian determinant. Let us note that Jacobian determinant and Jacobian are interchangeably used in this paper and should not be confounded with the Jacobian matrix.

Diffeomorphism—Diffeomoprhic transformations also preserve topology. A transformation function is a diffeomorphism, if it is invertible and both the function and its inverse are differentiable. A diffeomorphism maps a differentiable manifold to another.

In the following four subsections, the most important methods of the four classes are presented with emphasis on the approaches that endow the model under consideration with the above desirable properties.

A. Geometric Transformations Derived From Physical Models

Following [5], currently employed physical models can be further separated in five categories (see Fig. 1): i) elastic body models, ii) viscous fluid flow models, iii) diffusion models, iv) curvature registration, and v) flows of diffeomorphisms.

1) Elastic Body Models

a) Linear Models: In this case, the image under deformation is modeled as an elastic body. The Navier-Cauchy Partial Differential Equation (PDE) describes the deformation, or

$$\mu\nabla^2\mathbf{u}+(\mu+\lambda)\nabla(\nabla\cdot\mathbf{u})+\mathbf{F}=0, \quad (2)$$

where $\mathbf{F}(\mathbf{x})$ is the force field that drives the registration based on an image matching criterion, μ refers to the rigidity that quantifies the stiffness of the material and λ is Lamé's first coefficient.

Broit [15] first proposed to model an image grid as an elastic membrane that is deformed under the influence of two forces that compete until equilibrium is reached. An external

force tries to deform the image such that matching is achieved while an internal one enforces the elastic properties of the material.

Bajcsy and Kovacic [16] extended this approach in a hierarchical fashion where the solution of the coarsest scale is up-sampled and used to initialize the finer one. Linear registration was used at the lowest resolution.

Gee and Bajscy [17] formulated the elastostatic problem in a variational setting. The problem was solved under the Bayesian paradigm allowing for the computation of the uncertainty of the solution as well as for confidence intervals. The Finite Element Method (FEM) was used to infer the displacements for the element nodes, while an interpolation strategy was employed to estimate displacements elsewhere. The order of the interpolating or shape functions, determines the smoothness of the obtained result.

Linear elastic models have also been used when registering brain images based on sparse correspondences. Davatzikos [18] first used geometric characteristics to establish a mapping between the cortical surfaces. Then, a global transformation was estimated by modeling the images as inhomogeneous elastic objects. Spatially-varying elasticity parameters were used to compensate for the fact that certain structures tend to deform more than others. In addition, a non-zero initial strain was considered so that some structures expand or contract naturally.

In general, an important drawback of registration is that when source and target volumes are interchanged, the obtained transformation is not the inverse of the previous solution. In order to tackle this shortcoming, Christensen and Johnson [19] proposed to simultaneously estimate both forward and backward transformations, while penalizing inconsistent transformations by adding a constraint to the objective function. Linear elasticity was used as regularization constraint and $3D$ Fourier series were used to parametrize the transformation.

Leow *et al.* [20] took a different approach to tackle the inconsistency problem. Instead of adding a constraint that penalizes the inconsistency error, they proposed a unidirectional approach that couples the forward and backward transformation and provides inverse consistent transformations by construction. The coupling was performed by modeling the backward transformation as the inverse of the forward. This fact was also exploited during the optimization of the symmetric energy by only following the gradient direction of the forward mapping.

He and Christensen [21] proposed to tackle large deformations in an inverse consistent framework by considering a sequence of small deformation transformations, each modeled by a linear elastic model. The problem was symmetrized by considering a periodic sequence of images where the first (or last) and middle image are the source and target respectively. The symmetric objective function thus comprised terms that quantify the difference between any two successive pairs of images. The inferred incremental transformation maps were concatenated to map one input image to another.

b) Nonlinear Models: An important limitation of linear elastic models lies in their inability to cope with large deformations. In order to account for large deformations, nonlinear elastic models have been proposed. These models also guarantee the preservation of topology.

Rabbitt *et al.* [22] modeled the deformable image based on hyperelastic material properties. The solution of the nonlinear equations was achieved by local linearization and the use of the Finite Element method.

Pennec *et al.* [23] dropped the linearity assumption by modeling the deformation process through the St Venant-Kirchoff elasticity energy that extends the linear elastic model to the nonlinear regime. Moreover, the use of log-Euclidean metrics instead of Euclidean ones resulted in a Riemannian elasticity energy which is inverse consistent. Yanovsky *et al.* [24] proposed a symmetric registration framework based on the St Venant-Kirchoff elasticity. An auxiliary variable was added to decouple the regularization and the matching term. Symmetry was imposed by assuming that the Jacobian determinants of the deformation follow a zero mean, after log-transformation, log-normal distribution [25].

Droske and Rumpf [26] used an hyperelastic, polyconvex regularization term that takes into account the length, area and volume deformations. Le Guyader and Vese [27] presented an approach that combines segmentation and registration that is based on nonlinear elasticity. The authors used a poly-convex regularization energy based on the modeling of the images under deformation as Ciarlet-Geymonat materials [28]. Burger *et al.* [29] also used a polyconvex regularization term. The authors focused on the numerical implementation of the registration framework. They employed a discretize-then-optimize approach [9] that involved the partitioning voxels to 24 tetrahedra.

2) Viscous Fluid Flow Models—In this case, the image under deformation is modeled as a viscous fluid. The transformation is governed by the Navier-Stokes equation that is simplified by assuming a very low Reynold's number flow:

$$\mu_f \nabla^2 \mathbf{v} + (\mu_f + \lambda_f) \nabla (\nabla \cdot \mathbf{v}) + \mathbf{F} = 0. \quad (3)$$

These models do not assume small deformations, and thus are able to recover large deformations [30]. The first term of the Navier-Stokes equation (3), constrains neighboring points to deform similarly by spatially smoothing the velocity field. The velocity field is related to the displacement field as $\mathbf{v}(\mathbf{x}; t) = \partial_t \mathbf{u}(\mathbf{x}; t) + (\nabla \mathbf{u}(\mathbf{x}; t)\mathbf{v}(\mathbf{x}; t))$. The velocity field is integrated in order to estimate the displacement field. The second term allows structures to change in mass while μ_f and λ_f are the viscosity coefficients.

Christensen *et al.* [30] modeled the image under deformation as a viscous fluid allowing for large magnitude non-linear deformations. The PDE was solved for small time intervals and the complete solution was given by an integration over time. For each time interval a successive over-relaxation (SOR) scheme was used. To guarantee the preservation of topology, the Jacobian was monitored and each time its value fell under 0.5, the deformed image was re-gridded and a new one was generated to estimate a transformation. The final solution was the concatenation of all successive transformations occurring for each re-gridding step. In a subsequent work, Christensen *et al.* [31] presented a hierarchical way to recover the transformations for brain anatomy. Initially, global affine transformation was performed followed by a landmark transformation model. The result was refined by fluid transformation preceded by an elastic registration step.

An important drawback of the earliest implementations of the viscous fluid models, that employed SOR to solve the equations, was computational inefficiency. To circumvent this shortcoming, Christensen *et al.* employed a massive parallel computer implementation in [30]. Bro-Nielsen and Gramkow [32] proposed a technique based on a convolution filter in scale-space. The filter was designed as the impulse response of the linear operator $L = \mu_f \Delta \mathbf{u} + (\mu_f + \lambda_f) \nabla (\nabla \cdot \mathbf{v})$ defined in its eigen-function basis. Crun *et al.* [33] proposed a multi-grid approach towards handling anisotropic data along with a multi-resolution scheme opting for first recovering coarse velocity estimations and refining them in a subsequent step. Cahill *et al.* [34] showed how to use Fourier methods to efficiently solve the linear PDE system that

arises from equation (3) for any boundary condition. Furthermore, Cahill *et al.* extended their analysis to show how these methods can be applied in the case of other regularizers (diffusion, curvature and elastic) under Dirichlet, Neumann or periodic boundary conditions.

Wang and Staib [35] used fluid deformation models in an atlas-enhanced registration setting while D'Agostino *et al.* tackled multi-modal registration with the use of such models in [36]. More recently, Chiang *et al.* [37] proposed an inverse consistent variant of fluid registration to register Diffusion Tensor images. Symmetrized Kullback-Leibler (KL) divergence was used as the matching criterion. Inverse consistency was achieved by evaluating the matching and regularization criteria towards both directions.

3) Diffusion Models—In this case, the deformation is modeled by the diffusion equation:

$$\Delta \mathbf{u} + \mathbf{F} = 0. \quad (4)$$

Let us note that most of the algorithms, based on this transformation model and described in this section, do not explicitly state the equation (4) in their objective function. Nonetheless, they exploit the fact that the Gaussian kernel is the Green's function of the diffusion equation (4) (under appropriate initial and boundary conditions) to provide an efficient regularization step. Regularization is efficiently performed through convolutions with a Gaussian kernel.

Thirion, inspired by Maxwell's Demons, proposed to perform image matching as a diffusion process [38]. The proposed algorithm iterated between two steps: i) estimation of the demon forces for every demon (more precisely, the result of the application of a force during one iteration step, that is a displacement), and ii) update of the transformation based on the calculated forces. Depending on the way the demon positions are selected, the way the space of deformations is defined, the interpolation method that is used, and the way the demon forces are calculated, different variants can be obtained. The most suitable version for medical image analysis involved 1) selecting all image elements as demons, 2) calculating demon forces by considering the optical flow constraint, 3) assuming a non-parametric deformation model that was regularized by applying a Gaussian filter after each iteration, and 4) a trilinear interpolation scheme. The Gaussian filter can be applied either to the displacement field estimated at an iteration or the updated total displacement field. The bijectivity of the transformation was ensured by calculating for every point the difference between its initial position and the one that is reached after composing the forward with the backward deformation field, and redistributing the difference to each field. The bijectivity of the transformation can also be enforced by limiting the maximum length of the update displacement to half the voxel size and using composition to update the transformation. Variants for the contour-based registration and the registration between segmented images were also described in [38].

Most of the algorithms described in this section were inspired by the work of Thirion [38] and thus could alternatively be classified as "Demons approaches". These methods share the iterative approach that was presented in [38] that is, iterating between estimating the displacements and regularizing to obtain the transformation. This iterative approach results in increased computational efficiency. As it will be discussed later in this section, this feature led researchers to explore such strategies for different PDEs.

The use of Demons, as initially introduced, was an efficient algorithm able to provide dense correspondences but lacked a sound theoretical justification. Due to the success of the algorithm, a number of papers tried to give theoretical insight into its workings. Fischer and Modersitzki [39] provided a fast algorithm for image registration. The result was given as

the solution of linear system that results from the linearization of the diffusion PDE. An efficient scheme for its solution was proposed while a connection to the Thirion's Demons algorithm [38] was drawn.

Pennec *et al.* [40] studied image registration as an energy minimization problem and drew the connection of the Demons algorithm with gradient descent schemes. Thirion's image force based on optical flow was shown to be equivalent with a second order gradient descent on the Sum of Square Differences (SSD) matching criterion. As for the regularization, it was shown that the convolution of the global transformation with a Gaussian kernel corresponds to a single step of a first order gradient descent of a functional that penalizes the remainder of the transformation after convolving it with a high-pass filter.

Vercauteren *et al.* [41] adopted the alternate optimization framework that Cachier *et al.* [42] proposed, to relate symmetric Demons forces with the Efficient Second-order Minimization (ESM) [43]. In this framework, an auxiliary variable was used to decouple the matching and regularization terms. Matching was performed by minimizing the data term through ESM optimization while regularization was achieved by Gaussian smoothing.

In [44], Vercauteren *et al.* proposed a variant of Thirion's algorithm endowed with the diffeomorphic property. In contrast to classical Demons approaches, in every iteration of the algorithm an update field is estimated. In order to estimate the current transformation, a compositional update rule is used between the previous estimate and the exponential map of the update field. The exponential map is efficiently calculated by using the scaling and squaring method [45], [46] and the composition of displacement fields. The exponentiation of the displacement field ensures the diffeomorphism of the mapping.

To further facilitate the use of the Demons algorithm in anatomical computational studies, Vercauteren *et al.* [47] extended Demons to be symmetric. Initially, it was shown how the complete spatial transformation can be represented in the log-domain. Subsequently, a symmetric extension was provided by averaging the forward and backward forces that were computed separately.

The efficiency of this two-step iterative strategy spurred research interest in seeking a mathematical justification of the smoothing step to allow for deformations bearing different physical properties [32], [48]–[50].

Stefanescu *et al.* presented a way to perform adaptive smoothing by taking into account knowledge regarding the elasticity of tissues in [51]. A non-stationary diffusion filter was used to smooth less inside areas where greater deformations were expected and smooth more inside objects where coherence should be preserved. The authors also proposed to take into account the local image gradient content during smoothing. In areas with large image gradients where the local confidence for the established correspondences is higher, smoothing is scaled down. On the contrary, smoothing is scaled up in homogeneous areas.

Cahill *et al.* [48] showed that curvature and fluid registration can be formulated as two coupled diffusion equations. Their stationary solution may be approached via successive Gaussian convolutions, thus yielding a Demons algorithm for these cases. In a subsequent work, Cahill *et al.* [49] showed how to extend the curvature regularization to consider local image gradient content. The authors proposed a coupled PDE system whose stationary solution can be attained by consecutive convolutions with the Green's function of the diffusion equation.

In another example, Mansi *et al.* [50] introduced a physical constraint in the registration process to estimate the myocardium strain from Cine-MRI. The logDemons algorithm [47]

was endowed with the incompressibility constraint by making the velocity field divergence-free. This was achieved by solving the Poisson equation under 0-Dirichlet boundary conditions within a subdomain of the image showing the myocardium.

The earliest registration methods of this family of models used an SSD criterion to drive the matching. As a consequence, they were appropriate for mono-modal image registration. Subsequent approaches coped with the multi-modal registration problem. Guimond *et al.* [52] proposed a method that alternates between Demons based registration and intensity correction. Other efforts include the encoding of similarity metrics such as Normalized Mutual Information by Tristán-Vega *et al.* [53] and Modat *et al.* [54].

The application of the Demons algorithm is not limited to scalar images and has been extended to multi-channel images [55], diffusion tensor ones [56], as well as different geometries [57]. Peyrat *et al.* used multi-channel Demons to register $4D$ time-series of cardiac images by enforcing trajectory constraints in [55]. Each time instance was considered as a different channel while the estimated transformation between successive channels was considered as constraint. Yeo *et al.* [56] derived Demons forces from the squared difference between each element of the Log-Euclidean transformed tensors while taking into account the reorientation introduced by the transformation. Finally, the Demons framework was employed to register cortical surfaces parametrized as spheres by Yeo *et al.* [56]. To generalize Demons on the sphere, a method was introduced to measure the distance between two transformations and to regularize the transformation.

4) Curvature Registration—In this case, the deformation is modeled by the following equilibrium equation:

$$\Delta^2\mathbf{u}+\mathbf{F}=0. \quad (5)$$

This regularization scheme does not penalize affine linear transformations. As a consequence, unless an initial significant miss-alignment in space is present, these registration frameworks do not necessarily require an additional affine linear pre-registration step.

Fischer and Modersitzki used this constraint in [58], [59]. To solve equation (5), the Gâteaux derivatives with respect to the data and regularization terms were calculated and a finite difference scheme was employed to solve the resulting PDE. Neumann boundary conditions were used since they result in a highly structured matrix problem that can be solved efficiently. Despite this fact, the resulting underlying function space penalizes the affine linear displacements as pointed out by Henn in [60]. Thus, Henn proposed to include second-order terms as boundary conditions in the energy and applied a semi-implicit time discretization scheme to solve the full curvature registration problem.

Glocker *et al.* [61] used an approximation of the curvature penalty in the case of parametric grid-based deformation models. The approximation was derived by simultaneously examining the displacements of two neighboring grid nodes while the third was assumed to be fixed. Beuthien *et al.* [62], inspired by the approach presented in [32] for the viscous fluid registration scenario, proposed another way to solve the curvature based registration problem. Instead of devising a numerical scheme to solve the PDE that results from the equilibrium equation (5), recursive convolutions with an appropriate Green's function were used.

5) Flows of Diffeomorphisms—Flows of diffeomorphisms have also been proposed to model the deformation. In this case, the deformation is modeled by considering its velocity

over time according to the Lagrange transport equation [30], [63], [64]. The regularization term constrains the velocity field to be smooth:

$$\mathscr{R} = \int_0^1 \|\mathbf{v}_t\|_V^2 dt. \quad (6)$$

$\|\cdot\|_V$ is a norm on the space V of smooth velocity vector fields defined as $\|f\|_V = \|Df\|_{L_2}$, where D is a differential operator and $\|\cdot\|_{L_2}$ is the L_2 norm of square integrable functions. Choosing a kernel associated with V allows for the modeling of different types of spatial regularization [63]. While most often a single Gaussian kernel is used [65], it is possible to use multiple kernels and smooth the deformations adaptively at different scales [65], [66]. Lastly, the fact that the velocity field varies over time allows for the estimation of large deformations [67].

This framework, known as Large Deformation Diffeomorphic Metric Mapping (LDDMM), allows for the definition of a distance between images or sets of points [68], [69]. The distance between these elements is defined as a geodesic, according to a metric, that connects them and can be used for studies of anatomical variability [70]. A number of theoretical aspects of this framework and especially the ones related with computational analysis were further developed in [71]–[75]. The interested reader is referred to [76] for an overview of its evolution and the corresponding equations.

The LDDMM framework has been extended to solve a number of problems. Among its extensions, one may cite volume registration for scalar [67], [77]–[79] vector-[80] and tensor-valued data [81], point-matching [68], point-matching on spheres [82], matching sets of unlabeled points [83]–[85], shape-matching [65], [86], curve-mapping [87]–[90] and hybrid registration [91], [92].

Even though the LDDMM framework provides diffeomorphic transformations, it is not symmetric. To encode the symmetric property a number of approaches have been proposed [77], [78], [93]. Beg and Khan [77] focused on providing symmetric data terms. Younes [93] also discussed ways to render the alignment process symmetric while Avants *et al.* [78] presented a symmetric LDDMM registration process driven by cross-correlation

The mathematical rigor of the LDDMM framework comes at an important cost. The fact that the velocity field has to be integrated over time results in high computational and memory demands. Moreover, the gradient descent scheme that is usually employed to solve the optimization problem of the geodesic path estimation converges slowly [79]. More efficient optimization techniques for the LDDMM have been investigated in [79], [94], [95].

Cotter and Holm presented an approach that involves a particle mesh method in [95]. Marsland and McLachlan [94] formulated the problem in a PDE framework and used a particle method to solve for the diffeomorphism. More recently, Ashburner and Friston [79] gave a Gauss-Newton implementation of the algorithm in [95]. These approaches were based on the fact that the initial velocity field is sufficient to calculate the intermediate and final deformations. In other words, the diffeomorphism is parametrized by the initial velocity field. These calculations are possible by reformulating the initial boundary problem to an initial value one. The initial conditions comprise the initial velocity and the starting position. The optimization opts to estimate the initial velocity field that best aligns the images. This approach is known as geodesic shooting.

An alternative way to efficiently calculate diffeomorphisms involves the simplification of the problem by decreasing its degrees of freedom. Stationary velocity fields [96] have been

used towards this direction. Despite being limited with respect to the diffeomorphisms that they can capture, stationary velocity fields are a common choice among many researchers [97]–[100].

Hernandez *et al.* followed this approach and used stationary Ordinary Differential Equations (ODEs) in the LDDMM framework [101]. Ashburner [97] assumed the velocity field to be constant over time in order to propose a fast diffeomorphic image registration that was based on either membrane, bending or linear elastic energy. The solution was estimated through integration over time by composing successive solutions. Given an even number of steps, this was performed efficiently by a scaling and squaring approach [45], [46]. Furthermore, the exponential of the flow field was used to guarantee that the inferred mapping is diffeomorphic. The energy was optimized using the Levenberg-Marquardt algorithm coupled with a full multi-grid approach to efficiently compute its update step.

B. Geometric Transformations Derived From Interpolation Theory

Rather than being motivated by a physical model, the models of this class are derived from either interpolation theory or approximation theory. In interpolation theory, displacements, considered known in a restricted set of locations in the image, are interpolated for the rest of the image domain. In approximation theory, we assume that there is an error in the estimation of displacements. Thus, the transformation smoothly approximates the known displacements rather than taking the exact same values. These models are rich enough to describe the transformations that are present in image registration problems, while having low degrees of freedom and thus facilitating the inference of the parameters. Among the most important families of interpolation strategies, one may cite (see Fig. 1): i) Radial Basis Functions, ii) Elastic Body Splines, iii) Free-Form Deformations, iv) basis functions from signal processing, and v) piecewise affine models.

1) Radial Basis Functions—One of the most important families of interpolation strategies is that of Radial Basis Functions (RBFs), where the value at an interpolation point $\mathbf{x}$ is given as function of its distance r from the known sample $\mathbf{p}$, or

$$\mathbf{u}(\mathbf{x}) = \sum_{i=1}^{N} \omega_i \varphi(\|\mathbf{x} - \mathbf{p}_i\|). \quad (7)$$

Zagorchev and Goshtasby presented an evaluation study comparing RBFs used as transformation functions in non-rigid image registration in [102]. More recently, Yang *et al.* [103] presented an analysis with respect to the ability of RBFs to preserve topology. An important property of RBFs is that they are able to interpolate a deformation field from irregularly placed known values. A common property of most RBFs, that are described in this section, is their global support. Knowing the displacement at one point influences the values of points in the whole image domain. As a consequence, interpolation in sparsely populated areas is feasible. On the other hand, this behavior is undesirable when seeking local transformations. In order to counter it, sufficient landmarks are required in the regions of interest.

Bookstein proposed the use of Thin-Plate Splines (TPS) for image registration in [104], [105]. TPS minimize the bending energy assuming infinite boundary conditions. The solution is given in a closed-form and its uniqueness is guaranteed in most cases. Nonetheless, TPS, as proposed by Bookstein, are known to exhibit certain shortcomings. The transformation from one image domain to another is not inverse consistent [106]. Moreover, their support is global, which hinders the recovery of local image warpings

[107]–[109]. Furthermore, TPS do not take into consideration possible errors in the estimation of the displacements in the landmark positions [110]. Lastly, as the number of points increases, the interpolation becomes computationally demanding [111]. A number of researchers have worked to lessen the importance of these shortcomings [106]–[111].

In [106], Johnson and Christensen tackled the inverse inconsistency problem. They considered the minimization of the bending energy under cyclic boundary conditions in an effort to account for the great consistency error that they observed in the boundary of the images. Additionally, a term that penalizes the consistency error was introduced in the objective function to render the registration inverse consistent.

Li *et al.* coped with the problem of the global nature of TPS in [107]. TPS were constructed in such a way that their support is restricted locally. In a subsequent work, Yang *et al.* [108] defined the support of each point in an adaptive way by taking into consideration the distribution of the points in the image domain. These approaches [107], [108] were based on heuristics and a truncation of the original basis, to limit the influence of the control points. Rohr and Wörz [109] introduced a variant of TPS which assumes that the forces that act at the landmarks, also influence the region around them. These forces are described by a Gaussian function of the radial distance from the landmark instead of a Dirac delta function as in the classical TPS. The parametrization of the forces by the standard deviation of the Gaussian function allows for the control of the locality of the transformation.

Rohr *et al.* [110] proposed to take into consideration the landmark localization error when estimating the dense deformation field through the use of approximating Thin-Plate Splines. The authors proposed to weaken the interpolation constraint and estimate the transformation by minimizing a functional that weights the approximation error according to the (isotropic or anisotropic) landmark position estimation error. The approximation problem admits an analytical solution that consists of the same basis functions as the interpolation problem.

Three ways to address the computational problems related with the presence of a great number of landmarks were studied by Donato and Belongie [111]. The straightforward approach of sub-sampling the points was compared to two more elaborated ones that use either a subset of the basis functions or a matrix approximation technique based on the Nyström method. The more sophisticated methods were shown to outperform the naive approach in terms of mean squared error. The matrix approximation method was also shown to be useful when principal warp analysis was taken into account.

Marsland and Twining [69], [112] employed Clamped-Plate Splines for groupwise registration and groupwise analysis of deformable registrations. Clamped-Plate Splines minimize the same energy as TPS though under specific boundary conditions. Camion and Younes introduced Goedesic Interpolating Splines (GIS) following the LDDMM framework [113]. The dense deformation field that results from the interpolation with these splines is diffeomorphic. Younes extended this method to combine GIS with affine transformations in [114] while two ways to calculate them were presented by Mills *et al.* [115].

Ruprecht *et al.* have proposed another family of RBFs, that of multi-quadratics, that has global support [116]. Little *et al.* extended this approach to cope with the presence of a rigid object [117].

Arad *et al.* [118] suggested the use of Gaussian functions to parametrize the deformation. The choice of an appropriate Gaussian kernel allows for the control of their spatial influence. By choosing a small size for the Gaussian kernel, their influence can be greatly restricted and thus local displacements may be recovered. A recent example of the use of this deformation model in brain registration can be found in [119].

Zagorchev and Goshtasby [102] investigated the use of the normalized weighted average of sparse displacements to create dense deformation fields. Despite the global support of the control points, the locality of the transformation can be adapted by choosing an appropriate weighting function.

In medical image analysis, the presence of different anatomical structures characterized by different properties and the subsequent need to recover local deformations render the previous models not well suited. To cope successfully with such cases, interpolation methods where control points have spatially limited influence are appropriate.

Fornefett *et al.* [120] investigated the use of Wendland functions [121], [122] that exhibit the desired locality property, for deformable registration. Other local support radial basis functions include the C^2 smooth Wu functions [123] and the functions proposed by Buhmann [124]. Rohde *et al.* [125] applied the Wu functions in image registration and derived bounds for the basis function's coefficients so that the Jacobian of the computed transformation remains positive.

More recently, Siddiqui *et al.* [126] defined a new model based on the cosine function. Contrary to what is claimed in the paper, the new model is not positive definite [127]. A real-valued, continuously differentiable function is called positive definite on a neighborhood of the origin, if it is zero for the origin and greater than zero for the rest of the points in the neighborhood. The positive definiteness of the functions is important because it guarantees that the system of linear equations, that arises when estimating the coefficients of the interpolation problem, is solvable for all possible sets of pairs of corresponding landmarks in the two image domains, which are not colinear in $2D$ and coplanar in $3D$ [120]. Lowitzsch [128] introduced a class of RBFs that are vector-valued analogues of the Wendland functions [121], [122]. This class of RBFs provide interpolated displacement fields that are divergence free.

Yang *et al.* [103] compared the previous locally constrained radial basis functions by using transformations on random point sets, artificial images and medical images.

2) Elastic Body Splines—Splines, though mainly inspired by interpolation and approximation theory, may also be inspired by physical models. Such is the case of Elastic Body Splines (EBS), which were introduced by Davis *et al.* [129]. These splines are solutions of the Navier-Cauchy equilibrium equation for a homogeneous isotropic elastic body subjected to forces. When the force field that drives the registration based on the landmark correspondences is given as a radial symmetric function of the distance from the landmark, one can solve the equation analytically.

Kohlrausch *et al.* [130] extended the previous work by considering forces that are given as a Gaussian function of the distance from the landmark (Gaussian EBS). The size of the kernel of the Gaussian can be used to parametrize the compactness of the model's support. As a result, the transformation model can cope better with local deformations. An analytic solution for the equilibrium equation also exists for this type of force field.

Wörz and Rohr extended Gaussian EBS in [131]. Instead of opting for an exact interpolation, an approximation strategy was employed to account for errors in the landmark displacements. The PDE was extended to incorporate Gaussian forces that were weighted by the localization uncertainty. The uncertainties, depending on their isotropic or anisotropic nature, were represented as either scalar weights or matrices. An analytic solution was obtained for the extended equation.

3) Free Form Deformations—Free-Form Deformations (FFDs) is one of the most common types of transformation models in medical image registration. A rectangular grid $G = K_x \times K_y \times K_z$ is superimposed on the image (size $N_x \times N_y \times N_z$, $K_x \ll N_x$, $K_y \ll N_y$, $K_z \ll N_z$) that gets deformed under the influence of the control points. The dense deformation is given as a summation of tensor products of univariate splines. FFDs were first popularized in the computer graphics community [132], [133] but gained wide acceptance in the medical image analysis community when coupled with cubic-*B* splines [134]–[137].

The displacement field is given as

$$\mathbf{u}(\mathbf{x}) = \sum_{l=0}^{3}\sum_{m=0}^{3}\sum_{n=0}^{3} B_l(\mu_x) B_m(\mu_y) B_n(\mu_z) \mathbf{d}_{i+l,j+m,k+n}, \quad (8)$$

where $i = \lfloor x/N_x \rfloor - 1$, $j = \lfloor y/N_y \rfloor - 1$, $k = \lfloor z/N_z \rfloor - 1$, $\mu_x = x/N_x - \lfloor x/N_x \rfloor$, $\mu_y = y/N_y - \lfloor y/N_y \rfloor$ and $\mu_z = z/N_z - \lfloor z/N_z \rfloor$. B_l represents the lth basis function of the *B*-spline and **d** denotes displacement. This transformation model is simple and can efficiently provide smooth deformations. Moreover, it requires few degrees of freedom to describe local deformations.

While in general the transformations that result from cubic *B*-spline FFDs are smooth, the preservation of topology is not guaranteed. Rueckert *et al.* [138] imposed the hard constraints proven in [139] to produce diffeomorphic deformation fields. The required condition is that the maximum displacement should not be greater than four tenths of the grid spacing. Preservation of topology may also be ensured through the use of soft constraints (see Sec. II-D1).

Many extensions of FFDs have been proposed in the literature. While FFDs are usually uniform, non-uniform approaches have been proposed. Schnabel *et al.* [140] proposed to use multi-level B-splines. In this case, the transformation was given as a summation of the individual transformations of each level. The authors proposed to assign to every control point a status, either active or passive, in order to simulate a non-uniform control point distribution. Active control points were allowed to move, while passive control points remained fixed. Wang and Jiang [141] employed non-uniform rational *B*-splines (NURBS) to perform medical image registration in an adaptive focus manner. Shi *et al.* [142] used the multi-level B-splines model of [140] while imposing that only a sparse subset of the control points is active.

Noblet *et al.* [143] presented a symmetric extension of FFDs. The authors assumed that both images deform toward a common domain under the influence of two isomorphic grids. The common domain was assumed to be in an equal distance from the source and the target. Given the parametric nature of the transformation, this results in constraining the displacements of the corresponding nodes in the two grids to sum to zero. Moreover, in order to calculate the mapping from one image domain to the other, the respective estimated mappings toward the common domain should be invertible. Feng *et al.* [144] proposed an inverse consistent method based on FFDs. The proposed method did not require the inversion of the deformation field. It examined how well the composition of the two transformations mapped back to the image domain. Sotiras and Paragios [145] used a similar model to [143]. The two models differed in the way the invertibility of the mappings was guaranteed, and the fact that in [145], the registration problem was formulated as a discrete labeling one.

FFDs have been extended to tackle multiple-image registration where hard constraints are employed to define a reference domain [146]–[149]. Moreover, the transformation model

has been extended to the spatio-temporal domain where B-splines are also used for the temporal axis [150]–[152].

4) Basis Functions from Signal Representation—Inspired by the mathematical tools that are available to represent and analyze signals, many researchers have used Fourier and Wavelet analysis to model transformations. An important reason to use them is the fact that they can naturally provide a multi-resolution decomposition of the displacement field. This is a useful property for the coarse-to-fine schemes that are commonly applied in medical image registration to ease the computations and handle large deformations.

Christensen and Johnson employed a Fourier-based transformation scheme in their consistent registration framework [19]. The Fourier series representation of the transformation simplifies the linear elasticity constraint, thus allowing an efficient numerical implementation. Ashburner and Friston [153] tackled nonlinear registration by employing a transformation model that was parametrized as a linear combination of Discrete Cosine Transform basis functions. The separable nature of the basis functions was exploited by the authors to accelerate calculations.

Fourier basis functions are well localized in the frequency domain. On the contrary, they are not localized at all in the spatial domain. Wavelet basis functions, being localized in both domains, can model local deformations more efficiently than Fourier basis [154].

Amit [154] presented two variational approaches for $2D$ image matching. In the first case, the transformation was parametrized with respect to the Fourier basis, while in the second case, it was parametrized with respect to a wavelet basis. The reported experimental results indicated that the second method was able to capture local deformations with more accuracy than the Fourier method. Wu *et al.* [155] used a wavelet-based deformation model. The Cai-Wang wavelet was employed to generate a multi-resolution description in Sobolev space yielding intrinsically smooth deformations. Based on this model, the authors were able to treat global and local information simultaneously in a coarse-to-fine approach. Gefen *et al.* [156] modeled the deformation field with a finite-supported, semi-orthogonal wavelet toward tackling the problem of aligning rat brain histological images. In order to ease the optimization burden, the authors exploited the natural multi-resolution and multi-band decomposition of the wavelet coefficients. The transformation parameters were first inferred for low resolution levels, separately for each subband, before proceeding to finer resolution levels.

Musse *et al.* [157] presented a topology-preserving multi-resolution approach for $2D$ images. The authors used nonorthogonal Riesz basis of polynomial splines due to their compactness. The topology was preserved by controlling the Jacobian through hard linear constraints. Noblet *et al.* extended this approach to the $3D$ domain in [158] and further validated it in [159]. In the $3D$ case, the same multi-resolution framework was used, though the topology could not be preserved by satisfying linear constraints. This was made possible by solving a constrained optimization problem where the Jacobian was enclosed between two user specified bounds. Cathier [160] used the same wavelet basis as in [155] to decompose the transformation in a multi-resolution fashion. An L_1 penalty on the wavelet coefficients was used to regularize the registration problem. This regularization led to sparse transformations with respect to the wavelet basis and thus facilitated their storage in memory.

5) Locally Affine Models—Locally affine models parametrize the transformation by locally linear deformations. One may discern two different cases: i) piecewise affine models, and ii) poly-affine ones. In the first case, the image is mosaicked by a set of triangles or tetrahedra whose nodes parametrize the deformation. Inside each region, affine interpolation

takes place. Efficiency and invertibility are the main strengths of this method, while lack of smoothness in the region boundaries is its main limitation. In the second case, fuzzy regions are used in order to tackle the aforementioned drawback and produce a smooth transformation.

a) Piecewise Affine Models: Some of the most recent approaches using a piecewise affine model include, but are not limited to, the following. Hellier *et al.* [161] proposed a multi-resolution and multi-grid approach. The image was partitioned adaptively into cubes and an affine transformation was inferred for each one. A regularization energy term encouraged neighboring pairs to deform similarly. In a similar fashion, Zhang *et al.* [162] tackled diffusion tensor registration by taking into consideration tensor reorientation. The images were separated into contiguous blocks and an affine transformation was recovered for each one of them. Regularization on the interface of regions ensured the global smoothness of the transformation.

Pitiot *et al.* [163] reconstructed $3D$ volumes of histological images by employing a piecewise affine transformation model. The images were separated into independent components through hierarchical clustering. In a subsequent step, affine registration was performed for each pair of regions. The final transformation was estimated by calculating the affine transformation for each region and applying a non-linear interpolation in between the regions. Commowick *et al.* presented similar approach was presented in [164]. The main difference between the two methods lies in the fact that a regularization step followed to improve the smoothness in the interpolated areas. The regularization was based on the Log-Euclidean framework using Euclidean differences between the logarithms of the affine transformations.

Two more recent applications of piecewise affine models were presented in [165], [166]. Cootes *et al.* [165] favored the use of piecewise affine transformations as they can be easily inverted. Buerger *et al.* [166] proposed a hierarchical framework to adaptively separate the images into regions. Splitting was formulated as an energy minimization problem and three criteria were used. The first criterion tried to group regions with rich structural information. The second criterion grouped regions with significant residual error in large blocks, while the last criterion encouraged regions with similar motion to be considered together. The second was found to perform best.

Most approaches that employ piecewise linear strategies consider the affine transformations independently. As a result, singularities may occur and the transformation is not globally invertible. To account for this drawback, sophisticated methods have been introduced. Narayanan *et al.* proposed a transformation model that is affine at the center of a region and reduces to identity as the distance from the center increases [167]. This novel transformation model has a closed form and can be computed efficiently. Moreover, constraints were given in the form of bounds on the translation so that invertibility is ensured.

b) Poly-Affine Models: Arsigny *et al.* [168] presented a poly-rigid/affine transformation model. the transformation is parametrized by a set of anchor points a_i, a parameter p_i that defines the importance of every point and a distance σ_i. Fuzzy regions are defined by calculating the influence of an anchor point at each position $\mathbf{x}$ of the image as $p_i * G_{a_i, \sigma_i}(\mathbf{x})$, G_{a_i,σ_i} denotes a Gaussian function parametrized by a mean value a_i and a standard deviation σ_i. Given the transformation of the set of anchor points, the global transformation at each point is given by a distance-weighted sum of infinitesimal velocities at the known points, integrated over time. No closed form exists and a computationally expensive integration of ODEs is necessary. Arsigny *et al.* [169] extended the poly-affine transformation so that its

inverse is also poly-affine. Moreover, the fusion of affine transformations was rendered invariant to affine changes of the coordinate system.

C. Knowledge-based Geometric Transformations

In medical image analysis, there are registration scenarios that involve a specific well-defined task. More specifically, registration is either performed between any image and a specific target image or involves image acquisitions of specific anatomical organs. In these cases, it is possible to introduce knowledge about the deformations one tries to recover.

Introducing knowledge regarding the deformation may be achieved in two ways. In the case that the target domain is fixed in registration because it exhibits desired properties (*e.g.*, it is manually annotated), one can learn a high dimensional statistical model of deformations by performing pairwise registrations between the target image and the data that one has at their disposition. Subsequently, when a new image is to be registered to the target image, the learned model can be used to penalize configurations that diverge from it. The second method consists of exploiting our knowledge about the deformability of the tissues and constructing biomechanical/biophysical deformation models that mimic their properties.

The main motivation behind creating more informed priors is to render the registration method more robust and stable. A registration method is characterized as robust, when its performance does not drastically degrade for small deviations of the input images from the nominal assumptions. In other words, the presence of a small fraction of artifacts or outliers results in small changes in the result. Robustness is, for example, important when encountering images of pathology (*e.g.*, images characterized by the presence of tumors that can be regarded as outliers). A registration method is characterized as stable, when small changes in the input data result in small changes in the result. The stability of the method is, for example, important in longitudinal studies when temporal smoothness, or stable results, can be associated to normality and differences are attributed to temporal anatomical changes. On the other hand, the quality of the solution is conditioned on the quality of the learned model. Learning a high dimensional model is a challenging task that is further impeded by the limited number of training samples.

1) Statistically-Constrained Geometric Transformations—Statistical deformation models (SDMs) capture statistical information about deformation fields across a population of subjects. These methods are able to reduce the number of degrees of freedom, and consequently the computational demands of the problem, while achieving robust performance. Nonetheless, the use of SDMs implies important assumptions. First, one should be able to train the high dimensional statistical model from an often limited number of subjects. Second, it is assumed that the set of images used during the learning step is representative of the population that will be analyzed. Hence, a statistically-constrained registration framework is limited by previously-observed deformations. Subsequent refinement by conventional registration has been proposed to cope with this limitation.

Statistical models of variability have been applied successfully to many problems in medical image analysis. One of the most prominent examples concerns statistical models of shape variability applied to segmentation [170]. Cootes *et al.* [170] studied shape variability by performing Principal Component Analysis (PCA) on point correspondences. Wang and Staib [35] combined a statistical shape model over boundary points and a physics-based regularization term in a Bayesian approach to solve the atlas-based registration problem.

PCA has also been applied in the case of dense deformation fields to derive priors that can be used to constrain registration. Gee and Bajcsy [17] described a recursive way to update the model given new observations while accounting for the limited number of samples.

Wouters *et al.* [171] used PCA to model the deformation and registration was performed by adjusting the coefficients of the principal components while maximizing Mutual Information (MI).

Tang *et al.* [172] also used PCA to learn an SDM to accelerate image alignment. Once the model was learned, the authors created a set of intermediate target images by sampling along each dimension of the estimated multidimensional Gaussian distribution. The registration of a new image was performed by projecting it to the intermediate target image that is closest in intensity similarity, and by refining the result with a conventional registration method. In a similar approach, Kim *et al.* [173] used support vector regression models to predict the intermediate target image. The regression models had learned the correlations between deformations and image appearances.

Rueckert *et al.* [174] performed statistical analysis on the displacement of the control points of the FFD grid that deforms the image. Loeckx *et al.* [175] used a similar model to tackle lung radiograph registration. The statistical model was augmented by incorporating translation and scaling, to account for the fact that the training set was created by manual alignment of image pairs without prior global spatial normalization. Pszczolkowski *et al.* demonstrated that the model in [174] can encode landmark position information [176].

Glocker *et al.* [177] also proposed a model that captures variations in the displacements of the control points of the FFD grid. In the first place, a clustering step was performed to reveal the co-dependencies between node displacements. Then, Gaussian mixture models were used to represent the probability density function (PDF) of the relative displacement of two cluster centers and thus capture information about the global nature of the desired deformations. Similarly, PDFs were learned over the relative displacements of the cluster and its cluster members capturing the local information of the desired deformations. The learned priors were introduced as soft constraints in a discrete Markov Random Field registration framework through the consideration of appropriate pairwise interactions.

Xue *et al.* [178] tackled the problem of training a high dimensional SDM from a limited number of samples by employing wavelet-based decompositions and estimating the PDF of each band by applying PCA to each one. Two SDMs were trained, one captured variations about the deformation fields while the second encoded information about the Jacobian determinant of the deformation fields. The registration result was constrained by the these models as well as a nested Markov random field (MRF) regularization scheme. In a subsequent work, Xue and Shen [179] proposed the use of conventional registration to refine the result of the statistically-constrained method.

Pennec *et al.* [23] presented a statistical framework for nonlinear registration that takes into account the means and the covariances of the deformation tensors by computing their Mahalanobis distance. Brun *et al.* [180] further developed this framework by computing statistical priors on both the deformation tensors and the displacement vector fields in a nonconservative Lagrangian fluid registration algorithm. In both approaches, statistical priors were used to guide registration, instead of constraining it to follow the learned distribution.

Lester *et al.* [181] presented a modified version of the viscous fluid registration algorithm that incorporated tissue information by letting the viscosity vary according to the tissue. In a similar context, Commowick *et al.* [182] proposed to introduce prior knowledge regarding the stiffness of the deformability of different structures by weighting an elastic-type regularization term by a space-varying scalar or tensor field. The computation of the scalar map of deformability was based on the mean of the absolute value of the logarithm of the

determinant of the Jacobian while the stiffness tensor map was based on the mean of the absolute value of the logarithm of the deformation tensor.

Yeo *et al.* [183] presented a conceptually complementary approach. Instead of learning the set of admissible deformations, the weights for a weighted SSD similarity criterion were inferred by optimizing the cross-validation error of a specific task. One could argue that estimating these weights is implicitly equivalent to estimating a stiffness map.

2) Geometric Transformations Inspired by Biomechanical/Biophysical Models —Biomechanical/Biophysical models are also inspired by physical properties. Their difference with respect to the models presented in Sec. II-A is that they relate closely to anatomy and physiology. Usually, Finite Element Methods (FEMs) are employed to model the biomechanical/biophysical properties of the tissues under consideration.

The main motivation behind using the methods of this category is the surmise that more informed priors regarding the biomechanical properties of the tissues will allow the reliable estimation of complex deformation fields with the use of few degrees of freedom. What is more, the limited search space results in improved efficiency when compared to the standard approaches. Moreover, one assumes that by creating models of deforming organs that are consistent to their physical properties, the plausibility of the estimated deformation will improve and registration will be able to better cope with challenges due to the presence of outliers or large deformations. These models are more suitable for intra-individual registration since the biophysical model is no longer valid in inter-individual settings. Nonetheless, one may advocate in favor of their use in inter-individual settings on the basis that, depending on the application, it may be meaningful to let an anatomical structure behave realistically.

On the downside, when opting for models that aim to faithfully represent anatomical structures, one needs to accurately define the material properties as well as the necessary geometry and boundary conditions. This is a challenging procedure that is emphasized by our limited understanding of the material properties. As a consequence, the choice of the parameter values is approximately determined, while at the same time is general and not case-specific. The definition of the geometry requires an accurate segmentation of anatomical structures as well as appropriately meshing the image domain. Suitable boundary conditions can be specified by providing displacement constraints for the segmented organ surfaces. Uncertainty in the specification of these parameters may lead to undesirable bias.

a) Tumor growth models: Registration between normal atlas and pathological brain images in the presence of tumors is a problem that may profit from the existence of brain-tumor interaction models [184]–[187]. One approach to tackle such cases is to correct for the topological difference between the pair of images by accounting for the tumor and its effects in neighboring structures in the normal subject.

Kyriacou *et al.* [188] used a simple uniform expansion model for the tumor. The authors simulated a tumor-free anatomy that was subsequently used in a normal-to-normal atlas registration. The tumor influence was taken into account in order to produce the final deformation field. Cuadra *et al.* used a radial expansion model of the lesion in two cases [189], [190]. In the first case [189], the authors combined the model of lesion growth with the Demons registration algorithm [38]. In the second case [190], they used a variational method based on mutual information [191]. Ganser *et al.* also employed a simple radial growth model in order to perform registration between the Talairach atlas and a subject [192]. The matching process was driven by establishing point correspondences between segmented structures and the atlas. An RBF deformation model was used to estimate the

dense deformation field. Nowinski and Belov [193] refined the result of a Talairach landmark registration by assuming a radial mass-effect tumor model.

Richer models have also been considered. Clatz *et al.* [184] refined the result of an affine registration between a normal atlas and a patient's image by using a coupled model that predicts the anisotropic evolution of the tumor as well as its mass-effect. Methods that combine sophisticated brain-tumor interaction with deformable registration have been proposed in [194]–[197]. Mohamed *et al.* [194] trained a statistical model of the tumor-induced deformation based on a great number of tumor model simulations. This model was used to estimate the mass-effect in the atlas domain before applying deformable registration. Zacharaki *et al.* [195], [196] also trained a statistical model based on simulations of the tumor effect [185]. The parameters of the learned model were inferred through optimization that considered both deformation field information and image similarity. Gooya *et al.* [197] addressed the registration between a normal subject and a subject with Glioblastoma multiforme brain tumors. The tumor was modeled by [186]. An expectation-maximization setting was used to jointly estimate the parameters of the model and the warping.

b) Biomechanical models of the breast: Another field for application of biomechanical models is breast imaging. Biomechanical modeling is important in tackling large deformations which are typical in breast imaging applications such as image-guided interventions [198], cancer diagnosis [199] and surgical planning [200]. The ability of FEMs to realistically simulate breast deformations has led to their use for the validation of registration methods [201]–[203].

There are two main causes of breast deformation, gravity and plate compression. When patients are imaged under different positions (typically prone-supine), the breast is deformed greatly under the influence of gravity. FEMs have been used either to register the images [200], [204] or to provide a more appropriate initialization for standard intensity-based nonrigid registration methods [205]–[207].

The breast is typically compressed in mammography under the pressure of two plates in order to flatten and spread the tissue. As a consequence, alignment between 2D mammograms and images from other, (typically 3D), modalities is a challenging problem. FEMs have been used to tackle this problem [198], [208]–[212]. While these methods aim to align different images, they do not opt to optimize an image-similarity criterion. Instead, alignment is determined by the modeling assumptions and boundary conditions. Image driven approaches have been proposed toward estimating subject-specific tissue properties [213]–[215].

c) Biomechanical models of the prostate: Biomechanical models have also been used to model the prostate and its surrounding organs with applications in preoperative-intraoperative image registration problems [216] and treatment planning [217]. Mohamed *et al.* [218] and Hu *et al.* used a biomechanical model of the prostate to simulate training data to learn a statistical model that was subsequently used to constrain the registration. Alterovitz *et al.* [219] presented a 2D biomechanical model whose material properties and external forces were optimized by maximizing the overlap between the segmented prostate in both images. Crouch *et al.* [220] used medial shape models to facilitate meshing and boundary condition calculation.

d) Miscellaneous: Biomechanical models span a great range of applications. Detailing them all here is both out of scope and impossible. Nonetheless, let us note that they have been applied in the estimation of: cardiac movement [221]–[226], brain shift during surgical operations [227] and lung movement [228], [229].

D. Task-Specific Constraints

According to Hadamard's definition of well-posed problems [11], unregularized optimization of similarity measures for high-dimensional deformable transformation models is, in general, an ill-posed problem. In order to cope with the difficulty associated with the ill-posedness of the problem, regularization is necessary. Moreover, regularization allows us to introduce any prior knowledge we may have regarding the physical properties of the underlying anatomical structure and helps optimization avoid local minima.

There are two possible ways to regularize the problem: implicitly and explicitly. Implicit regularization may be achieved by parameterizing the deformation field with smooth functions. Explicit regularization may be achieved through the use of either hard constraints or soft constraints. Hard constraints are the constraints that the solution must satisfy in order for the registration to be successful. Soft constraints are introduced as additional terms in the energy function that penalize non-regular configurations. Soft constraints encode our preference regarding specific configurations, but deviations from the preferred configurations are allowed if driven by the other term(s) of the energy function. Physics-based deformation models are typical examples of explicit regularization. Moreover, explicit regularization may be used to achieve specific goals that are tailored to the problem at hand. Such goals include (see Fig. 1): i) topology preservation, ii) volume preservation, and iii) rigidity constraints. Task-specific constraints can be, and often are, used in conjunction with physics-based models (Sec. II-A) and interpolation-based models (Sec. II-B).

1) Topology Preservation—One of the most important properties that a registration algorithm should exhibit is the preservation of topology. The preservation of topology is equivalent to the invertibility of the deformation field. The Jacobian of the deformation field is very informative regarding the local properties of the deformation field. In order to avoid singularities in the deformation field, Christensen *et al.* [30] proposed to track the values of the Jacobian. When its value dropped below a threshold, an intermediate deformed image was created and the registration process was reinitialized.

Another way to enforce the preservation of topology is through the use of constraints, *i.e.*, by including in the objective function an appropriate term that acts upon the Jacobian. Christensen and Johnson [19] added to the objective function a term that penalizes small and large Jacobian values for both the forward and backward transformation. Similarly, Rueckert *et al.* [138] introduced a term in the objective function that penalizes values of the Jacobian determinant that are close to zero.

A different strategy is to formulate registration as a inequality constraint optimization problem. Musse *et al.* derived linear inequality constraints so that the topology is preserved [157]. The optimization was solved by employing a fast method that bears a resemblance to sequential linear programming. Noblet *et al.* extended the previous framework in the $3D$ case [158]. The authors optimized the energy under the constraint that the Jacobian will stay between user specified bounds. Interval analysis techniques were used in order to solve the optimization problem. Haber and Modersitzki [230] also used inequality constraints. They used a variant of a log-barrier method to solve the optimization problem. Instead of solving the initial constrained problem, a sequence of unconstrained ones was employed. The weight for the barrier terms increased gradually for each unconstrained problem that was optimized by applying a variant of the Gauss-Newton's method.

Sdika [137] also proposed a constrained optimization framework to ensure that the transformation is invertible. Two constraints were investigated for the case of a transformation model parametrized by cubic B-splines. The first constrained the Jacobian of every pixel to be greater than a threshold. This constraint did not control the value of the

Jacobian between the voxels. To account for that, the author proposed a second constraint that relates the Jacobian with its derivative. In that way, the Jacobian was restricted to be within a range of values. Moreover, its derivatives were constrained to be close to zero when approaching values close to the bounds. Chun and Fessler devised a simpler penalty for the case of *B*-splines [231]. The penalty takes into account the difference between two adjacent nodes and is memory efficient.

2) Volume Preservation—In many applications, volume preservation is also important. Such a constraint is of particular interest when we know that the imaged anatomical structure is not compressible and that all changes are due to either motion or intensity changes provoked by the action of a contrast agent. A simple example is a rigid part of the body such as a bone structure. More complicated cases include deformable structures that preserve their volume such as breast, myocardium and liver.

Tanner *et al.* [232] proposed a sequential approach for volume preserving deformable registration using an FFD model. First, a standard registration was performed. Based on its result, the areas whose volume should be preserved were identified. Then, the control points of the FFD that influenced these areas were grouped and restricted to move by a constant displacement that is equal to the mean value of their displacements during the initial registration step. Finally, the registration was solved again for the rest of the variables. Greene *et al.* also presented a sequential approach for image-guided adaptive radiotherapy using an FFD model [233]. First, the organs of interest and the bones were segmented and independently registered. Then, a constrained framework was used to estimate the FFD transformation that maps from one image to another. The displacements of the control points that influence the segmented objects were constrained to be close to the displacements that were calculated during the individual object registrations.

Rohlfing *et al.* employed a volume preserving strategy to register contrast-enhanced MR breast images [234]. The objective function comprised an image matching term and a term that penalized volume changes. The penalty integrated the absolute logarithm of the Jacobian determinant and was zero only when local volume was preserved. Haber and Modersitzki [235] presented a constrained optimization approach for volume preservation. The proposed energy function, consisting of a matching and regularization term, was minimized under the constraint that the determinant of the transformation is equal to one ($det(\mathbf{I} + \nabla\mathbf{u}) - 1 = 0$).

The myocardium is known to be a nearly incompressible material. Therefore, applications involving the deformation of the myocardium may profit from including an incompressibility constraint. Bistoquet *et al.* [236] approximated the previous constraint with $\nabla \cdot \mathbf{u} = 0$. This constraint was enforced by the use of divergence-free radial basis functions as deformation model [128]. In addition, a hard constraint was introduced in the objective function to penalize deviations from incompressibility. Dauguet *et al.* [237] constrained the determinant of the Jacobian to be close to one in a predefined region by using Lagrange multipliers. Mansi *et al.* took a different approach in [50]. They constrained the velocity field $\mathbf{v}$ to be divergence-free. This method was based on the fact that the integration over time of divergence-free velocities results in incompressible deformations.

3) Rigidity Constraints—The presence of rigid anatomical structures in medical images motivates the incorporation of rigidity constraints in image registration. Loeckx *et al.* [238] locally constrained a non-rigid FFD registration method by penalizing deviations of the Jacobian from orthogonality. Staring *et al.* [239] imposed rigidity by introducing three conditions. The first condition required the second derivatives of the transformation to be zero. The second condition forced the orthonormality of the rotation matrix, while the third

condition required the determinant of the Jacobian to be equal to one. Modersitzki [240] has also investigated local rigidity in a variational setting. Modersitzki introduced a third term in an objective function comprising a matching and a regularization term. The additional term controlled the rigidity of the transformation by forcing its Jacobian to be linear, orthogonal and orientation preserving.

III. Matching Criteria

We can distinguish three groups of registration methods according to how they exploit the available information to drive the matching process (see Fig. 2).

On one hand, geometric methods opt for the establishment of correspondences between landmarks. The landmarks are assumed to be placed in salient image locations which are considered to correspond to meaningful anatomical locations. The underlying assumption is that saliency in the image level is equivalent to anatomical regions of interest. Geometric registration is robust with respect to the initial conditions and the existence of large deformations. The solution of the registration problem is obtained in a relatively straightforward way once landmarks have been extracted. However, locating reliable landmarks is an open problem and an active topic of research. Most importantly, the sparse set of directly obtained correspondences gives rise to the need for extrapolation. Interpolation results in a decrease in accuracy as the distance from the landmarks increases. The interest regarding geometric methods has decreased during the past decade. Nevertheless, geometric methods constitute a reliable approach for specific applications. They are of interest when intensity information is undermined due to the presence of pathologies while geometric structures remain stable (*e.g.*, retina registration [241]). Geometric registration has also important applications in image-guided interventions [242], [243].

On the other hand, iconic methods, often referred to as either voxel-based or intensity-based methods, quantify the alignment of the images by evaluating an intensity-based criterion over the whole image domain. When compared to the geometric methods, this approach has the potential to better quantify and represent the accuracy of the estimated dense deformation field. Nonetheless, it comes at the cost of increased computational expense. Where geometric methods use a small subset of image voxels to evaluate the matching criterion, iconic methods may use them all. Moreover, due to the fact that salient points are not explicitly taken into account by the matching criterion, the important information they contain is not fully exploited to drive the registration. In addition, initial conditions greatly influence the quality of the obtained result due to the non-convexity of the problem.

Hybrid methods combine both types of information in an effort to get the best of both worlds.

A. Geometric Methods

Geometric methods aim to register two images by minimizing a criterion that takes into account landmark information. Before describing any methods, let us introduce the known and unknown variables of the problem.

The known variables consist of two sets of landmarks ($K = \{\kappa_1, \cdots, \kappa_n\}$ and $\Lambda = \{\lambda_1, \cdots, \lambda_m\}$). These sets of landmarks can be created using a key-point detector strategy. The first set of landmarks contains points belonging to the source domain Ω_S, while the second contains points that belong to the target one Ω_T. The set of unknown variables comprises: i) the correspondence, and ii) the transformation.

Three classes of methods can be separated based on which unknown variable is estimated [244] (see also Fig. 2): i) methods that infer only the correspondence, ii) methods that infer only the spatial transformation, and iii) methods that infer both variables. Let us emphasize that these are not the different components of geometric methods. Indeed, methods that infer only the correspondence can be used in conjunction with an interpolation to establish dense correspondences between two images. Nonetheless, these are different methods that exploit geometric information in order to solve distinct problems.

In the remainder of this section, we are going to first give a brief presentation of strategies for detecting point of interests. Then, we are going to continue with the presentation of methods based on the previous classification. In this section, we interchangeably use the terms landmarks, points of interest and key-points.

1) Detecting points of interest—The first step in geometric registration is to detect points of interest. Images that contain sufficient details facilitate point detection. Medical images are not as rich in details as natural images [4]. That is why, point detection has mainly drawn the interest of the computer vision community. Landmark extraction has been studied more in the case of $2D$ images and less in the case of $3D$ images. Before continuing, let us refer the interested reader to a recent book by Goshtasby [10] where point-detectors and descriptors are more extensively studied.

The detection and the matching of points of interest are inherently coupled with the way the landmarks are described. The richness of the description is important in order to detect salient points and better disambiguate between close potential candidates during matching. Moreover, as the imaged objects undergo deformations, the appearance of the points of interest will vary between images. Therefore, descriptors should be invariant to such changes in order to allow robust detection and matching under deformations.

A detailed overview of the point detectors that have been proposed in the computer vision literature is out of the scope of this review. Nonetheless, let us give a brief description of some important key-point detector methods. Harris *et al.* proposed to identify corners by exploiting the information conveyed by the structure tensor A [245]. Specifically, points of interest are determined by considering the following quantity: $det(A) - \alpha\ Tr(A)^2$. In similar lines, Shi and Tomasi [246] proposed to use the minimal eigenvalue of the structure tensor in order to track points of interest.

Many extensions to the Harris detector have been proposed in the literature. Their main aim was to impose a certain invariance. One may cite the approach proposed by Triggs [247] and affine-invariant Harris and Hessian [248]. Affine invariance is important as it enables the detection of points under affine transformations and a lot of efforts have been concentrated in defining such detectors. An evaluation study comparing the most important affine invariant detectors was presented by Mikolajczyk *et al.* [249]. For review of point detection methods, the interested reader is referred to the works of Schmid *et al.* [250] and Triggs [247]. Evaluation studies of point and corner detectors have been performed by Schmid *et al.* [250] and Mokhtarian and Mohanna [251].

An alternative way to determine point of interests is by performing scale-space analysis and detecting blob-like regions. The use of the Laplacian of Gaussian has been investigated to perform this task. The image is convolved with different scales of a Gaussian kernel and at each level the Laplacian operator is applied. Lindeberg proposed to track across scales the local maxima/minima of the response of the Laplacian operator in order to detect key-points

[2] http://www.mindboggle.info/papers/evaluationNeuroImage2009/data/

[252]. Kadir and Brady [253] proposed a multiscale approach for the detection of salient regions. The algorithm was based on the use of local entropy to quantify saliency. Matas *et al.* proposed a technique for blob detection [254]. A multiscale representation of image regions was created by thresholding for different values in the intensity domain. These regions were tracked and selected based on their area's stability to change of the threshold value.

Lowe [255] proposed to use the Difference of Gaussians, that is an approximation of the Laplacian, to create a scale-space representation. Feature points were detected by extracting the local minima/maxima of the this scale-space representation. The local Hessian information was used to reject spurious points. Lowe's Scale Invariant Feature Transform (SIFT) algorithm to describe key-points was based on the gradient information at the scale a point of interest was detected. For every pixel in a neighborhood of the key-point the gradient magnitude was computed. Its value was weighted depending on its distance from the key-point. From these values, gradient orientation histograms were computed and normalized to account for photometric variations. Many variants of SIFT have been proposed.

Ke and Sukthankar proposed PCA-SIFT [256] where the gradient image of the local patch is projected to lower dimensional space constructed by Principal Component Analysis (PCA). Mikolajczyk and Schmid proposed the use of Gradient Location and Orientation Histogram (GLOH) [257]. The authors proposed to use a log-polar pattern for the spatial sampling and PCA to decrease the dimensionality of the descriptor. Bay *et al.* [258] proposed the Speeded-Up Robust Features (SURF) that are based on the application of the Haar wavelet in the region of the point of the interest. Morel and Guoshen proposed an affine invariant version of SIFT [259]. Invariance was introduced by simulating the latitude and longitude angles.

For a comparison between the original SIFT and its variants see [260]. For a comparison of the performance of different feature descriptors, the interested reader is referred to [257], [261].

The development of such generic approaches to extract points of interest is less investigated in medical image analysis. Nonetheless, a number of extensions of SIFT in higher dimensions have been proposed. Cheung and Hamarneh extended SIFT in the nD domain [262] and reported results for the $3D$ and $4D$ case. Ni *et al.* also presented an extension of SIFT to the $3D$ image domain [263]. These approaches ignored the tilt-orientation information. Allaire *et al.* [264] proposed another extension of SIFT in the $3D$ domain that is fully orientation invariant. The authors proposed to create an additional histogram to determine the tilt angle. Flitton *et al.* [265] proposed the use of a tilt histogram for the full definition of the $3D$ orientation when extending SIFT in the $3D$ domain.

Cheung and Hamarneh [262] validated their extension of SIFT by matching landmarks between $3D$ MR images and $3D + t$ CT images. Ni *et al.* used $3D$ SIFT to $3D$ ultrasound volume stitching toward panorama creation [263]. Allaire *et al.* used $3D$ SIFT to register planning CT data to cone bean CT data [264]. Niemeijer *et al.* used matched SIFT points in order to tackle rigid registration between Optical Coherence Tomography (OCT) images [266]. Han extended the SURF descriptor [258] to $3D$ and used it in a hybrid registration framework [267]. Yang *et al.* used salient the scale invariant features [253] to tackle geometric registration that infers both the correspondence and the spatial transformation [268]. Toews and Wells used $3D$ scale invariant features for rigid model-to-image registration [269]. We are going to discuss in more detail these methods in the section that is more related to each one of them.

To the best of our knowledge, feature detection in medical image analysis is performed in a task specific manner, usually as product of a segmentation preprocessing step. Pennec *et al.* extracted points and lines in surfaces through the use of differential geometry for rigid brain registration [270]. In brain image registration, sulci information has been used in [89], [271]–[273]. The cortical surface information has also served as feature in [273]–[275].

Retina image registration is another application where extracting geometric cues has been investigated. The intensities in the nonvascular part of the image are homogeneous, while important information is conveyed by the vasculature. Can *et al.* used the branching and crossover points of the blood vessel structure as feature points [276]. Stewart *et al.* additionally used the centerlines of the segmented vasculature [241]. For each centerline point, its location, tangent direction and width were retained. Vascular structures are also important in brain sift correction [277], pulmonary CT images [278] and liver registration [279]. That is why a number of task-tailored detectors have been devised [280]–[283].

Lastly, fiducial markers are also used to guide image registration. Some resent studies regarding the errors in the process are given in [284]–[286].

2) Methods that infer only the correspondences—Methods that belong to this class aim to solve only the correspondence problem. In other words, these methods aim to assign every point $\kappa_i \in K$ to its corresponding point $\lambda_j \in \Lambda$. Establishing solely correspondences can be useful when they are used in combination with an interpolation-based transformation model to estimate dense displacements between the two images. Hybrid registration (see Sec. III-C) is another case where such methods are of interest. One uses the sparse geometric correspondences along with an iconic criterion to improve the estimation of the spatial transformation.

Having established a discriminative and ideally deformation invariant description of the key-points, correspondences may be established either by i) relying solely on the closeness of the descriptions, or ii) by incorporating structural constraints. For a different classification as well as the presentation of some earlier works in the field, the interested reader is referred to [244].

a) Matching by descriptor distance: In the first case, the information contained by the descriptor is used to determine the correspondences. There is an implicit assumption that the descriptors are constructed so that the use of the Euclidean distance is sufficient to rank potential matches. This construction can be achieved by appropriate rescaling of the feature vector values. Based on an established ranking, different matching strategies may be considered.

The simplest strategy is thresholding; points that exhibit a similarity higher than a threshold are matched. The definition of the threshold can be achieved by studying the Receiver Operating Characteristic (ROC) curve. A different strategy is to assign each point to its closest candidate. Closeness is de-fined based on the Euclidean distance in the descriptor space. As the probability of detecting a false positive is significant, a threshold is still needed to control it. The third strategy is to take into account the ratio between the distance with the nearest and the second nearest neighbor in the feature space. For an evaluation of these strategies, the interested reader is referred to [257]. A fourth strategy consists of verifying the uniqueness of the matching by evaluating the third criterion in both the forward and backward direction [262], [266], [267]. A point a is matched to b if and only if a is the best match for b, and b is the best match for a.

While being intuitive and efficient, these matching approaches discard any information regarding the spatial location of the key-points in the image. The incorporation of such knowledge aims to better constrain the matching problem and further reduce the number of erroneous correspondences.

b) Matching through geometric constraints: A popular way to introduce structural constraints is by formulating the problem as graph matching. Leordeanu and Hebert [287] proposed a spectral technique to solve the matching problem. Pairwise constraints were used to preserve pairwise geometry. Berg *et al.* [288] formulated the problem of recovering feature correspondences as an integer quadratic programming problem. Changes in the length and the direction of vectors defined by pairs of features were penalized. Torresani *et al.* also employed pairwise constraints to model local spatial coherence [289]. Moreover, the authors showed that is possible to handle outliers during the optimization.

Despite the success pairwise constraints have had in many applications, they are limited with respect to the relations they can model. Recently, a number of researchers have tried to tackle the graph matching problem with higher order constraints. Duchenne *et al.* [290] generalized the spectral matching method [287] to higher order constraints. A tensor power iteration method was employed to solve the matching problem. Zass and Shashua in [291] proposed a similar formulation, while using a different optimization method. Wang *et al.* [292] proposed a higher-order graph matching formulation that incorporates learned structural constraints in a segmentation framework. The inference was performed by a dual decomposition based method [293].

3) Methods that infer only the spatial transformation—The aim of these methods is to estimate the spatial transformation that, when applied, will align the two sets of landmarks K and Λ. These methods do not aim to explicitly establish correspondences between the two landmark sets. The output of the algorithm is the spatial transformation that relates the two point sets and not an explicit assignment of the every point $\kappa_i \in K$ to a point $\lambda_j \in \Lambda$.

Two different classes of methods can be distinguished according to whether the correspondences are known or not. The case of known correspondences is briefly presented for completeness reasons. We focus more on the case of unknown correspondences because it is more challenging and there is a number of recent algorithms that have been proposed to tackle the problem.

a) Known correspondences: Two categories of methods should be considered (see Fig. 2). The first one assumes that the correspondences are known in an exact or inexact way. This problem is known as exact or inexact landmark matching. In the exact case, a smooth transformation is sought so that the correspondences are respected exactly or a regularization energy is optimized under correspondence constraints. In the inexact case, a compromise between matching and smoothing the deformation is preferred.

Procrustes analysis is a popular method for shape analysis and is useful when homologies between point-sets are given [165], [294]–[296]. In Procrustes analysis, a least-squares distance is minimized. Given the correspondences, a solution that consists of translating, rotating and scaling can be analytically calculated [295].

Given the correspondences, one may estimate non-rigid transformations by adopting an interpolation strategy (Sec. II-B). Radial basis functions are able to produce dense deformation fields for any spatial distribution of points. Moreover, approximating splines are able to account for the uncertainty in the estimated correspondences [110], [131]. Guo *et*

al. has presented a solution for both the exact and inexact landmark matching problems for the case of diffeomorphic deformations [297]. Glaunes *et al.* have extended this method to the case where the domain is a sphere [82].

b) Unknown correspondences: The second subclass opts to estimate the transformation without concerning itself with the establishment of correspondences. These methods are more robust to missing correspondences and outliers. One may distinguish two different subclasses depending on the nature of the transformation that is estimated. The methods that belong in the first category estimate a global linear transformation, while the methods in the second category estimate a non-rigid transformation. For the description of some of the methods that belong to the first class, we refer the reader to [244]. Because the aim of this review is to describe the recent advances in deformable registration, we are going to focus here on the second class of methods.

The estimation of non-rigid transformations was achieved through the use of alternative representations of the geometric information. One possibility is to represent the point sets as probability distributions. In this case, the non-rigid transformation is estimated by minimizing a distance measure between the two distributions. Glaunes *et al.* [84] extended the large diffeomorphic deformation framework in the case of distributions and unlabeled point sets. Point sets were modeled as a weighted sum of Dirac measures and a kernel-based error measure was used. Tsin and Kanade [298] proposed to register point sets based on a measure called kernel correlation. The proposed measure is proportional to the correlation of two kernel density estimates. Singh *et al.* presented a similar approach based on kernel density correlation [299].

Gaussian Mixture Models (GMMs) are a common way to model distributions. Jian *et al.* [300] modeled each point set using GMMs and used a L_2 distance to compare them. Myronenko and Song [301] recast registration as a probability density estimation problem. The points of the first set were considered as the centroids of the GMMs which were fitted to the data (or points of the second set) by likelihood maximization. Special care was taken so that the centroids move in a coherent way. Roy *et al.* [302] modeled each feature of each shape as GMM. A mixture model was used to represent the shape by assuming that features are independent and identically distributed. A closed-form distance between the two distributions was used. Wang *et al.* used a similar model to tackle the problem of the simultaneous registration of multiple point sets [303]. Jensen-Shannon divergence was used as the similarity metric. The drawback of this approach was that the problem could not be solved in closed-form. Instead, a computationally and memory demanding estimation based on the law of large numbers was required. In a subsequent work, Wang *et al.* [304] alleviated this shortcoming by using the generalized L_2-divergence that allows for a closed-form solution. Tustison *et al.* also used a GMM with the difference that the Gaussians were not isotropic [305]. The Havrda-Charvat-Tsallis (HCT) divergence was used to compare the two distributions.

Another way to perform non-rigid registration of shapes and points without caring to establish correspondences is by adopting a representation of the geometric information based on the use of signed distance functions. In this case, the geometric primitives (*e.g.*, landmarks or shapes) are assigned to zero distance, while the rest of the image elements are assigned a signed value based on their euclidean distance from the geometric primitives. Based on this representation, the optimal transformation can be estimated by performing standard intensity-based registration.

Paragios *et al.* embedded shapes to the higher dimensional space defined by the signed distance transform and register them by evaluating the sum of squared differences criterion

over a narrow band around the shapes [306]. Huang *et al.* used the same shape representation and investigated the use of Mutual Information to globally align them [307]. The sum of squared differences was used to non-rigidly register the shapes. Savinaud *et al.* represented both silhouettes and landmarks using the Euclidean distance transform [308]. Leow *et al.* used implicit representation to tackle brain warping [83], [85]. Leow *et al.* formulated the energy minimization problem as a curve evolution problem motivated by the geodesic active contours [309].

4) Methods that infer both the correspondences and the transformation—The last class of methods aims to estimate the correspondences and the transformation at the same time. This is usually performed in an iterative way. First, one component is estimated, and then the other component is refined based on this estimation.

One of the most well known approaches is the Iterative Closest Point (ICP) method proposed by Besl and McKay [310]. Simplicity and speed are the main characteristics of this method. Correspondences are defined based on a closest (in a geometric sense) neighbor principle. Based on this estimation, the transformation is calculated. Then, a new closest neighbor is assigned to each key-point and the process continues until convergence. ICP has drawn a lot of attention and a number of researchers have tried to improve the method over the years. Rusinkiewicz and Levoy reviewed different variants of ICP [311]. Liu has reported an overview of the improvements over ICP [312]. Pottmann *et al.* presented a study of the convergence properties of the ICP algorithm [313].

Penney *et al.* [314] proposed to add Gaussian noise to the positions of the points in one set before each iteration of the original ICP. The magnitude of the noise was decreased as the process advanced. The motivation behind this strategy was to improve the precision and robustness of the algorithm. Granger and Pennec [315] proposed an approach named multi-scale EM-ICP. The method is similar to standard ICP with a Mahalanobis distance. The principal difference lies in the estimation of the transformation step where multiple matches weighted by Gaussian weights were considered. The problem was solved in an Expectation-Maximization fashion. Sharp *et al.* [316] investigated the use of shape features in addition to the positional information when estimating the correspondences.

Stewart *et al.* [241] proposed a dual-bootstrap ICP method to register retinal images. The method operated initially on small regions where accurate correspondences could be obtained. Based on these correspondences low order transformations were estimated. In the subsequent steps, the size of the regions as well as the order of the transformation model were refined. The region refinement was based on the uncertainty of the transformation. Liu [312] used collinearity and closeness constraints in order to increase the robustness and accuracy of the algorithm for free form deformation. Estepar *et al.* [317] allowed for anisotropic noise in both target and source point sets in order to render the algorithm more robust. The problem was cast in the form of a Generalized Total Least Square problem. Maier-Hein *et al.* [318] recently proposed a related work that accounts for localization error.

Let us note that ICP method, as well as its variants presented here, estimate a global linear transformation. An important extension to non-rigid scenarios was proposed by Chui *et al.* [244]. The proposed Thin-Plate Spline Robust Point Matching (TPS-RPM) algorithm iterates between estimating the correspondence with the softassign method and computing the transformation with a TPS model. Chui *et al.* [273] further refined the latter approach by iteratively solving a clustering and matching problem.

B. Iconic Methods

In iconic methods, the matching term integrates the evaluation of a dissimilarity criterion that takes into account the intensity information of the image elements. Devising an appropriate criterion is an important and difficult task. The criterion should be able to account for the different physical principles behind the acquisition of the two images and thus for the intensity relation between them. Moreover, the properties of the similarity function (*e.g.*, its convexity) may influence the difficulty of the inference and thus the quality of the obtained result.

An ideal dissimilarity criterion would take low values when points belonging to the same tissue class are examined and high values when points from different tissue classes are compared. Moreover, an ideal criterion should be convex, allowing for accurate inference. There is an important balance that should be struck between the convexity and ability to distinguish between points belonging to different tissues. On the one hand, convexifying the objective function will facilitate the solution of the problem. On the other hand, it may lead to a less realistic problem because the problem is non-convex in its nature.

At this point, two cases should be distinguished regarding the iconic methods (see also Fig. 2): i) the mono-modal case, involving images from one modality, and ii) the multi-modal one, involving images from multiple modalities.

1) Mono-Modal Registration—In the mono-modal case, the same imaging device is used to capture the same type of information for both volumes.

a) Intensity-based methods: Different matching criteria can be devised depending on the assumptions about the intensity relationship between the images. In the case that the same anatomical structures are assumed to correspond to similar intensity values, the Sum of Squared or Absolute Differences (SSD and SAD respectively) can be used as a matching criterion. The choice between the two depends on the assumption regarding the noise that corrupts the image intensities. In the case that a linear relation is assumed between the signal intensities, the optimal criterion is Cross Correlation (CCor) and Correlation Coefficient (CCoef) [1], [78], [319].

b) Attribute-based methods: Intensity information may lead to ambiguous matching and local minima in the objective function when pixels of the same anatomical structure take similar intensity values [119]. A number of researchers have proposed to increase the dimensionality of the feature space in order to cope with this shortcoming. A way to augment the feature space is by introducing local information through the use of attributes that represent the geometric structure of the underlying anatomy. These approaches are referred to as feature- or attribute-based ones. These approaches focus on a different way to represent image information, while they use standard similarity measures.

Shen and Davatzikos [119] proposed the use of an attribute vector including Geometric Moment Invariants in an attempt to capture local anatomical information at different spatial scales. The motivation was that a rich enough attribute vector would be able to differentiate voxels that would be considered the same based only on their intensity information. Thus, fewer local minima would be present and better accuracy may be achieved. To further reduce the effect of the local minima, they proposed a hierarchical scheme that successively approximated the objective function by progressively increasing the number of voxels where the matching criterion was evaluated.

The previous method requires a pre-segmentation step in order to introduce local spatial information. Xue *et al.* proposed the use of Daubechies wavelets to populate the attribute

vector in order to remove the requirement for segmentation [320]. The attribute vector was constructed in a multiscale fashion to be translation and rotation invariant. Shen proposed to tackle the above shortcoming by using local histograms and boundary information as attributes [321]. Wu *et al.* [322] proposed to use a learning approach in two ways. First, the authors proposed to learn the optimal scale for the geometric features for each voxel. Second, they proposed to learn which voxels should be used to drive the registration process. They proposed to take into account the saliency and the consistency of the description of the voxels across the training data.

Local information may also be incorporated by exploiting the local frequency representations obtained as response to Gabor filters [323], [324]. Gabor features have proven successful for both mono-modal and multi-modal image registration as they are able to capture information across different scales and orientations. Ou *et al.* [323] optimized the Gabor features to be more distinctive and employed the notion of mutual saliency to let the most reliable points drive the registration process. However, Liao and Chung [325] argued that frequency spectra of MRI brain images often exhibit non-Gaussian behavior and thus the choice of Gabor filters is not optimal. They proposed the use of symmetric alpha stable filters and showed experimentally that they outperform Gabor features in non-rigid MRI brain registration. Liao and Chung proposed a new feature for non-rigid registration in [326]. The feature is a uniform spherical region descriptor and is invariant with respect to rotation as well as monotonic gray-level transformation. Thus, it is able to account for the presence of a bias field. Myronenko and Song proposed to use Residual Complexity (RC) to account for complex spatially-varying intensity distortions [327]. This method attempts to register two images by minimizing the number of basis functions that are required to code the residual image.

2) Multi-Modal Registration—Multi-modal registration is more challenging as the choice of an appropriate matching criterion is a harder task. Two main approaches have been proposed to solve the problem (see also Fig. 2): i) use of information theoretic measures, and ii) reduction of the multimodal problem to a mono-modal problem. The latter can be achieved by either a) simulating one modality from another, or b) mapping both modalities to a common domain. Here, we are going to focus primarily on information theoretic approaches as they constitute the most frequently used way to tackle the challenges posed by multi-modal registration. Reduction techniques will also be briefly discussed.

a) Information theoretic approaches: Information theoretic approaches were popularized by two different groups, one in US [328], [329], and one in Belgium [330], [331]. Both teams investigated the use of Mutual Information (MI) in multi-modal image registration. The difference between their approaches is the way entropy is estimated. Wells *et al.* [328] and Viola and Wells [329] used a non-parametric estimator. Collignon *et al.* [330] and Maes *et al.* [331] used histograms instead. An important property of MI is its generality. MI does not assume any relationship between the image intensities. For a survey on MI-based registration methods, the interested reader is referred to the review by Pluim *et al.* [332].

The widespread use and study of MI has revealed some of its shortcomings. Primarily, it is not overlap invariant. Thus, in certain cases it may be possible for mutual information to be maximized when the images get misaligned. Studholme *et al.* proposed a Normalized version of Mutual Information (NMI) in order to remedy this shortcoming [333]. Recently, Cahill and co-workers elaborated upon the idea of overlap invariance and showed that neither NMI, MI, CR, CCor nor CCoef are invariant to changes of overlap and proposed appropriate invariant versions of the previous similarity measures in [334].

The success of MI paved the way for the introduction of an important number of statistical criteria in image registration. Roche *et al.* [335] argued that the generality of mutual information can be a drawback when a reasonable hypothesis can be made regarding the relationship between the intensities. They proposed to use the Correlation Ratio (CR) as the appropriate similarity measure when the assumption of functional dependence between the image intensities is valid.

Pluim *et al.* [336] compared the performance of a number of *f*-information measures (including MI) in medical image registration. In the context of registration, *f*-measures quantify the difference between the joint distribution of the intensities and the joint distribution that would arise if images were independent. The most important finding of the study was that there are *f*-measures that were able to perform better than MI at the cost of more difficult inference.

The idea to use divergence measures to compare joint intensity distributions has attracted significant attention and different divergence measures have been proposed for multimodal image registration. Chung *et al.* [337] and Guetter *et al.* [338] used Kullback-Leibler Divergence (KLD) to register multi-modal images. The joint intensity distribution was either learned from aligned pairs of images or by segmenting corresponding anatomical structures. Images got aligned by minimizing the divergence between the observed and estimated distributions. Liao *et al.* used Jensen-Shannon Divergence (JSD) to compare learned distributions in [339]. JSD is symmetric, bounded and true metric.

Another family of information theoretic approaches is built upon Renyi Entropy (RE) [340]. Let **p** be a random variable with n possible outcomes, then RE is defined as $R_\alpha(\mathbf{p}) = \frac{1}{1-\alpha} log(\sum_{i=1}^{n} p_i^\alpha)$, $\alpha \geq 0$ and $\alpha \neq 1$. p_i denotes the probability of the outcome i. Based on this entropy, the Jensen-Renyi divergence can be defined. It is symmetric, convex for $\alpha \in (0, 1)$ and is maximum when the distributions are degenerate. He *et al.* proposed its use for image registration [341]. Neemuchwala *et al.* [342] used a Minimum Spanning Tree (MST) to estimate the RE. Spanning graphs were also used by Sabuncu and Ramadge [343]. Martin and Durrani introduced a generalization of KLD in [344]. The new divergence measure was based on modified Bessel functions of the second kind and allowed for an efficient recursive computation. The generalization of KLD was shown to perform better than the standard measures of divergence.

Most of the aforementioned approaches share a common drawback; they are based on a single pixel joint probability model. As a consequence, by changing the positions of the pixels in a random way and evaluating the statistical criterion, the same similarity is obtained [345]. This extreme case demonstrates that when spatial information is ignored, registration may fail because the matching criterion is not able to quantify the difference between the two images. Shading artifacts pose a more reasonable challenge where information theoretic measures may fail [345]. To rectify this shortcoming, local context can be introduced in the used criterion.

One way to relax the way statistical criteria are globally taken into account consists of computing them locally, thus coping with the fact that the relation between the two image intensities is non stationary. This approach was investigated by Hermosillo *et al.* [191] and Karaçali [346]. Hermossilo *et al.* derived the Euler-Lagrange equations for MI, CR and CCoef based on locally estimated probability distribution functions. Karaçali followed a deterministic rationale to express the mutual information, joint entropy and the sum of marginal entropies over small spherical regions in closed form.

Local evaluation of mutual information has also been proposed by other researchers. For instance, Studholme *et al.* [347] investigated the use of Regional Mutual Information (RMI). The proposed similarity function is a linear weighted sum of local evaluations of MI and aims to reduce the error caused by local intensity changes. Sundar *et al.* proposed a robust way to compute MI [348]. The authors proposed to adaptively parcel late the image using octrees. The size of the octants is proportional to the homogeneity of the underlying image. These octant define the sampling strategy that is used to estimate the entropy. More samples are taken in regions where the density of octants is higher. In this case, the octree parcelation changes when objects move in the image and thus the estimation of the entropy changes. The method was applied in rigid registration. Loeckx *et al.* [349] proposed to condition the evaluation of MI upon the position. More recently, Zhuang *et al.* used locally evaluated MI in combination with standard global MI [350]. Under their approach, the local evaluation of the probability distribution function assesses pixels relatively to their distance from the FFD control points.

An alternative way to introduce local context is by inserting spatial information. This has been mainly achieved by incorporating additional features that capture local geometric information, which results in higher order entropic measures.

Pluim *et al.* [351] used the intensity image gradient as an additional cue. The proposed algorithm sought not only to maximize NMI but also intensity gradient information. This was simply achieved by multiplying NMI with a measure that takes into consideration both the intensity gradient magnitude and its orientation. This measure encourages the alignment of strong intensity gradients.

Rueckert *et al.* [345] proposed to use second-order MI to encode local information by considering co-occurrences of intensities between neighboring voxels. That approach requires a $4D$-histogram to estimate the information measures. To account for the high dimension of the histogram and the curse of dimensionality, the number of bins was kept reasonably small.

Russakoff *et al.* [352] proposed Regional Mutual Information that pushed forward the previous idea by taking into account co-occurrences between regions. Moreover, an efficient way to deal with the curse of dimensionality was presented. Assuming a high-dimensional distribution, the data points were transformed so that they were independent in each dimension. Then, the entropy was estimated by summing the distributed $1D$ entropies. Bardera *et al.* [353] investigated NMI between blocks of image elements. The high-dimensional NMI was estimated using random lines and a reduced number of bins. Recently, a similar approach was presented by Yi and Soatto [354]. Their approach is based upon learning a dictionary of image patches. Each image patch is represented by the label of its closest dictionary element. Then, higher-order mutual information can be estimated by using this label representation while accounting for the euclidean transformation that maps the patch to the label.

Instead of explicitly taking into account neighboring voxels, another way to consider local information is by extracting features that concisely describe regional characteristics. Holden *et al.* [355] employed Gaussian scale space derivatives and incorporated them as an additional information channel in a higher dimensional MI criterion. Gan *et al.* also employed a multi-dimensional NMI criterion [356]. The authors proposed to construct a new feature field by considering the average rate of intensity change between any two points in the images. The proposed feature, named Maximum Distance-Gradient, is calculated for a set of special points placed in important gradient areas by finding for which point the average rate of intensity change is maximized. This feature contains information regarding

the local edge content, the maximum rate of intensity change as well as the direction in which this change happens. The magnitude of the MDG vector field formed the supplementary channel, while its orientation was used as a second element in the similarity function.

The approaches that employ a higher dimensional statistical criterion are troubled by the curse of dimensionality. There are not enough samples to accurately calculate higher dimensional statistical criteria. To be able to handle such calculations, most researchers resort to crude implementation approximations such as limiting the number of histogram bins. Nevertheless, ways to estimate high dimensional entropies have been proposed and used to perform image registration.

Sabuncu and Ramadge [357] introduced spatial information through the construction of feature vectors. The resulting high dimensional entropy was estimated with the use of the MST estimator. Neemuchwala *et al.* used entropic graphs to tackle high dimensional α-MI registration of ultrasound images [358]. Both approaches coped with global linear registration. Staring *et al.* tackled deformable registration of Cervical MRI using high-dimensional MI in [359]. Features were used to describe local geometric information and a k-nearest neighbor graph was used to estimate the multi-dimensional MI.

Spatial information is not the only type of information that can be used to endow registration with increased robustness and accuracy. Assuming that a prior step of segmentation has been performed, tissue classification information may also help disambiguate between voxels that belong to different tissues but share common appearance properties.

Studholme *et al.* [360] segmented regions by thresholding and labeling connected components. The labels were used as an additional image and the matching criterion took into account the difference between the entropies of each image and the joint entropy.

Knops *et al.* [361] performed a k-means clustering before registration. Based on this clustering, voxels that shared similar intensity profiles but belonged to different anatomical structures were mapped to different intensity bins during the construction of the histogram. The new remapped intensities along with the initial one contributed to an NMI-based similarity criterion.

D'Agostino *et al.* [362] took into account voxel class probabilities in the matching criterion in order to tackle the labeled-to-labeled and intensity-to-labeled image registration. For the labeled-to-labeled case, KLD was used to compare the distribution of the joint classes. For the intensity-to-labeled registration, a version of MI was used with the difference that one of the features is a class probability and not intensity.

b) Reduction to mono-modal registration: An alternative way to proceed with multi-modal registration is to reduce the problem to a mono-modal one. By this reduction, one aims to simplify the problem and facilitate its solution. There are two possible ways to perform such a task. First, one can simulate one modality from another so that at the end both images come from the same modality. Second, one can map both images to a third domain where the registration will take place.

Simulating one modality from another can be achieved by taking advantage of the available knowledge regarding the physical properties of the imaging device. In this case, the goal is to model the imaging process. An alternative way is to exploit available co-registered pairs of images. In this case, machine learning techniques can be used to capture the relation between the intensities.

Roche *et al.* [363] tackled ultrasound (US) to MR rigid registration by simulating an US image from the MR one. The authors exploited MR intensities and MR gradient magnitude information in order to predict US intensities. Complex phenomena such as US signal attenuation and speckle were neglected. As a consequence, the simulated images roughly resembled actual US images. Wein *et al.* [364] simulated an US image in order to tackle the problem of CT-to-US rigid/affine registration. In order to simulate the US image, the authors employed a model that was based on the physical principles of ultrasound. A locally evaluated statistical criterion was used to drive the registration.

Michel and Paragios [365] used the mixture of experts methods to learn the conditional probability of the target intensity given a source patch. The conditional probability was then used to drive a Markov Random Field to regularize the simulated image.

In the second case, both modalities are mapped to a common space. As both modalities image the same anatomical structure, the assumption can be made that the local geometry would be helpful to establish meaningful correspondences. Thus, in principle, most methods apply filters to extract geometrical information. This information is subsequently used in a mono-modal registration setting.

Maintz *et al.* [366] tackled rigid multi-modal registration by using morphological tools to create new gray-value intensity images. The proposed method applied morphological opening and closing to extract edge information and then cross-correlation to align the images. It resembles a surface registration with the difference that instead of having binary values, real ones were used.

Droske and Rumpf [26] proposed an approach that was motivated by the mathematical morphology theory that states that an image can be characterized uniquely by the entity of its level sets. The common space was defined by mapping every point to its normalized intensity gradient. The registration was formulated in a variational framework where a morphological, contrast invariant, matching criterion was minimized under the influence of an appropriate regularization term. Haber and Modersitzki [367] assumed that borders of anatomical structures correspond to intensity changes and thus opted to exploit intensity gradient information. An intermediate image domain was created by taking into account the normalized intensity gradient field. This field conveys purely geometric information and accounts for the fact that the gradient magnitude may vary among different modalities. The similarity function was based on the difference in angles between the normalized gradient vectors.

Butz and Thiran [368] investigated the use of edge related information to cope with affine multi-modal registration. They used an edgeness operator that takes into account the local edge variance to map both images to a common space. Mutual information driven registration was then performed coupled with a multi-scale genetic optimization. Depending on the nature of the images, other operators may be applied. Penney *et al.* used the probability of vessel presence along with normalized cross-correlation to rigidly register MRI with ultrasound images [369].

Gabor filtering has also been used to map the images to a common domain because of their ability to capture local edge and texture information [370]. Liu *et al.* used local frequency representations to tackle rigid/affine multi-modal registration [324]. These representations are robust to edge strength and contrast differences. They were estimated by calculating the local phase gradient of the most significant Gabor filter response. Then, the integral squared error was chosen as the matching criterion. Jian *et al.* used local frequency maps for deformable registration [371]. The authors used the Riesz transform to estimate the local frequency information. Ou *et al.* used Gabor filters in deformable image registration [323].

Specifically, the responses of the filters were used to construct a rich vector descriptor. The images were aligned by minimizing a weighted sum of the vector differences.

Andronache *et al.* tackled the problems related to the estimation of MI in small patches in [372]. Their strategy consisted of identifying the patches where the estimation of MI becomes unreliable and then mapping them to a common pseudo-modality. The pseudo-modality depicted only common structures in both images and was constructed by decreasing the variance of the mapped intensities. In the intermediate domain, simpler criteria may be used to drive registration.

Recently, Heinrich *et al.* [373] presented a new descriptor for multi-modal registration. The driving idea behind the new descriptor is the use of similarities between neighboring patches as features. This idea is borrowed from the image de-noising literature. Once the descriptor is constructed a vector-difference can be used as a matching criterion. Wachinger *et al.* [374] proposed two techniques that derive from information theory and manifold learning to create the intermediate structural representation. The first one used the entropy of a patch centered around the voxel to assign a new intensity value. The second method used Laplacian Eigenmaps to embed the patches in a lower-dimensional manifold that preserves local distances.

Lee *et al.* presented a supervised technique to learn the similarity measure for multi-modal image registration [375]. The approach was formulated in a discriminative setting where the goal is to optimize a similarity function so that correct correspondences are assigned high values and erroneous ones low. Support vector machine regression was employed to learn the metric.

Bronstein *et al.* presented a supervised technique whose aim was to learn a similarity metric that discerns between corresponding and non-corresponding points [376]. This technique maps both modalities to a Hamming metric space where true correspondences are likely to have the same code, while wrong ones are not. The embedding was constructed by using AdaBoost. Michel *et al.* investigated the application of the previous method to the problem of $3D$ deformable registration [377].

It should also be noted that some of the techniques that were previously presented under the *information theoretic* class of methods learn a similarity measure. The difference is that a generative framework is employed. Given co-registered data, the joint distribution of the intensities is learned. Then, either a maximum likelihood approach [378] or a divergence criterion [337]–[339], [343] is used to compare the estimated and learned distributions.

C. Hybrid Methods

Iconic and geometric registration methods each bear certain advantages while suffering from shortcomings. Hybrid methods try to capitalize on the advantages of each by using complementary information in an effort to get the best of both worlds. Among hybrid methods, the following subclasses may be distinguished based on the way the geometric information is exploited, that is (see also Fig. 2): i) as initialization, ii) as constraint, or iii) in a coupled fashion.

1) Additional information used independently—In the first subclass, each type of information is taken into account in a separate and sequential way. Registration is decomposed into two independent steps, each one acting on a different type of information. Typically, geometric registration precedes, resulting in a rough alignment of the two images. Subsequently, iconic registration is performed to refine the result.

a) Exploiting landmarks information: Johnson and Christensen initialized their consistent intensity algorithm with the result of a consistent landmark approach in [379]. The landmark and intensity registration were solved independently in an iterative way until a criterion on the number of iterations was met. Paquin *et al.* proposed a multiscale approach for hybrid image registration [380]. The authors identified bony structure landmarks and used them to coarsely align the images. In the finer levels, intensity-based deformable registration was performed. Yin *et al.* [381] inferred the optimal displacements of a cubic *B*-spline FFD model by alternately minimizing the sum of squared intensity differences and the distance between corresponding landmarks.

b) Exploiting surface information: Liu *et al.* [274] proposed a hybrid algorithm that combined surface and volume information to register cortical structures. The algorithm was initialized with the result of a volumetric approach [119] and was subsequently refined using a surface warping method. Postelnicu *et al.* [382] started from the geometric registration, propagated the result to the whole volume using a biophysical model of the brain and refined it with a non-linear optical flow registration algorithm. Gibson *et al.* [383] presented an approach where brain images are initially registered using an intensity-based method [67] and the result is refined by cortical surface registration [57]. Auzias *et al.* investigated the use of the diffeomorphic sulcal-based cortical registration (DISCO) [92] in collaboration with an intensity method (DARTEL [97]). The methods were used in a sequential manner.

c) Exploiting segmented structures information: Camara *et al.* [384] presented an approach where the result of the registration of segmented structures is refined by iconic registration.

2) Additional information used as constraint—Using one type of information independently of the other to initialize the following step usually results in an increase of the robustness of the registration procedure. However, there is no guarantee that the correspondences that were established during the previous step will be preserved. To overcome this limitation, a number of researchers have proposed to use the correspondences that were estimated during the first step to constrain the estimation of the correspondences during the following step. The spatial influence of these constraints varies from point-wise to global.

a) Additional information used as soft constraint: The Hellier and Barillot proposed to couple dense and landmark-based approaches for non-rigid brain registration in [272]. In a first step, sulci were extracted and modeled as active ribbons. Then, a matching point algorithm was used to establish geometric correspondences. These correspondences were subsequently used in a robust function as constraints with local spatial support. Hartkens *et al.* combined normalized mutual information with geometric cues to tackle brain registration in [385]. Two kinds of geometric cues were employed, landmarks and surfaces. The correspondences for the landmarks were fixed while the surface correspondences were estimated in an ICP fashion. The ratio between the iconic and geometric terms was calculated automatically based on their derivatives. Papademetris *et al.* [386] used sulcal constraints to constrain iconic registration. A robust point matching method was used to establish correspondences between the sulcal landmarks while accounting for outliers. The matching criterion comprised an intensity similarity term and a term ensuring that the estimated deformation field adhered to the point correspondences.

Rohr *et al.* [387] used the local correlation coefficient as intensity similarity criterion along with the adherence to point correspondences to register $2D$ electrophoresis images. Avants *et al.* [91] added a landmark inexact matching term in the LDDMM framework in order to

compare human and chimpanzee cortices. Landmarks were provided manually to establish either anatomical or functional correspondences between the two species.

Azar *et al.* proposed a user-guided registration method [388]. The proposed algorithm iterated between estimating the transformation W that maps one image to another and the estimation of two dense deformation fields. The landmark-based deformation field was initialized by using the user provided landmark correspondences and TPS interpolation. In subsequent iterations it was estimated by taking into account the landmark correspondences and the transformation W of the previous iteration. The intensity-based deformation field was estimated by minimizing an intensity based similarity criterion while taking into account the transformation W of the previous iteration. The transformation W was given as an adaptive combination of the intensity- and landmark-based deformation fields. Landmark information was weighted more in their vicinity of landmarks. This method was able to incorporate any intensity-based algorithm though it could not guarantee convergence.

Wörz and Rohr proposed a spline-based registration framework that uses both intensity and landmark information [389]. The authors proposed to estimate a dense deformation field by using a set of corresponding landmarks and their localization uncertainties. The solution of the registration problem was a compromise between matching the image data, being regular and being close to the landmark-based deformation field. Biesdorf *et al.* presented a similar approach in [390]. The difference was that a local measure of mutual information was used as an intensity criterion. Lu *et al.* [391] incorporated landmark information in the diffeomorphic Demons registration algorithm [99]. The authors proposed to include the sum of squared landmark Euclidean distances in the matching criterion along with point-wise mutual information [392].

b) Additional information used as hard constraint: While most methods establish geometric correspondences and then encourage the intensity driven deformation field to comply with them without guaranteeing their preservation, Joshi *et al.* [393] imposed geometric correspondences as hard constraints. First correspondences were established between the cortical gray/white matter and gray/CSF surfaces using sulcal constraints. The correspondences were then propagated to the whole cortical volume with the use of an harmonic map. Following that, the dense deformation field was refined by considering image intensity information under the hard constraint that the deformation is zero for the previously registered surfaces.

3) Coupled approaches—In the previous approaches, the information flows in one direction. By formulating the problems in a decoupled way, iconic registration may profit from geometric methods either by being initialized closer to the solution or by being driven by an extra force of adherence to correspondences. However, geometric registration does not benefit from iconic registration because its solution is independently obtained. In this class of methods, the two problems are unified and solved by minimizing a single objective function simultaneously. As a consequence, the solution of each problem takes advantage of the information coming from the other problem, and the final solution of the registration is consistent with both types of information.

Cachier *et al.* [271] proposed such a universal energy function for the problem of deformable registration. The coupling of the two problems was performed through the introduction of an auxiliary smooth deformation field. The authors proposed to extract sulci modeled as point distributions and use them in the coupled formulation to accomplish brain registration. The problem was solved by iterating between three steps: i) solving for the deformation that minimizes the iconic criterion, ii) solving the geometric problem by establishing correspondences between the closest points of the geometrical structures, iii)

and finally opting for a smooth deformation that respects both iconic and geometric constraints.

Joshi *et al.* [394] proposed an approach to couple surface-and intensity-based registration. An approach to tackle surface registration is to map both surfaces to a sphere and perform registration there. Joshi *et al.* proposed to additionally map the interior brain volumes to the interior of the spheres through harmonic maps. Then, correspondences can be established by involving the complete sphere domain, or both the surface and iconic information at the same time.

Sotiras *et al.* [148] presented a coupled approach that aims to simultaneously estimate the correspondences between two landmark sets, and a dense displacement field parametrized by cubic *B*-splines that maps one image space to another. The problem was formulated as a first-order Markov Random Field described by a two-layer undirected graph. The graph nodes represent the latent variables (displacement parameters and landmark correspondences), while the edges represent the relationships between the variables. The first layer of the graph modeled the iconic registration problem, while the second layer modeled the geometric correspondence problem. Inter-layer edges imposed the consistency between the two problems by approximating a coupling constraint.

Some of the limitations of this work were addressed in subsequent attempts. Honnorat *et al.* [395] used the exact L_2 distance to couple the geometric and iconic information for the problem of guide-wire tracking. The inner product was developed to allow its modeling by pairwise relations. Kurkure *et al.* [396] used learned higher-order potential for the layer of the graph that models the geometric problem. As a consequence, the requirement for a global linear registration was reduced.

Siless *et al.* [397] proposed a coupled approach based on the diffeomorphic Demons algorithm [99]. The authors proposed to define the update field as the addition of an intensity-based update field and a geometric-based update field. The intensity-based update field was calculated as in [99]. The geometric-based update field was estimated by minimizing the squared Euclidean distance between each point and its closest one. In a subsequent work, Siless *et al.* extended log-domain diffeomorphic demons [47] to take into account geometric information represented in the space of currents [398]. Cifor *et al.* [399] also extended [47] to take into account geometric information.

IV. Optimization Methods

The aim of optimization is to infer the optimal transformation (see Sec. II) that best aligns two images according to an objective function comprising a matching term (see Sec. III) and a regularization term (see Eq. 1). As a consequence, the choice of the optimization methods impacts the quality of the obtained result.

Optimization methods may be separated into two categories based on the nature of the variables that they try to infer (see Fig. 3): i) continuous, and ii) discrete. The first class of methods solves optimization problems where the variables assume real values. On the contrary, methods in the second class solve problem the variables take values from a discrete set. Both classes of methods are constrained with respect to the nature of the objective function as well as the structure to be optimized. Heuristic and metaheuristic methods do not bear the previous constraints. However, they do not enjoy theoretical guarantees regarding the optimality of the solution.

A. Continuous Optimization

Continuous optimization methods are constrained to problems where the variables take real values and the objective function is differentiable. Image registration is a problem where the application of continuous optimization methods has been studied. Continuous optimization methods estimate the optimal parameters following an update rule of the following form:

$$\theta_{t+1}=\theta_t+\alpha_t \mathbf{g}_t(\theta_t), \quad (9)$$

where $\boldsymbol{\theta}$ denotes the vector of parameters of the transformation, t indexes the number of iteration, α_t is the step size or gain factor, and $\mathbf{g}$ defines the search direction. The search direction is calculated by taking into account both the matching and the regularization term. Therefore, it should be written as $\mathbf{g}_t(\mathcal{M}(\boldsymbol{\theta}_t) + \mathcal{R}(\boldsymbol{\theta}_t))$. Nonetheless, we prefer the use of $\mathbf{g}_t(\boldsymbol{\theta}_t)$ in order to reduce the clutter of unnecessary notation.

There are various ways to define the previous parameters. For example, the step size may be constant, decrease with each iteration or such that it minimizes the objective function along the search direction (exact or inexact line search). The search direction can be specified by exploiting only first-order information or, for example, by also taking into consideration second-order information. It is the choice of these parameters that distinguishes different methods.

Commonly used methods include (see also Fig. 3): i) Gradient Descent (GD), ii) Conjugate Gradient (CG), iii) Powell's conjugate directions, iv) Quasi-Newton (QN), v) Levenberg-Marquardt (LM), and vi) Stochastic gradient descent. Klein *et al.* [400] reported a study comparing optimization strategies in image registration using mutual information as similarity metric and cubic *B*-spline FFDs as deformation model.

1) Gradient descent methods—An approach to optimize the objective function is by following the direction that decreases the energy, or its negative gradient. In other words, the direction is given as $\mathbf{g} = -\nabla_{\theta}(\boldsymbol{\theta})$. Klein *et al.* [400] studied two variants of gradient descent. The first employed a function of the step size that decayed with each iteration, while the second was based on the inexact line search algorithm of Moré and Thuente [401]. Other line strategies include keeping the step size fixed, monotone line search [402], line search and golden section search [403].

Gradient descent has been used to solve various registration problems. In the LDDMM framework, usually posed in a variational setting, gradient descent is often used to solve the problem [67], [72], [80]. Johnson and Christensen's consistent registration approach [379] as well as Rueckert *et al.*'s FFD registration algorithm [135] were also based on a gradient descent optimization scheme. Without trying to give a full account of all registration methods that employ gradient descent, let us also cite two more variational approaches [26], [307].

2) Conjugate gradient methods—Techniques that have better convergence rates than gradient descent have also been tested. Conjugate gradient descent methods try to exploit the knowledge conveyed by the previous gradients and propose a search direction that does not follow the new gradient but is conjugate to the previous direction. Thus, the direction now is given as $\mathbf{g}_t = f(\nabla_{\theta}(\boldsymbol{\theta}_t), \mathbf{g}_{t-1})$, where f usually denotes a linear combination, $\mathbf{g}_t = -\nabla_{\theta}(\boldsymbol{\theta}_t) + \beta_t \mathbf{g}_{t-1}$. Different ways to define the weighting factor β_t. Among the well-known formulas for β_t, one may cite the Fletcher-Reeves [404], the Polak-Ribière [405], the Polak-Ribière-Polyak [406] and the Hestenes-Stiefel [407]. For a review on CG methods, the interested reader is referred to the work of Hager and Zhang [408].

Some examples of registration methods that use conjugate gradient descent as an optimizer are [71], [82], [382], [393]. An interesting approach tailored for FFD image registration using a preconditioned gradient scheme was presented in [409]. Tustison *et al.* [409] observed that problematic energy topologies appear in the standard gradient schemes for FFD image registration. This is caused by the nature of the uniform *B*-splines that leads to disproportionate weighting of the control points. The authors proposed an approach to account for this fact by normalizing the gradient based on the spline basis functions.

3) Powell's conjugate directions method—Powell's optimization approach or the Direction Set method [403] is another method that has been used in image registration. Powell's method aims to minimize the objective function by following conjugate directions. Contrary to the CG methods, the conjugate directions are calculated without the use of gradient information. The basic procedure that Powell proposed sets the initial direction to the basis vectors $\mathbf{g}^i = \mathbf{e}^i$, $i = 1, \cdots, N$; optimizes along each parameter axis independently from the rest; performs the replacement $\mathbf{g}_t^i = \mathbf{g}_{t-1}^{i+1}$ while adding $\mathbf{g}_t^N = \theta_{t-1} - \theta_0$ and iterates until convergence.

Powell's method is gradient free and has been applied in low degrees of freedom registration tasks *e.g.*, [331], [336], [337], [351], [356]. A drawback of Powell's method is that it tends to find search directions that are linearly dependent [403]. As a consequence, the optimization fails even for moderate scale problems.

4) Quasi-Newton methods—Another class of optimization methods that has been tested in registration applications is that of Quasi-Newton (QN) methods [403]. This class of methods aims to accumulate information from the previous iterations and take advantage of it in order to achieve better convergence. More specifically, these methods aim to estimate the inverse Hessian matrix $H^{-1}(\boldsymbol{\theta})$ and use it to define the search direction. Thus, the search direction is defined as $\mathbf{g} = -\hat{H}^{-1}(\boldsymbol{\theta})\,\nabla_{\theta}(\boldsymbol{\theta})$, where the ^ denotes that an approximation is used (the true Hessian is used in the case of Newton's or the Newton-Raphson method). Two main algorithms exist in this category, the Davidon-Fletcher-Powell (DFP) and the Broyden-Fletcher-Goldfarb-Shanno (BFGS). BFGS is considered to be more efficient than DFP [410], [411].

A version of BFGS that uses less memory (L-BFGS) was tested in [400]. Other efforts where researchers have investigated the use of Quasi-Newton methods in image registration can be found in [100], [152], [303], [349].

5) Gauss-Newton method—An optimization method of the same family is the Gauss-Newton (GN) algorithm. It is devised to solve optimization problems involving sum of squared function values. This is of particular interest for image registration as this type of objective function is common when aligning images of the same modality. This algorithm does not require the computation of second derivatives. Instead, the Hessian is approximated by ignoring derivatives higher than first order with $\hat{H} = 2J^TJ$ where J denotes the Jacobian. The search direction is now given as $\mathbf{g} = -(J^T(\boldsymbol{\theta})J(\boldsymbol{\theta}))^{-1}\nabla_{\theta}(\boldsymbol{\theta})$.

The Gauss-Newton optimizer has been used in [79], [230], [240]. The Gauss-Newton algorithm is frequently used in the Demons registration framework to optimize the similarity measure when tackling mono-modal registration [41], [44], [56], [57], [99]. In the demons registration setting, an extension of Gauss-Newton by Malis [43] was employed to derive the symmetric demons forces [47], [50]. This algorithm exploits more knowledge with respect to the problem at hand. More specifically, it takes advantage of the fact that when the images are aligned, the gradient of the source can be approximated by the gradient of the target. Recently, Zikic *et al.* [412] proposed a preconditioning scheme that improves the

convergence speed of registration algorithms. The scheme is based on normalizing the length of the point force vectors.

6) Levenberg-Marquardt algorithm—A method related to the previous one that has been applied to the problem of image registration is the Levenberg-Marquardt algorithm. The search direction in this case is given by: $\mathbf{g} = -(\hat{H}^{-1}(\boldsymbol{\theta}) + \zeta\mathbf{I})\,\nabla_{\boldsymbol{\theta}}(\boldsymbol{\theta})$. $\mathbf{I}$ is the identity matrix and ζ is a weighting factor that regulates the performance of the optimizer with respect to its speed and stability. By decreasing its value, greater speed may be achieved. At the limit, when ζ equals to zero, we fall to the previous algorithm. On the contrary, when its value increases, the stability increases as well.

For some applications of the LM approach the interested reader is referred to [97], [136], [155], [156]. Based on the LM algorithm, Thevanez and Unser [413] proposed an efficient optimizer for mutual information driven registration. Kybic and Unser [136] compared the LM algorithm with GD, GD with a quadratic step size estimation and CG to find that it performs the best for an FFD registration task.

7) Stochastic gradient descent methods—The aforementioned techniques cover the deterministic gradient methods that are used most often to solve the optimization problems that arise when tackling image registration. In medical image registration, the computation of the derivative information can be computationally demanding because of the great dimensionality of both the data and the search space. Thus, to alleviate the computational burden, researchers have investigated the use of stochastic gradient approaches. Their update rule is based on an approximation of the gradient, or $\boldsymbol{\theta}_{t+1} = \boldsymbol{\theta}_t + \alpha_t \hat{\mathbf{g}}_t(\boldsymbol{\theta}_t)$.

The variants of the stochastic gradient approach differ with respect to how the gradient is approximated. In [400], three approaches were discussed. The first one, referred to as Kiefer-Wolfowitz (KW), approximates the gradient by a finite difference scheme. The second one, known as Simultaneous Perturbation (SP), estimates the gradient by perturbing it not along the basis axis but instead along a random perturbation vector $\boldsymbol{\Delta}$ whose elements are independent and symmetrically Bernoulli distributed. The last method was proposed by Robbins and Monro (RM). It is more general, in the sense that it only assumes that an approximation of the gradient exists. This method uses a step-size that decreases with time in order to decrease the inaccuracy. [400] estimated the gradient by using a subset of the image voxels sampled uniformly. The conclusion of [400] is that the RM method performs best.

The RM method was extended in two subsequent works by employing adaptive image-driven strategies. Klein *et al.* [414] presented an adaptive step mechanism, while Bhagalia *et al.* [415] proposed an edge-driven importance sampling to improve the gradient approximation. Stochastic gradient descent schemes have been applied in image registration settings that employ lower degrees of freedom deformation models (*e.g.*, global linear or cubic *B*-spline FFDs). For some applications of stochastic gradient see [147], [328], [329], [359].

8) Constrained optimization methods—All the previous approaches aim to solve an unconstrained optimization problem. As discussed in Sec. II-D, constrained optimization problems arise when trying to impose task-specific conditions on the deformation field. The solution of such optimization problems is more challenging. The optimization strategies that are usually employed transform the constrained to an unconstrained one that can be solved efficiently. For example, a log-barrier method was used in [230]. Another way to solve the problem is by augmenting the dimensionality of the problem using the method of Lagrange multipliers [235], [237].

B. Discrete Optimization

Discrete optimization methods are constrained to problems where the variables take discrete values. Recently, discrete Markov Random Field (MRF) formulations have been investigated to tackle image registration.

An MRF is a probabilistic graphical model represented by an undirected graph $\mathcal{G}$, consisting of set of vertices $\mathcal{V}$ and a set of edges $\mathcal{E}$($\mathcal{G}$ = { $\mathcal{V}$, $\mathcal{E}$}). The set of nodes encodes the random variables, while the set of edges represents the relationships between the variables. The random variables take values in a discrete label set $\mathcal{L}$. The corresponding energy is the sum of all unary potentials $\mathcal{U}_p$ of the nodes $p \in \mathcal{V}$ (*i.e.*, data cost) along with the pairwise potentials $\mathcal{P}_{pq}$ (*i.e.*, regularization cost) modeled by the edges connecting nodes p and q (*i.e*, $pq \in \mathcal{E}$). Minimizing the previous energy results in an assigning to each random variable p an optimal label $l_p^\star$.

Discrete optimization methods can be classified according to the techniques they employ into three categories (see also Fig. 3): i) graph-based methods, ii) message passing methods, and iii) Linear-Programming (LP) approaches.

1) Graph-based methods—The first class of methods is based on the max-flow min-cut principle [416] that states that the maximum amount of flow that can pass from the source to the sink is equal to the minimum cut that separates the two terminal nodes. The two terminal nodes are defined as source and sink depending on the direction of their edges. The cost of a cut is given by the sum of the weights of the edges that were removed.

Greig *et al.* [417] showed how to calculate the exact maximum a posteriori estimation for the case of the Ising model through a single graph cut computation. Boykov *et al.* [418] proposed the α-expansion algorithm that extended [417] to the multi-label case. This algorithm starts from an initial labeling and then checks every label to see if the energy may be decreased by allowing any set of nodes to change their label to the one under study. The optimal labeling at each iteration is estimated by performing a single graph cut.

In medical image registration, α-expansion is the optimizer used by Tang and Chung [419], So *et al.* [420]–[422] and Liao and Chung [326]. The authors constructed a graph the size of the image assuming a 6-connectivity scheme and densely sampled the solution space resulting in a large set of candidate solutions. The size of the graph as well as the large label set resulted in important computational times.

2) Belief propagation methods—Belief Propagation (BP) methods [423] constitute the second class of methods. These methods are based on local message exchange between the nodes of the graph and then backtracking to recover the best solution to the problem. Belief propagation methods can provide an exact inference for chain and tree-structured graphs. In the case of graphs that contain loops, Loopy Belief propagation methods have been shown to converge to satisfactory solutions [424], [425].

A drawback related to the messages is the large storage requirement when a large set of solutions is involved. Yang *et al.* [426] proposed a constant space $O(1)$ BP method that does not depend on the number of labels. The basic idea of the method was to a apply a coarse-to-fine strategy to the solution space so that the overall complexity remains constant. The numbers of labels decreased from coarser to finer levels by keeping only the ones for whose the cost was the smallest. Heinrich *et al.* [427] applied this technique in a discrete registration setting to recover respiratory motion.

Shekhovtsov *et al.* [428] proposed an efficient MRF deformation model for non-rigid $2D$ image matching by decomposing the original grid graph into two isomorphic layers. The nodes of each layer modeled the displacement along each axis. Nodes placed at corresponding positions in each layer were connected with an edge that modeled the data matching term. Intra-layer edges encoded the regularization term. This decomposition reduced the number of operations required to update the messages. Lee *et al.* extended this model to the $3D$ case [429]. The graph was decomposed into three layers and ternary interactions were used to model the data cost.

Liu *et al.* [430] used the $2D$ decomposed model [428] along with loopy BP to match SIFT-descriptors along the flow vectors. Kwon *et al.* proposed a similar approach that matches dense local descriptors using a higher-order smoothness prior [431].

3) Linear-Programming approaches—The last class of methods comprises techniques that are based on Linear Programming. These approaches aim to solve an LP relaxation of the original problem that is in general *NP*-hard. Komodakis *et al.* [432], [433] cast the original problem as a linear integer program and proposed a method (FastPD) that takes into account the primal and dual LP relaxations.

Glocker *et al.* [434], [435] used FastPD to infer the displacements of a grid-based deformation model in image registration. Hard constraints on the set of solutions, imposed through the construction of the label set, enforced the diffeomorphic property on the deformation field despite the use of a simple first-order regularization term. Glocker *et al.* extended this method to tackle atlas-based registration in [436], and to knowledge-based registration with the use of learned pairwise relations in [177]. Ou *et al.* [323] used it to solve feature-based registration, while Sotiras *et al.* to solve diffusion tensor registration [437] and symmetric iconic registration [145].

Sotiras *et al.* used this optimizer to tackle group-wise registration [438], [439]. Savinaud *et al.* extended this method to multi-channel images [440]. These methods modeled the registration problem with the use of an n-layer graph where intra-layer edges encoded a smoothing term and inter-layer edges encoded the data matching term. Zikic *et al.* [441] tackled linear registration by using FastPD to perform inference in a graph where each node encoded a different parameter of the transformation, while the edges relating them modeled their interactions.

TRW-S or sequential tree-reweighted message passing is also based on an LP relaxation. The algorithm aims to solve the dual of the relaxation that provides a lower bound of the optimal MRF energy. The goal is to maximize the lower bound that is given by a convex combination of trees.

Shekhovtsov *et al.* [428] used it to optimize their efficient decomposed MRF deformation model. Kwon *et al.* [442] used TRW-S to perform inference in a factor graph that models higher-order spatial smoothness constraints for image registration. Sotiras *et al.* used it to perform hybrid registration [148]. Lee *et al.* [443] used TRW-S to solve the optical flow estimation problem based on an adaptive convolution kernel prior.

C. Miscellaneous

The continuous and discrete methods are limited regarding what objective functions and structures they can optimize. Heuristic and metaheuristic methods, on the contrary, can handle a wide range of problems and explore large solution spaces. Nevertheless, they are not able to provide any guarantee with respect to the optimality of the solution.

1) Greedy approaches—Making at each step the locally optimal choice is an approach that has been used in image registration. This greedy strategy requires the definition of a set of plausible solutions and a score function. Being gradient free and intuitive, it was applied to tackle the problem of feature-driven image registration. The candidate sets were constructed in a multi-resolution fashion while a standard similarity measure was used. More information about the practical implementation of this strategy can be found in [119], [274], [320]–[322].

2) Evolutionary algorithms—Evolutionary algorithms have been used in medical image registration to mainly tackle linear registration [444]. These algorithms derive from the theory of evolution and natural selection. They start from an initial set of solutions that are ranked according to a fitness measure and a subset of them is chosen in a stochastic fashion to generate a new set of solutions. The new set of solutions is generated by adapting the current set following a nature-motivated strategy such as mutation. In [400], the covariance matrix adaptation method was investigated [445] and found to converge slowly. For a more elaborated presentation and comparison of state-of-the-art evolutionary methods for image registration the interested reader is referred to the work of Santamaria *et al.* [444].

V. Discussion

Deformable registration is a mature field that has been extensively studied. As a consequence, an important body of research work has been devoted to its improvement and application in clinical settings. In this review, we have made an effort to provide a comprehensive survey of the recent developments in the field of deformable medical image registration. Our approach was structured around the three core registration components, i) deformation models, ii) matching criteria, and iii) optimization methods. For every component, particular emphasis was placed on classifying the methods appertaining to it according to their theoretical foundations. We focused our presentation on giving an account of recent approaches that have not be be covered in previous reviews. Let us now summarize the contents of this paper.

In Sec. II we have presented the transformation models for deformable image registration. We discussed physics-based models (see Sec. II-A) which provide transformations that comply with a physical model. The transformation is estimated through the solution of a PDE that can be computationally demanding. Interpolation-based methods were presented in Sec. II-B). These models do not assume, in general, that the deformed object behaves according to a natural law. Instead, they exploit interpolation and approximation theory to construct the deformation field. In Sec. II-C we discussed knowledge-based approaches that exploit our knowledge regarding the problem through the use of more informed priors at the cost of being constrained to well-defined settings. We concluded this section by presenting constraints (see Sec. II-D) that have been devised to enforce certain properties on the resulting transformation.

In Sec. III we have classified similarity criteria based on the type of information they exploit. We have presented intensity-based matching criteria in Sec. III-B according to whether they tackle mono-modal or multi-modal registration problems. In the mono-modal case, the use of standard similarity criteria (*e.g.*, SSD or SAD) involving either intensities or multi-channel data extracted from the image through the application of filters is well-accepted by the community. In the multimodal case, the use of information theoretic measures has become the prevalent solution. In Sec. III-A, we presented registration approaches that exploit geometric information. The presentation was organized according to the unknown variables the methods estimate. We concluded the section by presenting

coupled approaches that opt to bridge the gap between the iconic and the geometric methods (see Sec. III-C).

The third component of registration, optimization, is discussed in Sec. IV. Registration is an inherently continuous problem. As a consequence, continuous optimization methods have been the main driving force behind registration algorithms. These methods are presented in Sec. IV-A. Recently, discrete optimization techniques have been proposed to tackle deformable registration. We discuss these approaches in Sec. IV-B. Heuristic and metaheuristic approaches are briefly introduced in Sec. IV-C.

Image registration is a particularly active field of research. New methods, spanning all aspects of registration, are devised that tackle the shortcomings of the existing ones resulting in a fluid research domain. In this review, we opted to map the research field by reporting the recent advances related to the methodological aspects of registration.

An important topic that was not covered is the evaluation of registration methods. Evaluation of registration methods is a particularly difficult problem because of the lack of a "ground truth". The absence of knowledge of correspondences between images makes the quantitative validation of the registration performance a challenging task. Moreover, because of the different requirements of the applications that are based on deformable registration, the notion of correspondence should vary according to application context, aiming to properly characterize error [446].

Nonetheless, the increasing availability of annotated data sets (*e.g.*, the LONI Probabilistic Brain Atlas [447], the Internet Brain Segmentation Repository - IBSR [448], the CUMC12 dataset[2] acquired at the Columbia University Medical Center, the MGH10 dataset[2] scanned at the MGH/MIT/HMS Athinoula A. Martinos Center for Biomedical Imaging) has made possible evaluation studies like the one by Klein *et al.* [449]. Moreover, the development of evaluation projects for image registration (*i.e.*, Non-rigid Image Registration Evaluation Project - NIREP [450]) and the increasing understanding regarding the use of surrogate measures for the measurement of the accuracy of registration [451] will further facilitate the comparison between different algorithms.

Landmark correspondences can also be used for the evaluation of registration accuracy. Manual identification and matching of landmarks across scans is a tedious task. As a consequence few datasets are available providing such reference standards. One may cite the POPI model [452] containing 40 landmarks in every frame of a $4D$ lung CT acquisition, or the $4D$ CT dataset made available by Castillo *et al.* [453] with landmarks in the maximum inhale and exhale phase. The development of dedicated methods for reference standard construction [454] and the organization of registration challenges [455] create the necessary conditions for objective comparison of registration methods.

The increased availability of data along with the publication of the source code of the methods will lead to evaluation studies that will allow us to quantify the performance of the registration components and draw conclusions regarding their applicability in specific registration settings.

Acknowledgments

The authors would like to thank the anonymous reviewers for their helpful and constructive comments that greatly improved the paper.

References

1. Brown LG. A survey of image registration techniques. ACM Computing Surveys. 1992; 24(4):325–376.
2. Maintz JA, Viergever MA. A survey of medical image registration. Medical Image Analysis. 1998; 2(1):1–36. [PubMed: 10638851]
3. Hajnal, JV.; Hill, DL.; Hawkes, DJ., editors. Medical image registration. Boca Raton, FL: CRC Press; 2001.
4. Zitova B, Flusser J. Image registration methods: a survey. Image and Vision Computing. 2003; 21(11):977–1000.
5. Modersitzki, J. Numerical methods for image registration. New York: Oxford University Press; 2004.
6. Goshtasby, A. 2-D and 3-D image registration for medical, remote sensing, and industrial applications. Hoboken, NJ: John Wiley & Sons, Inc; 2005.
7. Szeliski R. Image alignment and stitching: A tutorial. Foundations and Trends® in Computer Graphics and Vision. 2006; 2(1):1–104.
8. Fischer B, Modersitzki J. Ill-posed medicine–an introduction to image registration. Inverse Problems. 2008; 24(3):034008.
9. Modersitzki, J. FAIR: Flexible algorithms for image registration. Philadelphia: SIAM; 2009.
10. Goshtasby, AA. Image registration: Principles, tools and methods. Springer; 2012.
11. Hadamard, J. Lectures on the Cauchy's Problem in Linear Partial Differential Equations. New Haven, CT: Yale University Press; 1923.
12. Fleet, D.; Weiss, Y. Handbook of Mathematical Models in Computer Vision. Springer Verlag; 2006. Optical flow estimation; p. 237-257.
13. Baker S, Scharstein D, Lewis JP, Roth S, Black MJ, Szeliski R. A Database and Evaluation Methodology for Optical Flow. International Journal of Computer Vision. 2010; 92(1):1–31.
14. Holden M. A review of geometric transformations for nonrigid body registration. IEEE Transactions on Medical Imaging. 2008; 27(1):111–128. [PubMed: 18270067]
15. Broit, C. PhD dissertation. University of Pennsylvania; 1981. Optimal registration of deformed images.
16. Bajcsy R, Kovačič S. Multiresolution elastic matching. Computer Vision, Graphics, and Image Processing. 1989; 46(1):1–21.
17. Gee JC, Bajcsy R. Elastic matching: Continuum mechanical and probabilistic analysis. Brain Warping. 1999:183–197.
18. Davatzikos C. Spatial transformation and registration of brain images using elastically deformable models. Computer Vision and Image Understanding. 1997; 66(2):207–222. [PubMed: 11543561]
19. Christensen GE, Johnson HJ. Consistent image registration. IEEE Transactions on Medical Imaging. 2001; 20(7):568–582. [PubMed: 11465464]
20. Leow A, Huang S-C, Geng A, Becker J, Davis S, Toga A, Thompson P. Inverse consistent mapping in 3D deformable image registration: its construction and statistical properties. International Conference on Information Processing in Medical Imaging. 2005:493–503.
21. He J, Christensen GE. Large deformation inverse consistent elastic image registration. International Conference on Information Processing in Medical Imaging. 2003:438–449.
22. Rabbitt RD, Weiss JA, Christensen GE, Miller MI. Mapping of hyperelastic deformable templates using the finite element method. Proceedings SPIE Vision Geometry. 1995:252–265.
23. Pennec X, Stefanescu R, Arsigny V, Fillard P, Ayache N. Riemannian elasticity: A statistical regularization framework for nonlinear registration. International Conference on Medical Image Computing and Computer-Assisted Intervention. 2005:943–950.
24. Yanovsky I, Le Guyader C, Leow A, Toga AW, Thompson PM, Vese L, et al. Unbiased volumetric registration via nonlinear elastic regularization. Workshop on Mathematical Foundations of Computational Anatomy: Medical Image Computing and Computer-Assisted Intervention. 2008

25. Leow AD, Yanovsky I, Chiang MC, Lee AD, Klunder AD, Lu A, Becker JT, Davis SW, Toga AW, Thompson PM. Statistical properties of Jacobian maps and the realization of unbiased large-deformation nonlinear image registration. IEEE Transactions on Medical Imaging. 2007; 26(6): 822–832. [PubMed: 17679333]
26. Droske M, Rumpf M. A variational approach to nonrigid morphological image registration. SIAM Journal on Applied Mathematics. 2004; 64(2):668–687.
27. Le Guyader C, Vese LA. A combined segmentation and registration framework with a nonlinear elasticity smoother. Computer Vision and Image Understanding. 2011; 115(12):1689–1709.
28. Ciarlet PG, Geymonat G. Sur les lois de comportement en élasticité non linéaire compressible. C R Acad Sci Paris Sér II. 1982; 295:423–426.
29. Burger M, Modersitzki J, Ruthotto L. A hyperelastic regularization energy for image registration. SIAM Journal on Scientific Computing. 2013; 35(1):B132–B148.
30. Christensen GE, Rabbitt RD, Miller MI. Deformable templates using large deformation kinematics. IEEE Transactions on Image Processing. 1996; 5(10):1435–1447. [PubMed: 18290061]
31. Christensen GE, Joshi SC, Miller MI. Volumetric transformation of brain anatomy. IEEE Transactions on Medical Imaging. 1997; 16(6):864–877. [PubMed: 9533586]
32. Bro-Nielsen M, Gramkow C. Fast fluid registration of medical images. Visualization in Biomedical Computing. 1996:265–276.
33. Crum WR, Tanner C, Hawkes DJ. Anisotropic multi-scale fluid registration: evaluation in magnetic resonance breast imaging. Physics in Medicine and Biology. 2005; 50(21):5153–5174. [PubMed: 16237247]
34. Cahill ND, Noble JA, Hawkes DJ. Fourier methods for nonparametric image registration. International Conference on Computer Vision and Pattern Recognition. 2007:1–8.
35. Wang Y, Staib LH. Physical model-based non-rigid registration incorporating statistical shape information. Medical Image Analysis. 2000; 4(1):7–20. [PubMed: 10972317]
36. D'Agostino E, Maes F, Vandermeulen D, Suetens P. A viscous fluid model for multimodal non-rigid image registration using mutual information. Medical Image Analysis. 2003; 7(4):565–575. [PubMed: 14561559]
37. Chiang MC, Leow AD, Klunder AD, Dutton RA, Barysheva M, Rose SE, McMahon KL, De Zubicaray GI, Toga AW, Thompson PM. Fluid registration of diffusion tensor images using information theory. IEEE Transactions on Medical Imaging. 2008; 27(4):442–456. [PubMed: 18390342]
38. Thirion JP. Image matching as a diffusion process: an analogy with Maxwell's demons. Medical Image Analysis. 1998; 2(3):243–260. [PubMed: 9873902]
39. Fischer B, Modersitzki J. Fast diffusion registration. AMS Contemporary Mathematics, Inverse Problems, Image Analysis, and Medical Imaging. 2002; 313:117–127.
40. Pennec X, Cachier P, Ayache N. Understanding the "Demon's algorithm": 3D non-rigid registration by gradient descent. International Conference on Medical Image Computing and Computer-Assisted Intervention. 1999:597–606.
41. Vercauteren T, Pennec X, Malis E, Perchant A, Ayache N. Insight into efficient image registration techniques and the Demons algorithm. International Conference on Information Processing in Medical Imaging. 2007:495–506.
42. Cachier P, Bardinet E, Dormont D, Pennec X, Ayache N. Iconic feature based nonrigid registration: the PASHA algorithm. Computer Vision and Image Understanding. 2003; 89(2–3): 272–298.
43. Malis E. Improving vision-based control using efficient second-order minimization techniques. International Conference on Robotics and Automation. 2004:1843–1848.
44. Vercauteren T, Pennec X, Perchant A, Ayache N. Non-parametric diffeomorphic image registration with the demons algorithm. International Conference on Medical Image Computing and Computer-Assisted Intervention. 2007:319–326.
45. Higham NJ. The scaling and squaring method for the matrix exponential revisited. SIAM Journal on Matrix Analysis and Applications. 2005; 26(4):1179–1193.

46. Moler C, Van Loan C. Nineteen dubious ways to compute the exponential of a matrix, twenty-five years later. SIAM Review. 2003; 45(1):3–49.
47. Vercauteren T, Pennec X, Perchant A, Ayache N. Symmetric log-domain diffeomorphic registration: A demons-based approach. International Conference on Medical Image Computing and Computer-Assisted Intervention. 2008:754–761.
48. Cahill ND, Noble JA, Hawkes DJ. Demons algorithms for fluid and curvature registration. International Symposium on Biomedical Imaging. 2009:730–733.
49. Cahill ND, Noble JA, Hawkes DJ. A Demons algorithm for image registration with locally adaptive regularization. International Conference on Medical Image Computing and Computer-Assisted Intervention. 2009:574–581.
50. Mansi T, Pennec X, Sermesant M, Delingette H, Ayache N. ilogdemons: A demons-based registration algorithm for tracking incompressible elastic biological tissues. International Journal of Computer Vision. 2011; 92(1):92–111.
51. Stefanescu R, Pennec X, Ayache N. Grid powered nonlinear image registration with locally adaptive regularization. Medical Image Analysis. 2004; 8(3):325–342. [PubMed: 15450226]
52. Guimond A, Roche A, Ayache N, Meunier J. Three-dimensional multimodal brain warping using the demons algorithm and adaptive intensity corrections. IEEE Transactions on Medical Imaging. 2001; 20(1):58–69. [PubMed: 11293692]
53. Tristán-Vega A, Vegas-Sánchez-Ferrero G, Santiago A-F. Local similarity measures for demons-like registration algorithms. International Symposium on Biomedical Imaging. 2008:1087–1090.
54. Modat M, Vercauteren T, Ridgway GR, Hawkes DJ, Fox NC, Ourselin S. Diffeomorphic Demons using normalized mutual information, evaluation on multimodal brain MR images. Proceedings SPIE Medical Imaging: Image Processing. 2010:76, 232K–1–76, 232K–8.
55. Peyrat J-M, Delingette H, Sermesant M, Pennec X, Xu C, Ayache N. Registration of 4D time-series of cardiac images with multichannel diffeomorphic Demons. International Conference on Medical Image Computing and Computer-Assisted Intervention. 2008:972–979.
56. Yeo BTT, Vercauteren T, Fillard P, Peyrat JM, Pennec X, Golland P, Ayache N, Clatz O. DT-REFinD: Diffusion tensor registration with exact finite-strain differential. IEEE Transactions on Medical Imaging. 2009; 28(12):1914–1928. [PubMed: 19556193]
57. Yeo BTT, Sabuncu MR, Vercauteren T, Ayache N, Fischl B, Golland P. Spherical Demons: fast diffeomorphic landmark-free surface registration. IEEE Transactions on Medical Imaging. 2010; 29(3):650–668. [PubMed: 19709963]
58. Fischer B, Modersitzki J. Curvature based image registration. Journal of Mathematical Imaging and Vision. 2003; 18(1):81–85.
59. Fischer B, Modersitzki J. A unified approach to fast image registration and a new curvature based registration technique. Linear Algebra and its Applications. 2004; 380:107–124.
60. Henn S. A full curvature based algorithm for image registration. Journal of Mathematical Imaging and Vision. 2006; 24(2):195–208.
61. Glocker B, Komodakis N, Paragios N, Navab N. Approximated curvature penalty in non-rigid registration using pairwise mrfs. Advances in Visual Computing. 2009:1101–1109.
62. Beuthien B, Kamen A, Fischer B. Recursive greens function registration. International Conference on Medical Image Computing and Computer-Assisted Intervention. 2010:546–553.
63. Dupuis P, Grenander U, Miller MI. Variational problems on flows of diffeomorphisms for image matching. Quarterly of Applied Mathematics. 1998; 56(3):587–600.
64. Trouvé A. Diffeomorphisms groups and pattern matching in image analysis. International Journal of Computer Vision. 1998; 28(3):213–221.
65. Risser L, Vialard F, Wolz R, Murgasova M, Holm DD, Rueckert D. Simultaneous multi-scale registration using large deformation diffeomorphic metric mapping. IEEE Transactions on Medical Imaging. 2011; 30(10):1746–1759. [PubMed: 21521665]
66. Sommer S, Nielsen M, Lauze F, Pennec X. A multi-scale kernel bundle for lddmm: towards sparse deformation description across space and scales. International Conference on Information Processing in Medical Imaging. 2011:624–635.

67. Beg MF, Miller MI, Trouvé A, Younes L. Computing large deformation metric mappings via geodesic flows of diffeomorphisms. International Journal of Computer Vision. 2005; 61(2):139–157.
68. Joshi SC, Miller MI. Landmark matching via large deformation diffeomorphisms. IEEE Transactions on Image Processing. 2000; 9(8):1357–1370. [PubMed: 18262973]
69. Marsland S, Twining CJ. Constructing diffeomorphic representations for the groupwise analysis of nonrigid registrations of medical images. IEEE Transactions on Medical Imaging. 2004; 23(8): 1006–1020. [PubMed: 15338734]
70. Miller MI, Trouvé A, Younes L. On the metrics and Euler-Lagrange equations of computational anatomy. Annual Review of Biomedical Engineering. 2002; 4(1):375–405.
71. Miller MI, Younes L. Group actions, homeomorphisms, and matching: A general framework. International Journal of Computer Vision. 2001; 41(1–2):61–84.
72. Vaillant M, Miller MI, Younes L, Trouvé A, et al. Statistics on diffeomorphisms via tangent space representations. NeuroImage. 2004; 23(Supplement 1):S161–S169. [PubMed: 15501085]
73. Trouvé A, Younes L. Metamorphoses through lie group action. Foundations of Computational Mathematics. 2005; 5(2):173–198.
74. Miller MI, Trouvé A, Younes L. Geodesic shooting for computational anatomy. Journal of Mathematical Imaging and Vision. 2006; 24(2):209–228. [PubMed: 20613972]
75. Younes L, Qiu A, Winslow RL, Miller MI. Transport of relational structures in groups of diffeomorphisms. Journal of Mathematical Imaging and Vision. 2008; 32(1):41–56. [PubMed: 19809583]
76. Younes L, Arrate F, Miller MI. Evolutions equations in computational anatomy. NeuroImage. 2009; 45(1, Supplement 1):S40–S50. [PubMed: 19059343]
77. Beg MF, Khan A. Symmetric data attachment terms for large deformation image registration. IEEE Transactions on Medical Imaging. 2007; 26(9):1179–1189. [PubMed: 17896591]
78. Avants BB, Epstein CL, Grossman M, Gee JC. Symmetric diffeomorphic image registration with cross-correlation: Evaluating automated labeling of elderly and neurodegenerative brain. Medical Image Analysis. 2008; 12(1):26–41. [PubMed: 17659998]
79. Ashburner J, Friston KJ. Diffeomorphic registration using geodesic shooting and gauss–newton optimisation. NeuroImage. 2011; 55(3):954–967. [PubMed: 21216294]
80. Cao Y, Miller MI, Winslow RL, Younes L. Large deformation diffeomorphic metric mapping of vector fields. IEEE Transactions on Medical Imaging. 2005; 24(9):1216–1230. [PubMed: 16156359]
81. Cao Y, Miller MI, Mori S, Winslow RL, Younes L. Diffeomorphic matching of diffusion tensor images. Computer Vision and Pattern Recognition Workshop. 2006:67.
82. Glaunès J, Vaillant M, Miller MI. Landmark matching via large deformation diffeomorphisms on the sphere. Journal of Mathematical Imaging and Vision. 2004; 20(1–2):179–200.
83. Leow A, Thompson R, Protas H, Huang S-C. Brain warping with implicit representations. International Symposium on Biomedical Imaging. 2004:603–606.
84. Glaunès J, Trouvé A, Younes L. Diffeomorphic matching of distributions: A new approach for unlabelled point-sets and sub-manifolds matching. International Conference on Computer Vision and Pattern Recognition. 2004:712–718.
85. Leow A, Yu CL, Lee SJ, Huang SC, Protas H, Nicolson R, Hayashi KM, Toga AW, Thompson PM. Brain structural mapping using a novel hybrid implicit/explicit framework based on the level-set method. NeuroImage. 2005; 24(3):910–927. [PubMed: 15652325]
86. Vaillant M, Glaunès J. Surface matching via currents. International Conference on Information Processing in Medical Imaging. 2005:381–392.
87. Qiu A, Younes L, Wang L, Ratnanather JT, Gillepsie SK, Kaplan G, Csernansky J, Miller MI. Combining anatomical manifold information via diffeomorphic metric mappings for studying cortical thinning of the cingulate gyrus in schizophrenia. NeuroImage. 2007; 37(3):821–833. [PubMed: 17613251]
88. Glaunès J, Qiu A, Miller MI, Younes L. Large deformation diffeomorphic metric curve mapping. International Journal of Computer Vision. 2008; 80(3):317–336. [PubMed: 20419045]

89. Durrleman S, Pennec X, Trouvé A, Thompson P, Ayache N. Inferring brain variability from diffeomorphic deformations of currents: an integrative approach. Medical Image Analysis. 2008; 12(5):626–637. [PubMed: 18658005]

90. Durrleman S, Pennec X, Trouvé A, Ayache N. Statistical models of sets of curves and surfaces based on currents. Medical Image Analysis. 2009; 13(5):793–808. [PubMed: 19679507]

91. Avants BB, Schoenemann PT, Gee JC. Lagrangian frame diffeomorphic image registration: Morphometric comparison of human and chimpanzee cortex. Medical Image Analysis. 2006; 10(3):397–412. [PubMed: 15948659]

92. Auzias G, Colliot O, Glaunès JA, Perrot M, Mangin JF, Trouvé A, Baillet S. Diffeomorphic brain registration under exhaustive sulcal constraints. IEEE Transactions on Medical Imaging. 2011; 30(6):1214–1227. [PubMed: 21278014]

93. Younes L. Jacobi fields in groups of diffeomorphisms and applications. Quarterly of Applied Mathematics. 2007; 65(1):113–134.

94. Marsland S, McLachlan R. A Hamiltonian particle method for diffeomorphic image registration. International Conference on Information Processing in Medical Imaging. 2007:396–407.

95. Cotter CJ, Holm DD. Singular solutions, momentum maps and computational anatomy. Arxiv preprint nlin/0605020. 2006

96. Arsigny V, Commowick O, Pennec X, Ayache N. A log-Euclidean framework for statistics on diffeomorphisms. International Conference on Medical Image Computing and Computer-Assisted Intervention. 2006:924–931.

97. Ashburner J. A fast diffeomorphic image registration algorithm. NeuroImage. 2007; 38(1):95–113. [PubMed: 17761438]

98. Bossa M, Hernandez M, Olmos S. Contributions to 3D diffeomorphic atlas estimation: application to brain images. International Conference on Medical Image Computing and Computer-Assisted Intervention. 2007:667–674.

99. Vercauteren T, Pennec X, Perchant A, Ayache N. Diffeomorphic Demons: Efficient non-parametric image registration. NeuroImage. 2009; 45(1, Supplement 1):S61–S72. [PubMed: 19041946]

100. De Craene M, Camara O, Bijnens BH, Frangi AF. Large diffeomorphic FFD registration for motion and strain quantification from 3D-US sequences. International Conference on Functional Imaging and Modeling of the Heart. 2009:437–446.

101. Hernandez M, Bossa MN, Olmos S. Registration of anatomical images using paths of diffeomorphisms parameterized with stationary vector field flows. International Journal of Computer Vision. 2009; 85(3):291–306.

102. Zagorchev L, Goshtasby A. A comparative study of transformation functions for nonrigid image registration. IEEE Transactions on Image Processing. 2006; 15(3):529–538. [PubMed: 16519341]

103. Yang X, Xue Z, Liu X, Xiong D. Topology preservation evaluation of compact-support radial basis functions for image registration. Pattern Recognition Letters. 2011; 32(8):1162–1177.

104. Bookstein FL. Principal warps: Thin-plate splines and the decomposition of deformations. IEEE Transactions on Pattern Analysis and Machine Intelligence. 1989; 11(6):567–585.

105. Bookstein FL. Thin-plate splines and the atlas problem for biomedical images. International Conference on Information Processing in Medical Imaging. 1991:326–342.

106. Johnson HJ, Christensen GE. Landmark and intensity-based, consistent thin-plate spline image registration. International Conference on Information Processing in Medical Imaging. 2001:329–343.

107. Li J, Yang X, Yu J. Compact support thin plate spline algorithm. Journal of Electronics (China). 2007; 24(4):515–522.

108. Yang X, Zhang Z, Pei J. Elastic image deformation using adaptive support radial basic function. International Conference on Wavelet Analysis and Pattern Recognition. 2008:158–162.

109. Rohr K, Wörz S. An extension of thin-plate splines for image registration with radial basis functions. International Symposium on Biomedical Imaging. 2012:442–445.

110. Rohr K, Stiehl HS, Sprengel R, Buzug TM, Weese J, Kuhn M. Landmark-based elastic registration using approximating thin-plate splines. IEEE Transactions on Medical Imaging. 2001; 20(6):526–534. [PubMed: 11437112]
111. Donato G, Belongie S. Approximate thin plate spline mappings. European Conference on Computer Vision. 2002:13–31.
112. Marsland S, Twining C, Taylor C. Groupwise non-rigid registration using polyharmonic clamped-plate splines. International Conference on Medical Image Computing and Computer-Assisted Intervention. 2003:771–779.
113. Camion V, Younes L. Geodesic interpolating splines. Workshop on Energy Minimization Methods in Computer Vision and Pattern Recognition. 2001:513–527.
114. Younes L. Combining geodesic interpolating splines and affine transformations. IEEE Transactions on Image Processing. 2006; 15(5):1111–1119. [PubMed: 16671292]
115. Mills A, Shardlow T, Marsland S. Computing the geodesic interpolating spline. International Workshop on Biomedical Image Registration. 2006:169–177.
116. Ruprecht D, Nagel R, Müller H. Spatial free-form deformation with scattered data interpolation methods. Computer & Graphics. 1995; 19(1):63–71.
117. Little JA, Hill DLG, Hawkes DJ. Deformations incorporating rigid structures. Computer Vision and Image Understanding. 1997; 66(2):223–232.
118. Arad N, Dyn N, Reisfeld D, Yeshurun Y. Image warping by radial basis functions: Application to facial expressions. CVGIP: Graphical Models and Image Processing. 1994; 56(2):161–172.
119. Shen D, Davatzikos C. HAMMER: hierarchical attribute matching mechanism for elastic registration. IEEE Transactions on Medical Imaging. 2002; 21(11):1421–1439. [PubMed: 12575879]
120. Fornefett M, Rohr K, Stiehl HS. Radial basis functions with compact support for elastic registration of medical images. Image and Vision Computing. 2001; 19(1–2):87–96.
121. Wendland H. Piecewise polynomial, positive definite and compactly supported radial functions of minimal degree. Advances in Computational Mathematics. 1995; 4(1):389–396.
122. Wendland H. Error estimates for interpolation by compactly supported radial basis functions of minimal degree. Journal of Approximation Theory. 1998; 93(2):258–272.
123. Wu Z. Compactly supported positive definite radial functions. Advances in Computational Mathematics. 1995; 4(1):283–292.
124. Buhmann MD. A new class of radial basis functions with compact support. Mathematics of Computation. 2001; 70(233):307–318.
125. Rohde GK, Aldroubi A, Dawant BM. The adaptive bases algorithm for intensity-based nonrigid image registration. IEEE Transactions on Medical Imaging. 2003; 22(11):1470–1479. [PubMed: 14606680]
126. Siddiqui AM, Masood A, Saleem M. A locally constrained radial basis function for registration and warping of images. Pattern Recognition Letters. 2009; 30(4):377–390.
127. Tristán-Vega A, García-Pérez V. Comments on: A locally constrained radial basis function for registration and warping of images. 2011:586–589.
128. Lowitzsch, S. PhD dissertation. Texas A&M University; 2002. Approximation and interpolation employing sivergence–free radial basis functions with applications.
129. Davis MH, Khotanzad A, Flamig DP, Harms SE. A physics-based coordinate transformation for 3-D image matching. IEEE Transactions on Medical Imaging. 1997; 16(3):317–328. [PubMed: 9184894]
130. Kohlrausch J, Rohr K, Stiehl HS. A new class of elastic body splines for nonrigid registration of medical images. Journal of Mathematical Imaging and Vision. 2005; 23(3):253–280.
131. Wörz S, Rohr K. Physics-based elastic registration using non-radial basis functions and including landmark localization uncertainties. Computer Vision and Image Understanding. 2008; 111(3): 263–274.
132. Sederberg TW, Parry SR. Free-form deformation of solid geometric models. SIGGRAPH Computer Graphics. 1986; 20(4):151–160.

133. Hsu WM, Hughes JF, Kaufman H. Direct manipulation of free-form deformations. SIGGRAPH Computer Graphics. 1992; 26(2):177–184.

134. Declerck J, Feldmar J, Goris ML, Betting F. Automatic registration and alignment on a template of cardiac stress and rest reoriented SPECT images. IEEE Transactions on Medical Imaging. 1997; 16(6):727–737. [PubMed: 9533574]

135. Rueckert D, Sonoda LI, Hayes C, Hill DLG, Leach MO, Hawkes DJ. Nonrigid registration using free-form deformations: application to breast MR images. IEEE Transactions on Medical Imaging. 1999; 18(8):712–721. [PubMed: 10534053]

136. Kybic J, Unser M. Fast parametric elastic image registration. IEEE Transactions on Image Processing. 2003; 12(11):1427–1442. [PubMed: 18244700]

137. Sdika M. A fast nonrigid image registration with constraints on the jacobian using large scale constrained optimization. IEEE Transactions on Medical Imaging. 2008; 27(2):271–281. [PubMed: 18334448]

138. Rueckert D, Aljabar P, Heckemann RA, Hajnal JV, Hammers A. Diffeomorphic registration using B-splines. International Conference on Medical Image Computing and Computer-Assisted Intervention. 2006:702–709.

139. Choi Y, Lee S. Injectivity conditions of 2d and 3d uniform cubic b-spline functions. Graphical Models. 2000; 62(6):411–427.

140. Schnabel J, Rueckert D, Quist M, Blackall JM, Castellano-Smith AD, Hartkens T, Penney GP, Hall WA, Liu H, Truwit CL, Gerritsen FA, Hill DLG, Hawkes DJ. A generic framework for non-rigid registration based on non-uniform multi-level free-form deformations. International Conference on Medical Image Computing and Computer-Assisted Intervention. 2001:573–581.

141. Wang J, Jiang T. Nonrigid registration of brain MRI using NURBS. Pattern Recognition Letters. 2007; 28(2):214–223.

142. Shi W, Zhuang X, Pizarro L, Bai W, Wang H, Tung K-P, Edwards P, Rueckert D. Registration using sparse free-form deformations. International Conference on Medical Image Computing and Computer-Assisted Intervention. 2012:659–66.

143. Noblet V, Heinrich C, Heitz F, Armspach J-P. Symmetric nonrigid image registration: application to average brain templates construction. International Conference on Medical Image Computing and Computer-Assisted Intervention. 2008:897–904.

144. Feng W, Reeves SJ, Denney TS Jr, Lloyd S, Dell'Italia L, Gupta H. A new consistent image registration formulation with B-spline deformation model. International Symposium on Biomedical Imaging. 2009:2–5.

145. Sotiras A, Paragios N. Discrete symmetric image registration. International Symposium on Biomedical Imaging. 2012:342–345.

146. Bhatia KK, Hajnal JV, Puri BK, Edwards AD, Rueckert D. Consistent groupwise non-rigid registration for atlas construction. International Symposium on Biomedical Imaging. 2004:908–911.

147. Balci SK, Golland P, Shenton M, Wells WM III. Free-form b-spline deformation model for groupwise registration. Statistical Registration Workshop: Medical Image Computing and Computer-Assisted Intervention. 2007:23–30.

148. Sotiras A, Ou Y, Glocker B, Davatzikos C, Paragios N. Simultaneous geometric–iconic registration. International Conference on Medical Image Computing and Computer-Assisted Intervention. 2010:676–683.

149. Metz CT, Klein S, Schaap M, Van Walsum T, Niessen WJ. Nonrigid registration of dynamic medical imaging data using nd + t b-splines and a groupwise optimization approach. Medical Image Analysis. 2011; 15(2):238–249. [PubMed: 21075672]

150. Perperidis D, Mohiaddin RH, Rueckert D. Spatio-temporal free-form registration of cardiac MR image sequences. Medical Image Analysis. 2005; 9(5):441–456. [PubMed: 16029955]

151. Ledesma-Carbayo MJ, Kybic J, Desco M, Santos A, Sühling M, Hunziker P, Unser M. Spatio-temporal nonrigid registration for ultrasound cardiac motion estimation. IEEE Transactions on Medical Imaging. 2005; 24(9):1113–1126. [PubMed: 16156350]

152. Vandemeulebroucke J, Rit S, Kybic J, Clarysse P, Sarrut D. Spatiotemporal motion estimation for respiratory-correlated imaging of the lungs. Medical Physics. 2011; 38(1):166–178. [PubMed: 21361185]
153. Ashburner J, Friston KJ. Nonlinear spatial normalization using basis functions. Human Brain Mapping. 1999; 7(4):254–266. [PubMed: 10408769]
154. Amit Y. A nonlinear variational problem for image matching. SIAM Journal on Scientific Computing. 1994; 15(1):207–224.
155. Wu YT, Kanade T, Li CC, Cohn J. Image registration using wavelet-based motion model. International Journal of Computer Vision. 2000; 38(2):129–152.
156. Gefen S, Tretiak O, Nissanov J. Elastic 3-D alignment of rat brain histological images. IEEE Transactions on Medical Imaging. 2003; 22(11):1480–1489. [PubMed: 14606681]
157. Musse O, Heitz F, Armspach JP. Topology preserving deformable image matching using constrained hierarchical parametric models. IEEE Transactions on Image Processing. 2001; 10(7):1081–1093. [PubMed: 18249681]
158. Noblet V, Heinrich C, Heitz F, Armspach JP. 3-D deformable image registration: A topology preservation scheme based on hierarchical deformation models and interval analysis optimization. IEEE Transactions on Image Processing. 2005; 14(5):553–566. [PubMed: 15887550]
159. Noblet V, Heinrich C, Heitz F, Armspach J-P. Retrospective evaluation of a topology preserving non-rigid registration method. Medical Image Analysis. 2006; 10(3):366–384. [PubMed: 16497537]
160. Cathier P. Iconic feature registration with sparse wavelet coefficients. International Conference on Medical Image Computing and Computer-Assisted Intervention. 2006:694–701.
161. Hellier P, Barillot C, Mémin É, Pérez P. Hierarchical estimation of a dense deformation field for 3-D robust registration. IEEE Transactions on Medical Imaging. 2001; 20(5):388–402. [PubMed: 11403198]
162. Zhang H, Yushkevich PA, Alexander DC, Gee JC. Deformable registration of diffusion tensor MR images with explicit orientation optimization. Medical Image Analysis. 2006; 10(5):764–785. [PubMed: 16899392]
163. Pitiot A, Bardinet E, Thompson PM, Malandain G. Piecewise affine registration of biological images for volume reconstruction. Medical Image Analysis. 2006; 10(3):465–483. [PubMed: 15963755]
164. Commowick O, Arsigny V, Isambert A, Costa J, Dhermain F, Bidault F, Bondiau PY, Ayache N, Malandain G. An efficient locally affine framework for the smooth registration of anatomical structures. Medical Image Analysis. 2008; 12(4):427–441. [PubMed: 18325825]
165. Cootes TF, Twining CJ, Petrović VS, Babalola KO, Taylor CJ. Computing accurate correspondences across groups of images. IEEE Transactions on Pattern Analysis and Machine Intelligence. 2010; 32(11):1994–2005. [PubMed: 20847389]
166. Buerger C, Schaeffter T, King AP. Hierarchical adaptive local affine registration for fast and robust respiratory motion estimation. Medical Image Analysis. 2011; 15(4):551–564. [PubMed: 21454119]
167. Narayanan R, Fessler JA, Park H, Meyer CR. Diffeomorphic nonlinear transformations: a local parametric approach for image registration. International Conference on Information Processing in Medical Imaging. 2005:174–185.
168. Arsigny V, Pennec X, Ayache N. Polyrigid and polyaffine transformations: A novel geometrical tool to deal with non-rigid deformations – Application to the registration of histological slices. Medical Image Analysis. 2005; 9(6):507–523. [PubMed: 15948656]
169. Arsigny V, Commowick O, Ayache N, Pennec X. A fast and log-euclidean polyaffine framework for locally linear registration. Journal of Mathematical Imaging and Vision. 2009; 33(2):222–238.
170. Cootes TF, Taylor CJ, Cooper DH, Graham J. Active shape models – their training and application. Computer Vision and Image Understanding. 1995; 61(1):38–59.

171. Wouters J, D'Agostino E, Maes F, Vandermeulen D, Suetens P. Non-rigid brain image registration using a statistical deformation model. Proceedings SPIE Medical Imaging: Image Processing. 2006:614, 411–1–614, 411–8.

172. Tang S, Fan Y, Wu G, Kim M, Shen D. Rabbit: Rapid alignment of brains by building intermediate templates. NeuroImage. 2009; 47(4):1277–1287. [PubMed: 19285145]

173. Kim M, Wu G, Yap PT, Shen D. A general fast registration framework by learning deformation–appearance correlation. IEEE Transactions on Image Processing. 2012; 21(4):1823–1833. [PubMed: 21984505]

174. Rueckert D, Frangi AF, Schnabel JA. Automatic construction of 3-D statistical deformation models of the brain using nonrigid registration. IEEE Transactions on Medical Imaging. 2003; 22(8):1014–1025. [PubMed: 12906255]

175. Loeckx D, Maes F, Vandermeulen D, Suetens P. Temporal subtraction of thorax cr images using a statistical deformation model. IEEE Transactions on Medical Imaging. 2003; 22(11):1490–1504. [PubMed: 14606682]

176. Pszczolkowski S, Pizarro L, Guerrero R, Rueckert D. Nonrigid free-form registration using landmark-based statistical deformation models. Proceedings SPIE Medical Imaging: Image Processing. 2012; 831:418–1–831. 418–9.

177. Glocker B, Komodakis N, Navab N, Tziritas G, Paragios N. Dense registration with deformation priors. International Conference on Information Processing in Medical Imaging. 2009:540–551.

178. Xue Z, Shen D, Davatzikos C. Statistical representation of high-dimensional deformation fields with application to statistically constrained 3d warping. Medical Image Analysis. 2006; 10(5): 740–751. [PubMed: 16887376]

179. Xue Z, Shen D. Statistically-constrained deformable registration of mr brain images. International Symposium on Biomedical Imaging. 2007:25–28.

180. Brun CC, Leporé N, Pennec X, Chou YY, Lee AD, De Zubicaray G, McMahon KL, Wright MJ, Gee JC, Thompson PM. A nonconservative lagrangian framework for statistical fluid registration – safira. IEEE Transactions on Medical Imaging. 2011; 30(2):184–202. [PubMed: 20813636]

181. Lester H, Arridge S, Jansons K, Lemieux L, Hajnal J, Oatridge A. Non-linear registration with the variable viscosity fluid algorithm. International Conference on Information Processing in Medical Imaging. 1999:238–251.

182. Commowick O, Stefanescu R, Fillard P, Arsigny V, Ayache N, Pennec X, Malandain G. Incorporating statistical measures of anatomical variability in atlas-to-subject registration for conformal brain radiotherapy. International Conference on Medical Image Computing and Computer-Assisted Intervention. 2005:927–934.

183. Yeo BTT, Sabuncu MR, Vercauteren T, Holt DJ, Amunts K, Zilles K, Golland P, Fischl B. Learning task-optimal registration cost functions for localizing cytoarchitecture and function in the cerebral cortex. IEEE Transactions on Medical Imaging. 2010; 29(7):1424–1441. [PubMed: 20529736]

184. Clatz O, Sermesant M, Bondiau PY, Delingette H, Warfield SK, Malandain G, Ayache N. Realistic simulation of the 3-d growth of brain tumors in mr images coupling diffusion with biomechanical deformation. IEEE Transactions on Medical Imaging. 2005; 24(10):1334–1346. [PubMed: 16229419]

185. Hogea C, Biros G, Abraham F, Davatzikos C. A robust framework for soft tissue simulations with application to modeling brain tumor mass effect in 3d mr images. Physics in Medicine and Biology. 2007; (23):6893–6908. [PubMed: 18029982]

186. Hogea C, Davatzikos C, Biros G. An image-driven parameter estimation problem for a reaction–diffusion glioma growth model with mass effects. Journal of Mathematical Biology. 2008; 56(6): 793–825. [PubMed: 18026731]

187. Konukoglu E, Clatz O, Menze BH, Stieltjes B, Weber MA, Mandonnet E, Delingette H, Ayache N. Image guided personalization of reaction-diffusion type tumor growth models using modified anisotropic eikonal equations. IEEE Transactions on Medical Imaging. 2010; 29(1):77–95. [PubMed: 19605320]

188. Kyriacou SK, Davatzikos C, Zinreich JS, Bryan NR. Nonlinear elastic registration of brain images with tumor pathology using a biomechanical model. IEEE Transactions on Medical Imaging. 1999; 18(7):580–592. [PubMed: 10504092]
189. Bach Cuadra M, Pollo C, Bardera A, Cuisenaire O, Villemure J-G, Thiran J-P. Atlas-based segmentation of pathological mr brain images using a model of lesion growth. IEEE Transactions on Medical Imaging. 2004; 23(10):1301–1314. [PubMed: 15493697]
190. Bach Cuadra M, De Craene M, Duay V, Macq B, Pollo C, Thiran JP. Dense deformation field estimation for atlas-based segmentation of pathological mr brain images. Computer Methods and Programs in Biomedicine. 2006; 84(2–3):66–75. [PubMed: 16979256]
191. Hermosillo G, Chefd'Hotel C, Faugeras O. Variational methods for multimodal image matching. International Journal of Computer Vision. 2002; 50(3):329–343.
192. Ganser KA, Dickhaus H, Metzner R, Wirtz CR. A deformable digital brain atlas system according to talairach and tournoux. Medical Image Analysis. 2004; 8(1):3–22. [PubMed: 14644143]
193. Nowinski WL, Belov D. Toward atlas-assisted automatic interpretation of mri morphological brain scans in the presence of tumor. Academic Radiology. 2005; 12(8):1049–1057. [PubMed: 16087098]
194. Mohamed A, Zacharaki EI, Shen D, Davatzikos C. Deformable registration of brain tumor images via a statistical model of tumor-induced deformation. Medical Image Analysis. 2006; 10(5):752–763. [PubMed: 16860588]
195. Zacharaki EI, Shen D, Lee SK, Davatzikos C. Orbit: a multiresolution framework for deformable registration of brain tumor images. IEEE Transactions on Medical Imaging. 2008; 27(8):1003–1017. [PubMed: 18672419]
196. Zacharaki EI, Hogea CS, Shen D, Biros G, Davatzikos C. Non-diffeomorphic registration of brain tumor images by simulating tissue loss and tumor growth. NeuroImage. 2009; 46(3):762–774. [PubMed: 19408350]
197. Gooya A, Biros G, Davatzikos C. Deformable registration of glioma images using em algorithm and diffusion reaction modeling. IEEE Transactions on Medical Imaging. 2011; 30(2):375–390. [PubMed: 20876010]
198. Azar FS, Metaxas DN, Schnall MD. A deformable finite element model of the breast for predicting mechanical deformations under external perturbations. Academic Radiology. 2001; 8(10):965–975. [PubMed: 11699849]
199. Ruiter NV, Müller TO, Stotzka R, Gemmeke H, Reichenbach JR, Kaiser WA. Automatic image matching for breast cancer diagnostics by a 3d deformation model of the mamma. Biomedizinische Technik/Biomedical Engineering. 2002; 47(s1b):644–647.
200. del Palomar AP, Calvo B, Herrero J, López J, Doblaré M. A finite element model to accurately predict real deformations of the breast. Medical Engineering & Physics. 2008; 30(9):1089–1097. [PubMed: 18329940]
201. Schnabel JA, Tanner C, Castellano-Smith AD, Degenhard A, Leach MO, Hose DR, Hill DLG, Hawkes DJ. Validation of nonrigid image registration using finite-element methods: application to breast mr images. IEEE Transactions on Medical Imaging. 2003; 22(2):238–247. [PubMed: 12716000]
202. Richard FJ, Bakic PR, Maidment AD. Mammogram registration: a phantom-based evaluation of compressed breast thickness variation effects. IEEE Transactions on Medical Imaging. 2006; 25(2):188–197. [PubMed: 16468453]
203. Hipwell JH, Tanner C, Crum WR, Schnabel JA, Hawkes DJ. A new validation method for x-ray mammogram registration algorithms using a projection model of breast x-ray compression. IEEE Transactions on Medical Imaging. 2007; 26(9):1190–1200. [PubMed: 17896592]
204. Rajagopal V, Lee A, Chung J-H, Warren R, Highnam R, Nielsen P, Nash M. Towards tracking breast cancer across medical images using subject-specific biomechanical models. International Conference on Medical Image Computing and Computer-Assisted Intervention. 2007:651–658.
205. Lee A, Schnabel J, Rajagopal V, Nielsen P, Nash M. Breast image registration by combining finite elements and free-form deformations. Workshop on Digital Mammography. 2010:736–743.

206. Carter T, Tanner C, Beechey-Newman N, Barratt D, Hawkes D. Mr navigated breast surgery: method and initial clinical experience. International Conference on Medical Image Computing and Computer-Assisted Intervention. 2008:356–363.

207. Han L, Hipwell J, Mertzanidou T, Carter T, Modat M, Ourselin S, Hawkes D. A hybrid fem-based method for aligning prone and supine images for image guided breast surgery. International Symposium on Biomedical Imaging. 2011:1239–1242.

208. Samani A, Bishop J, Yaffe MJ, Plewes DB. Biomechanical 3-d finite element modeling of the human breast using mri data. IEEE Transactions on Medical Imaging. 2001; 20(4):271–279. [PubMed: 11370894]

209. Pathmanathan P, Gavaghan DJ, Whiteley JP, Chapman SJ, Brady JM. Predicting tumor location by modeling the deformation of the breast. IEEE Transactions on Biomedical Engineering. 2008; 55(10):2471–2480. [PubMed: 18838373]

210. Ruiter NV, Stotzka R, Müller TO, Gemmeke H, Reichenbach JR, Kaiser WA. Model-based registration of x-ray mammograms and mr images of the female breast. IEEE Transactions on Nuclear Science. 2006; 53(1):204–211.

211. Chung J, Rajagopal V, Nielsen P, Nash M. A biomechanical model of mammographic compressions. Biomechanics and Modeling in Mechanobiology. 2008; 7(1):43–52. [PubMed: 17211616]

212. Kellner AL, Nelson TR, Cerviño LI, Boone JM. Simulation of mechanical compression of breast tissue. IEEE Transactions on Biomedical Engineering. 2007; 54(10):1885–1891. [PubMed: 17926687]

213. Ou JJ, Ong RE, Yankeelov TE, Miga MI. Evaluation of 3d modality-independent elastography for breast imaging: a simulation study. Physics in Medicine and Biology. 2008; 53(1):147–163. [PubMed: 18182693]

214. Tanner C, White M, Hawkes DJ, Salvatore G, Michael D, Hall-Craggs MA. Large breast compressions: Observations and evaluation of simulations. Medical Physics. 2011; 38(2):682–690. [PubMed: 21452705]

215. Han L, Hipwell JH, Tanner C, Taylor Z, Mertzanidou T, Cardoso J, Ourselin S, Hawkes DJ. Development of patient-specific biomechanical models for predicting large breast deformation. Physics in Medicine and Biology. 2012; 57(2):455–472. [PubMed: 22173131]

216. Bharatha A, Hirose M, Hata N, Warfield SK, Ferrant M, Zou KH, Suarez-Santana E, Ruiz-Alzola J, D'Amico A, Cormack RA, Kikinis R, Jolesz FA, Tempany CMC. Evaluation of three-dimensional finite element-based deformable registration of pre- and intraoperative prostate imaging. Medical Physics. 2001; 28(12):2551–2560. [PubMed: 11797960]

217. Hensel JM, Ménard C, Chung PW, Milosevic MF, Kirilova A, Moseley JL, Haider MA, Brock KK. Development of multiorgan finite element-based prostate deformation model enabling registration of endorectal coil magnetic resonance imaging for radiotherapy planning. International Journal of Radiation Oncology*Biology*Physics. 2007; 68(5):1522–1528.

218. Mohamed A, Davatzikos C, Taylor R. A combined statistical and biomechanical model for estimation of intra-operative prostate deformation. International Conference on Medical Image Computing and Computer-Assisted Intervention. 2002:452–460.

219. Alterovitz R, Goldberg K, Pouliot J, Hsu ICJ, Kim Y, Noworolski SM, Kurhanewicz J. Registration of mr prostate images with biomechanical modeling and nonlinear parameter estimation. Medical Physics. 2006; 33(2):446–454. [PubMed: 16532952]

220. Crouch JR, Pizer SM, Chaney EL, Hu YC, Mageras GS, Zaider M. Automated finite-element analysis for deformable registration of prostate images. IEEE Transactions on Medical Imaging. 2007; 26(10):1379–1390. [PubMed: 17948728]

221. Papademetris X, Sinusas AJ, Dione DP, Constable RT, Duncan JS. Estimation of 3-d left ventricular deformation from medical images using biomechanical models. IEEE Transactions on Medical Imaging. 2002; 21(7):786–800. [PubMed: 12374316]

222. Sermesant M, Forest C, Pennec X, Delingette H, Ayache N. Deformable biomechanical models: Application to 4d cardiac image analysis. Medical Image Analysis. 2003; 7(4):475–488. [PubMed: 14561552]

223. Veress AI, Gullberg GT, Weiss JA. Measurement of strain in the left ventricle during diastole with cine-mri and deformable image registration. Journal of Biomechanical Engineering. 2005; 127:1195–1207. [PubMed: 16502662]

224. Moireau P, Chapelle D, Tallec PL. Joint state and parameter estimation for distributed mechanical systems. Computer Methods in Applied Mechanics and Engineering. 2008; 197(6–8):659–677.

225. Phatak NS, Maas SA, Veress AI, Pack NA, Di Bella EV, Weiss JA. Strain measurement in the left ventricle during systole with deformable image registration. Medical Image Analysis. 2009; 13(2):354–361. [PubMed: 18948056]

226. Sundar H, Davatzikos C, Biros G. Biomechanically-constrained 4d estimation of myocardial motion. International Conference on Medical Image Computing and Computer-Assisted Intervention. 2009:257–265.

227. Škrinjar O, Nabavi A, Duncan J. Model-driven brain shift compensation. Medical Image Analysis. 2002; 6(4):361–373. [PubMed: 12494947]

228. Werner R, Ehrhardt J, Schmidt R, Handels H. Patient-specific finite element modeling of respiratory lung motion using 4d ct image data. Medical Physics. 2009; 36(5):1500–1511. [PubMed: 19544766]

229. Al-Mayah A, Moseley J, Brock KK. Contact surface and material nonlinearity modeling of human lungs. Physics in Medicine and Biology. 2008; 53(1):305–317. [PubMed: 18182705]

230. Haber E, Modersitzki J. Image registration with guaranteed displacement regularity. International Journal of Computer Vision. 2007; 71(3):361–372.

231. Chun SY, Fessler JA. Regularized methods for topology-preserving smooth nonrigid image registration using b-spline basis. International Symposium on Biomedical Imaging. 2008:1099–1102.

232. Tanner C, Schnabel JA, Chung D, Clarkson MJ, Rueckert D, Hill DLG, Hawkes DJ. Volume and shape preservation of enhancing lesions when applying non-rigid registration to a time series of contrast enhancing mr breast images. International Conference on Medical Image Computing and Computer-Assisted Intervention. 2000:327–337.

233. Greene WH, Chelikani S, Purushothaman K, Knisely JPS, Chen Z, Papademetris X, Staib LH, Duncan JS. Constrained non-rigid registration for use in image-guided adaptive radiotherapy. Medical Image Analysis. 2009; 13(5):809–817. [PubMed: 19682945]

234. Rohlfing T, Maurer CR Jr, Bluemke DA, Jacobs MA. Volume-preserving nonrigid registration of MR breast images using free-form deformation with an incompressibility constraint. IEEE Transactions on Medical Imaging. 2003; 22(6):730–741. [PubMed: 12872948]

235. Haber E, Modersitzki J. Numerical methods for volume preserving image registration. Inverse Problems. 2004; 20(5):1621–1638.

236. Bistoquet A, Oshinski J, Škrinjar O. Myocardial deformation recovery from cine MRI using a nearly incompressible biventricular model. Medical Image Analysis. 2008; 12(1):69–85. [PubMed: 18234539]

237. Dauguet J, Herard A-S, Declerck J, Delzescaux T. Locally constrained cubic b-spline deformations to control volume variations. International Symposium on Biomedical Imaging. 2009:983–986.

238. Loeckx D, Maes F, Vandermeulen D, Suetens P. Nonrigid image registration using free-form deformations with a local rigidity constraint. International Conference on Medical Image Computing and Computer-Assisted Intervention. 2004:639–646.

239. Staring M, Klein S, Pluim JPW. A rigidity penalty term for nonrigid registration. Medical Physics. 2007; 34(11):4098–4108. [PubMed: 18072476]

240. Modersitzki J. Flirt with rigidity–image registration with a local non-rigidity penalty. International Journal of Computer Vision. 2008; 76(2):153–163.

241. Stewart CV, Tsai CL, Roysam B. The dual-bootstrap iterative closest point algorithm with application to retinal image registration. IEEE Transactions on Medical Imaging. 2003; 22(11): 1379–1394. [PubMed: 14606672]

242. Fitzpatrick JM, West JB, Maurer CR Jr. Predicting error in rigid-body point-based registration. IEEE Transactions on Medical Imaging. 1998; 17(5):694–702. [PubMed: 9874293]

243. Tomazevic D, Likar B, Slivnik T, Pernus F. 3-d/2-d registration of ct and mr to x-ray images. IEEE Transactions on Medical Imaging. 2003; 22(11):1407–1416. [PubMed: 14606674]
244. Chui H, Rangarajan A. A new point matching algorithm for non-rigid registration. Computer Vision and Image Understanding. 2003; 89(2–3):114–141.
245. Harris C, Stephens M. A combined corner and edge detector. Alvey Vision Conference. 1988:147–151.
246. Shi J, Tomasi C. Good features to track. International Conference on Computer Vision and Pattern Recognition. 1994:593–600.
247. Triggs B. Detecting keypoints with stable position, orientation, and scale under illumination changes. European Conference on Computer Vision. 2004:100–113.
248. Mikolajczyk K, Schmid C. Scale & affine invariant interest point detectors. International Journal of Computer Vision. 2004; 60(1):63–86.
249. Mikolajczyk K, Tuytelaars T, Schmid C, Zisserman A, Matas J, Schaffalitzky F, Kadir T, Gool LV. A comparison of affine region detectors. International Journal of Computer Vision. 2005; 65(1–2):43–72.
250. Schmid C, Mohr R, Bauckhage C. Evaluation of interest point detectors. International Journal of Computer Vision. 2000; 37(2):151–172.
251. Mokhtarian F, Mohanna F. Performance evaluation of corner detectors using consistency and accuracy measures. Computer Vision and Image Understanding. 2006; 102(1):81–94.
252. Lindeberg T. Feature detection with automatic scale selection. International Journal of Computer Vision. 1998; 30(2):79–116.
253. Kadir T, Brady M. Saliency, scale and image description. International Journal of Computer Vision. 2001; 45(2):83–105.
254. Matas J, Chum O, Urban M, Pajdla T. Robust wide-baseline stereo from maximally stable extremal regions. Image and Vision Computing. 2004; 22(10):761–767.
255. Lowe DG. Distinctive image features from scale-invariant key-points. International Journal of Computer Vision. 2004; 60(2):91–110.
256. Ke Y, Sukthankar R. Pca-sift: A more distinctive representation for local image descriptors. International Conference on Computer Vision and Pattern Recognition. 2004:506–513.
257. Mikolajczyk K, Schmid C. A performance evaluation of local descriptors. IEEE Transactions on Pattern Analysis and Machine Intelligence. 2005; 27(10):1615–1630. [PubMed: 16237996]
258. Bay H, Ess A, Tuytelaars T, Van Gool L. Speeded-up robust features (surf). Computer Vision and Image Understanding. 2008; 110(3):346–359.
259. Morel JM, Yu G. Asift: A new framework for fully affine invariant image comparison. SIAM Journal on Imaging Sciences. 2009; 2(2):438–469.
260. Juan L, Gwun O. A comparison of sift, pca-sift and surf. International Journal of Image Processing. 2009; 3(5):143–152.
261. Gil A, Mozos OM, Ballesta M, Reinoso O. A comparative evaluation of interest point detectors and local descriptors for visual SLAM. Machine Vision and Applications. 2010; 21(6):905–920.
262. Cheung W, Hamarneh G. n-SIFT: n-dimensional scale invariant feature transform. IEEE Transactions on Image Processing. 2009; 18(9):2012–2021. [PubMed: 19502129]
263. Ni D, Qu Y, Yang X, Chui Y, Wong T-T, Ho S, Heng P. Volumetric ultrasound panorama based on 3d sift. International Conference on Medical Image Computing and Computer-Assisted Intervention. 2008:52–60.
264. Allaire S, Kim JJ, Breen SL, Jaffray DA, Pekar V. Full orientation invariance and improved feature selectivity of 3d sift with application to medical image analysis. Computer Vision and Pattern Recognition Workshop. 2008:1–8.
265. Flitton G, Breckon TP, Megherbi N. Object recognition using 3d sift in complex ct volumes. British Machine Vision Conference. 2010:11.1–11.12.
266. Niemeijer M, Garvin MK, Lee K, van Ginneken B, Abrámoff MD, Sonka M. Registration of 3d spectral oct volumes using 3d sift feature point matching. Proceedings SPIE Medical Imaging: Image Processing. 2009:72, 591I–1–72, 591I–8.

267. Han X. Feature-constrained nonlinear registration of lung ct images. Medical Image Analysis for the Clinic: A Grand Challenge. 2010:63–72.
268. Yang J, Williams JP, Sun Y, Blum RS, Xu C. A robust hybrid method for nonrigid image registration. Pattern Recognition. 2011; 44(4):764–776.
269. Toews M, WMW. Efficient and robust model-to-image alignment using 3d scale-invariant features. Medical Image Analysis. 2012
270. Pennec, X.; Ayache, N.; Thirion, J-P. Handbook of Medical Imaging - Processing and Analysis. Elsevier; 2000. Landmark-based registration using features identified through differential geometry; p. 499-513.
271. Cachier P, Mangin J-F, Pennec X, Rivière D, Papadopoulos-Orfanos D, Regis J, Ayache N. Multisubject non-rigid registration of brain MRI using intensity and geometric features. International Conference on Medical Image Computing and Computer-Assisted Intervention. 2001:734–742.
272. Hellier P, Barillot C. Coupling dense and landmark-based approaches for nonrigid registration. IEEE Transactions on Medical Imaging. 2003; 22(2):217–227. [PubMed: 12715998]
273. Chui H, Win L, Schultz R, Duncan JS, Rangarajan A. A unified non-rigid feature registration method for brain mapping. Medical Image Analysis. 2003; 7(2):113–130. [PubMed: 12868617]
274. Liu T, Shen D, Davatzikos C. Deformable registration of cortical structures via hybrid volumetric and surface warping. NeuroImage. 2004; 22(4):1790–1801. [PubMed: 15275935]
275. Qiu A, Miller MI. Cortical hemisphere registration via large deformation diffeomorphic metric curve mapping. International Conference on Medical Image Computing and Computer-Assisted Intervention. 2007:186–193.
276. Can A, Stewart CV, Roysam B, Tanenbaum HL. A feature-based, robust, hierarchical algorithm for registering pairs of images of the curved human retina. IEEE Transactions on Pattern Analysis and Machine Intelligence. 2002; 24(3):347–364.
277. Reinertsen I, Descoteaux M, Siddiqi K, Collins DL. Validation of vessel-based registration for correction of brain shift. Medical Image Analysis. 2007; 11(4):374–388. [PubMed: 17524702]
278. Xiao C, Staring M, Shamonin D, Reiber JHC, Stolk J, Stoel BC. A strain energy filter for 3D vessel enhancement with application to pulmonary CT images. Medical Image Analysis. 2011; 15(1):112–124. [PubMed: 20951629]
279. Comparison of vesselness functions for multiscale analysis of the liver vasculature. International Conference on Information Technology and Applications in Biomedicine. 2010:1–5.
280. Sato Y, Nakajima S, Shiraga N, Atsumi H, Yoshida S, Koller T, Gerig G, Kikinis R. Three-dimensional multi-scale line filter for segmentation and visualization of curvilinear structures in medical images. Medical Image Analysis. 1998; 2(2):143–168. [PubMed: 10646760]
281. Frangi AF, Niessen WJ, Vincken KL, Viergever MA. Multiscale vessel enhancement filtering. International Conference on Medical Image Computing and Computer-Assisted Intervention. 1998:130–137.
282. Cañero C, Radeva P. Vesselness enhancement diffusion. Pattern Recognition Letters. 2003; 24(16):3141–3151.
283. Manniesing R, Viergever MA, Niessen WJ. Vessel enhancing diffusion: A scale space representation of vessel structures. Medical Image Analysis. 2006; 10(6):815–825. [PubMed: 16876462]
284. Fitzpatrick JM, West JB. The distribution of target registration error in rigid-body point-based registration. IEEE Transactions on Medical Imaging. 2001; 20(9):917–927. [PubMed: 11585208]
285. Wiles AD, Likholyot A, Frantz DD, Peters TM. A statistical model for point-based target registration error with anisotropic fiducial localizer error. IEEE Transactions on Medical Imaging. 2008; 27(3):378–390. [PubMed: 18334433]
286. Moghari MH, Abolmaesumi P. Distribution of fiducial registration error in rigid-body point-based registration. IEEE Transactions on Medical Imaging. 2009; 28(11):1791–1801. [PubMed: 19884067]
287. Leordeanu M, Hebert M. A spectral technique for correspondence problems using pairwise constraints. International Conference on Computer Vision. 2005:1482–1489.

288. Berg AC, Berg TL, Malik J. Shape matching and object recognition using low distortion correspondences. International Conference on Computer Vision and Pattern Recognition. 2005:26–33.
289. Torresani L, Kolmogorov V, Rother C. Feature correspondence via graph matching: Models and global optimization. European Conference on Computer Vision. 2008:596–609.
290. Duchenne O, Bach F, Kweon IS, Ponce J. A Tensor-Based Algorithm for High-Order Graph Matching. IEEE Transactions on Pattern Analysis and Machine Intelligence. 2011; 33(12):2383–2395.
291. Zass R, Shashua A. Probabilistic graph and hypergraph matching. International Conference on Computer Vision and Pattern Recognition. 2008:1–8.
292. Wang C, Teboul O, Michel F, Essafi S, Paragios N. 3D knowledge-based segmentation using pose-invariant higher-order graphs. International Conference on Medical Image Computing and Computer-Assisted Intervention. 2010:189–196.
293. Komodakis N, Paragios N, Tziritas G. MRF energy minimization and beyond via dual decomposition. IEEE Transactions on Pattern Analysis and Machine Intelligence. 2011; 33(3): 531–552. [PubMed: 20479493]
294. Goodall C. Procrustes methods in the statistical analysis of shape. Journal of the Royal Statistical Society Series B (Methodological). 1991; 53(2):285–339.
295. Cootes TF, Taylor CJ. A mixture model for representing shape variation. Image and Vision Computing. 1999; 17(8):567–573.
296. Duta N, Jain AK, Dubuisson-Jolly MP. Automatic construction of 2D shape models. IEEE Transactions on Pattern Analysis and Machine Intelligence. 2001; 23(5):433–446.
297. Guo, H.; Rangarajan, A.; Joshi, SC. Handbook of Mathematical Models in Computer Vision. Springer Verlag; 2006. Diffeomorphic point matching; p. 205-219.
298. Tsin Y, Kanade T. A correlation-based approach to robust point set registration. European Conference on Computer Vision. 2004:558–569.
299. Singh M, Himanshu A, Ahuja N. Robust registration and tracking using kernel density correlation. Computer Vision and Pattern Recognition Workshop. 2004
300. Jian B, Vemuri B. Robust point set registration using gaussian mixture models. IEEE Transactions on Pattern Analysis and Machine Intelligence. 2011; 33(8):1633–1645.
301. Myronenko A, Song X. Point set registration: coherent point drift. IEEE Transactions on Pattern Analysis and Machine Intelligence. 2010; 32(12):2262–2275. [PubMed: 20975122]
302. Roy AS, Gopinath A, Rangarajan A. Deformable density matching for 3D non-rigid registration of shapes. International Conference on Medical Image Computing and Computer-Assisted Intervention. 2007:942–949.
303. Wang F, Vemuri BC, Rangarajan A, Eisenschenk SJ. Simultaneous nonrigid registration of multiple point sets and atlas construction. IEEE Transactions on Pattern Analysis and Machine Intelligence. 2008; 30(11):2011–2022. [PubMed: 18787248]
304. Wang F, Vemuri B, Syeda-Mahmood T. Generalized L2-divergence and its application to shape alignment. International Conference on Information Processing in Medical Imaging. 2009:227–238.
305. Tustison NJ, Awate SP, Song G, Cook TS, Gee JC. Point set registration using Havrda-Charvat-Tsallis entropy measures. IEEE Transactions on Medical Imaging. 2011; 30(2):451–460. [PubMed: 20937578]
306. Paragios N, Rousson M, Ramesh V. Non-rigid registration using distance functions. Computer Vision and Image Understanding. 2003; 89(2–3):142–165.
307. Huang X, Paragios N, Metaxas DN. Shape registration in implicit spaces using information theory and free form deformations. IEEE Transactions on Pattern Analysis and Machine Intelligence. 2006; 28(8):1303–1318. [PubMed: 16886865]
308. Savinaud M, Paragios N, Maitrejean S. Motion-based enhancement of optical imaging. International Symposium on Biomedical Imaging. 2009:738–741.
309. Caselles V, Kimmel R, Sapiro G. Geodesic active contours. International Journal of Computer Vision. 1997; 22(1):61–79.

310. Besl PJ, McKay ND. A method for registration of 3-D shapes. IEEE Transactions on Pattern Analysis and Machine Intelligence. 1992; 14(2):239–256.
311. Rusinkiewicz S, Levoy M. Efficient variants of the icp algorithm. International Conference on 3-D Digital Imaging and Modeling. 2001:145–152.
312. Liu Y. Improving ICP with easy implementation for free-form surface matching. Pattern Recognition. 2004; 37(2):211–226.
313. Pottmann H, Huang QX, Yang YL, Hu SM. Geometry and convergence analysis of algorithms for registration of 3d shapes. International Journal of Computer Vision. 2006; 67(3):277–296.
314. Penney G, Edwards P, King A, Blackall J, Batchelor P, Hawkes D. A stochastic iterative closest point algorithm (stochas-tICP). International Conference on Medical Image Computing and Computer-Assisted Intervention. 2001:762–769.
315. Granger S, Pennec X. Multi-scale EM-ICP: A fast and robust approach for surface registration. European Conference on Computer Vision. 2002:69–73.
316. Sharp GC, Lee SW, Wehe DK. ICP registration using invariant features. IEEE Transactions on Pattern Analysis and Machine Intelligence. 2002; 24(1):90–102.
317. Estépar R, Brun A, Westin C-F. Robust generalized total least squares iterative closest point registration. International Conference on Medical Image Computing and Computer-Assisted Intervention. 2004:234–241.
318. Maier-Hein L, Franz AM, dos Santos TR, Schmidt M, Fangerau M, Meinzer H, Fitzpatrick JM. Convergent iterative closest-point algorithm to accomodate anisotropic and inhomogenous localization error. IEEE Transactions on Pattern Analysis and Machine Intelligence. 2012; 34(8): 1520–1532. [PubMed: 22184256]
319. Kim J, Fessler JA. Intensity-based image registration using robust correlation coefficients. IEEE Transactions on Medical Imaging. 2004; 23(11):1430–1444. [PubMed: 15554130]
320. Xue Z, Shen D, Davatzikos C. Determining correspondence in 3-D MR brain images using attribute vectors as morphological signatures of voxels. IEEE Transactions on Medical Imaging. 2004; 23(10):1276–1291. [PubMed: 15493695]
321. Shen D. Image registration by local histogram matching. Pattern Recognition. 2007; 40(4):1161–1172.
322. Wu G, Qi F, Shen D. Learning-based deformable registration of MR brain images. IEEE Transactions on Medical Imaging. 2006; 25(9):1145–1157. [PubMed: 16967800]
323. Ou Y, Sotiras A, Paragios N, Davatzikos C. DRAMMS: Deformable registration via attribute matching and mutual-saliency weighting. Medical Image Analysis. 2011; 15(4):622–639. [PubMed: 20688559]
324. Liu J, Vemuri BC, Marroquin JL. Local frequency representations for robust multimodal image registration. IEEE Transactions on Medical Imaging. 2002; 21(5):462–469. [PubMed: 12071617]
325. Liao S, Chung ACS. Feature based nonrigid brain MR image registration with symmetric alpha stable filters. IEEE Transactions on Medical Imaging. 2010; 29(1):106–119. [PubMed: 19666334]
326. Liao S, Chung ACS. Non-rigid brain MR image registration using uniform spherical region descriptor. IEEE Transactions on Image Processing. 2012; 21(1):157–169. [PubMed: 21690014]
327. Myronenko A, Song X. Intensity-based image registration by minimizing residual complexity. IEEE Transactions on Medical Imaging. 2010; 29(11):1882–1891. [PubMed: 20562036]
328. Wells WM III, Viola P, Atsumi H, Nakajima S, Kikinis R. Multi-modal volume registration by maximization of mutual information. Medical Image Analysis. 1996; 1(1):35–51. [PubMed: 9873920]
329. Viola P, Wells WM III. Alignment by maximization of mutual information. International Journal of Computer Vision. 1997; 24(2):137–154.
330. Collignon A, Maes F, Delaere D, Vandermeulen D, Suetens P, Marchal G. Automated multi-modality image registration based on information theory. International Conference on Information Processing in Medical Imaging. 1995:263–274.
331. Maes F, Collignon A, Vandermeulen D, Marchal G, Suetens P. Multimodality image registration by maximization of mutual information. IEEE Transactions on Medical Imaging. 1997; 16(2): 187–198. [PubMed: 9101328]

332. Pluim JPW, Maintz JA, Viergever MA. Mutual-information-based registration of medical images: A survey. IEEE Transactions on Medical Imaging. 2003; 22(8):986–1004. [PubMed: 12906253]
333. Studholme C, Hill DLG, Hawkes DJ. An overlap invariant entropy measure of 3D medical image alignment. Pattern Recognition. 1999; 32(1):71–86.
334. Cahill ND, Schnabel JA, Noble JA, Hawkes DJ. Revisiting overlap invariance in medical image alignment. Computer Vision and Pattern Recognition Workshop. 2008:1–8.
335. Roche A, Malandain G, Pennec X, Ayache N. The correlation ratio as a new similarity measure for multimodal image registration. International Conference on Medical Image Computing and Computer-Assisted Intervention. 1998:1115–1124.
336. Pluim JPW, Maintz JBA, Viergever MA. F-information measures in medical image registration. IEEE Transactions on Medical Imaging. 2004; 23(12):1508–1516. [PubMed: 15575408]
337. Chung AC, Wells WM III, Norbash A, Grimson WEL. Multi-modal image registration by minimizing Kullback-Leibler distance. International Conference on Medical Image Computing and Computer-Assisted Intervention. 2002:525–532.
338. Guetter C, Xu C, Sauer F, Hornegger J. Learning based non-rigid multi-modal image registration using Kullback-Leibler divergence. International Conference on Medical Image Computing and Computer-Assisted Intervention. 2005:255–262.
339. Liao R, Guetter C, Xu C, Sun Y, Khamene A, Sauer F. Learning-based 2D/3D rigid registration using Jensen-Shannon divergence for image-guided surgery. Workshop on Medical Imaging and Augmented Reality. 2006:228–235.
340. Rényi A. On measures of entropy and information. Berkeley Symposium on Mathematical Statistics and Probability. 1961:547–561.
341. He Y, Hamza AB, Krim H. A generalized divergence measure for robust image registration. IEEE Transactions on Signal Processing. 2003; 51(5):1211–1220.
342. Neemuchwala H, Hero AO III, Carson P. Image registration using entropic graph-matching criteria. Asilomar Conference on Signals, Systems and Computers. 2002:134–138.
343. Sabuncu MR, Ramadge P. Using spanning graphs for efficient image registration. IEEE Transactions on Image Processing. 2008; 17(5):788–797. [PubMed: 18390383]
344. Martin S, Durrani TS. A new divergence measure for medical image registration. IEEE Transactions on Image Processing. 2007; 16(4):957–966. [PubMed: 17405429]
345. Rueckert D, Clarkson MJ, Hill DLG, Hawkes DJ. Non-rigid registration using higher-order mutual information. Proceedings SPIE Medical Imaging: Image Processing. 2000:438–447.
346. Karaçali B. Information Theoretic Deformable Registration Using Local Image Information. International Journal of Computer Vision. 2007; 72(3):219–237.
347. Studholme C, Drapaca C, Iordanova B, Cardenas V. Deformation-based mapping of volume change from serial brain MRI in the presence of local tissue contrast change. IEEE Transactions on Medical Imaging. 2006; 25(5):626–639. [PubMed: 16689266]
348. Sundar H, Shen D, Biros G, Xu C, Davatzikos C. Robust computation of mutual information using spatially adaptive meshes. International Conference on Medical Image Computing and Computer-Assisted Intervention. 2007:950–958.
349. Loeckx D, Slagmolen P, Maes F, Vandermeulen D, Suetens P. Nonrigid image registration using conditional mutual information. IEEE Transactions on Medical Imaging. 2010; 29(1):19–29. [PubMed: 19447700]
350. Zhuang X, Arridge S, Hawkes DJ, Ourselin S. A nonrigid registration framework using spatially encoded mutual information and free-form deformations. Medical Imaging, IEEE Transactions on. 2011; 30(10):1819–1828.
351. Pluim JPW, Maintz JBA, Viergever MA. Image registration by maximization of combined mutual information and gradient information. IEEE Transactions on Medical Imaging. 2000; 19(8):809–814. [PubMed: 11055805]
352. Russakoff D, Tomasi C, Rohlfing T, Maurer CR Jr. Image similarity using mutual information of regions. European Conference on Computer Vision. 2004:596–607.
353. Bardera A, Feixas M, Boada I, Sbert M. High-dimensional normalized mutual information for image registration using random lines. International Workshop on Biomedical Image Registration. 2006:264–271.

354. Yi Z, Soatto S. Multimodal registration via spatial-context mutual information. International Conference on Information Processing in Medical Imaging. 2011:424–435.

355. Holden M, Griffin LD, Saeed N, Hill DLG. Multi-channel mutual information using scale space. International Conference on Medical Image Computing and Computer-Assisted Intervention. 2004:797–804.

356. Gan R, Chung ACS, Liao S. Maximum distance-gradient for robust image registration. Medical Image Analysis. 2008; 12(4):452–468. [PubMed: 18337156]

357. Sabuncu MR, Ramadge PJ. Spatial information in entropy-based image registration. International Workshop on Biomedical Image Registration. 2003:132–141.

358. Neemuchwala H, Hero AO III, Carson P. Image matching using alpha-entropy measures and entropic graphs. Signal Processing. 2005; 85(2):277–296.

359. Staring M, van der Heide UA, Klein S, Viergever MA, Pluim JPW. Registration of cervical MRI using multifeature mutual information. IEEE Transactions on Medical Imaging. 2009; 28(9): 1412–1421. [PubMed: 19278929]

360. Studholme C, Hill DLG, Hawkes DJ. Incorporating connected region labelling into automated image registration using mutual information. Workshop on Mathematical Methods in Biomedical Image Analysis. 1996:23–31.

361. Knops ZF, Maintz JBA, Viergever MA, Pluim JPW. Registration using segment intensity remapping and mutual information. International Conference on Medical Image Computing and Computer-Assisted Intervention. 2004:805–812.

362. D'Agostino E, Maes F, Vandermeulen D, Suetens P. An information theoretic approach for non-rigid image registration using voxel class probabilities. Medical Image Analysis. 2006; 10(3): 413–431. [PubMed: 15919230]

363. Roche A, Pennec X, Malandain G, Ayache N. Rigid registration of 3-D ultrasound with MR images: a new approach combining intensity and gradient information. IEEE Transactions on Medical Imaging. 2001; 20(10):1038–1049. [PubMed: 11686439]

364. Wein W, Brunke S, Khamene A, Callstrom MR, Navab N. Automatic CT-ultrasound registration for diagnostic imaging and image-guided intervention. Medical Image Analysis. 2008; 12(5): 577–585. [PubMed: 18650121]

365. Michel F, Paragios N. Image transport regression using mixture of experts and discrete markov random fields. International Symposium on Biomedical Imaging. 2010:1229–1232.

366. Maintz JBA, van den Elsen PA, Viergever MA. 3D multimodality medical image registration using morphological tools. Image and Vision Computing. 2001; 19(1–2):53–62.

367. Haber E, Modersitzki J. Intensity gradient based registration and fusion of multi-modal images. Methods of Information in Medicine. 2007; 46(3):292–299. [PubMed: 17492115]

368. Butz T, Thiran J-P. Affine registration with feature space mutual information. International Conference on Medical Image Computing and Computer-Assisted Intervention. 2001:549–556.

369. Penney GP, Blackall JM, Hamady MS, Sabharwal T, Adam A, Hawkes DJ. Registration of freehand 3D ultrasound and magnetic resonance liver images. Medical Image Analysis. 2004; 8(1):81–91. [PubMed: 14644148]

370. Jain AK, Farrokhnia F. Unsupervised texture segmentation using gabor filters. Pattern Recognition. 1991; 24(12):1167–1186.

371. Jian B, Vemuri BC, Marroquin JL. Robust nonrigid multimodal image registration using local frequency maps. International Conference on Information Processing in Medical Imaging. 2005:504–515.

372. Andronache A, von Siebenthal M, Székely G, Cattin P. Non-rigid registration of multi-modal images using both mutual information and cross-correlation. Medical Image Analysis. 2008; 12(1):3–15. [PubMed: 17669679]

373. Heinrich MP, Jenkinson M, Bhushan M, Matin T, Gleeson FV, Brady SM, Schnabel JA. MIND: Modality independent neighbourhood descriptor for multi-modal deformable registration. Medical Image Analysis. 2012; 16(7):1423–1435. [PubMed: 22722056]

374. Wachinger C, Navab N. Entropy and laplacian images: Structural representations for multi-modal registration. Medical Image Analysis. 2012; 16(1):1–17. [PubMed: 21632274]

375. Lee D, Hofmann M, Steinke F, Altun Y, Cahill ND, Scholkopf B. Learning similarity measure for multi-modal 3D image registration. International Conference on Computer Vision and Pattern Recognition. 2009:186–193.

376. Bronstein MM, Bronstein AM, Michel F, Paragios N. Data fusion through cross-modality metric learning using similarity-sensitive hashing. International Conference on Computer Vision and Pattern Recognition. 2010:3594–3601.

377. Michel F, Bronstein MM, Bronstein AM, Paragios N. Boosted metric learning for 3d multi-modal deformable registration. International Symposium on Biomedical Imaging. 2011:1209–1214.

378. Leventon M, Grimson W. Multi-modal volume registration using joint intensity distributions. International Conference on Medical Image Computing and Computer-Assisted Intervention. 1998:1057–1066.

379. Johnson HJ, Christensen GE. Consistent landmark and intensity-based image registration. IEEE Transactions on Medical Imaging. 2002; 21(5):450–461. [PubMed: 12071616]

380. Paquin D, Levy D, Xing L. Hybrid multiscale landmark and deformable image registration. Mathematical Biosciences and Engineering. 2007; 4(4):711–737. [PubMed: 17924721]

381. Yin Y, Hoffman EA, Ding K, Reinhardt JM, Lin CL. A cubic b-spline-based hybrid registration of lung ct images for a dynamic airway geometric model with large deformation. Physics in Medicine and Biology. 2011; 56(1):203–218. [PubMed: 21149947]

382. Postelnicu G, Zollei L, Fischl B. Combined volumetric and surface registration. IEEE Transactions on Medical Imaging. 2009; 28(4):508–522. [PubMed: 19273000]

383. Gibson E, Khan AR, Beg MF. A combined surface and volumetric registration (SAVOR) framework to study cortical biomarkers and volumetric imaging data. International Conference on Medical Image Computing and Computer-Assisted Intervention. 2009:713–720.

384. Camara O, Delso G, Colliot O, Moreno-Ingelmo A, Bloch I. Explicit incorporation of prior anatomical information into a non-rigid registration of thoracic and abdominal CT and 18-FDG whole-body emission PET images. IEEE Transactions on Medical Imaging. 2007; 26(2):164–178. [PubMed: 17304731]

385. Hartkens T, Hill DLG, Castellano-Smith A, Hawkes DJ, Maurer CR, Martin A, Hall W, Liu H, Truwit C. Using points and surfaces to improve voxel-based non-rigid registration. International Conference on Medical Image Computing and Computer-Assisted Intervention. 2002:565–572.

386. Papademetris X, Jackowski AP, Schultz RT, Staib LH, Duncan JS. Integrated intensity and point-feature nonrigid registration. International Conference on Medical Image Computing and Computer-Assisted Intervention. 2004:763–770.

387. Rohr K, Cathier P, Wörz S. Elastic registration of electrophoresis images using intensity information and point landmarks. Pattern Recognition. 2004; 37(5):1035–1048.

388. Azar A, Xu C, Pennec X, Ayache N. An interactive hybrid non-rigid registration framework for 3d medical images. International Symposium on Biomedical Imaging. 2006:824–827.

389. Wörz S, Rohr K. Hybrid spline-based elastic image registration using analytic solutions of the navier equation. Bildverarbeitung für die Medizin. 2007:151–155.

390. Biesdorf A, Wörz S, Kaiser H-J, Stippich C, Rohr K. Hybrid spline-based multimodal registration using local measures for joint entropy and mutual information. International Conference on Medical Image Computing and Computer-Assisted Intervention. 2009:607–615.

391. Lu H, Cattin PC, Reyes M. A hybrid multimodal non-rigid registration of mr images based on diffeomorphic demons. International Conference of the IEEE Engineering in Medicine and Biology Society. 2010:5951–5954.

392. Lu H, Reyes M, Šerifović A, Weber S, Sakurai Y, Yamagata H, Cattin PC. Multi-modal diffeomorphic demons registration based on point-wise mutual information. International Symposium on Biomedical Imaging. 2010:372–375.

393. Joshi AA, Shattuck DW, Thompson PM, Leahy RM. Surface-constrained volumetric brain registration using harmonic mappings. IEEE Transactions on Medical Imaging. 2007; 26(12): 1657–1669. [PubMed: 18092736]

394. Joshi A, Leahy R, Toga AW, Shattuck D. A framework for brain registration via simultaneous surface and volume flow. International Conference on Information Processing in Medical Imaging. 2009:576–588.

395. Honnorat N, Vaillant R, Paragios N. Graph-based geometric-iconic guide-wire tracking. International Conference on Medical Image Computing and Computer-Assisted Intervention. 2011:9–16.
396. Kurkure U, Le YH, Paragios N, Carson JP, Ju T, Kakadiaris IA. Landmark/image-based deformable registration of gene expression data. International Conference on Computer Vision and Pattern Recognition. 2011:1089–1096.
397. Siless V, Guevara P, Pennec X, Fillard P. Joint t1 and brain fiber diffeomorphic registration using the demons. Workshop on Multimodal Brain Image Analysis, Medical Image Computing and Computer-Assisted Intervention. 2011:10–18.
398. Durrleman S, Fillard P, Pennec X, Trouvé A, Ayache N. Registration, atlas estimation and variability analysis of white matter fiber bundles modeled as currents. NeuroImage. 2011; 55(3): 1073–1090. [PubMed: 21126594]
399. Cifor A, Risser L, Chung D, Anderson EM, Schnabel JA. Hybrid feature-based log-demons registration for tumour tracking in 2-d liver ultrasound images. International Symposium on Biomedical Imaging. 2012:724–727.
400. Klein S, Staring M, Pluim JPW. Evaluation of optimization methods for nonrigid medical image registration using mutual information and B-splines. IEEE Transactions on Image Processing. 2007; 16(12):2879–2890. [PubMed: 18092588]
401. Moré JJ, Thuente DJ. Line search algorithms with guaranteed sufficient decrease. ACM Transactions on Mathematical Software. 1994; 20(3):286–307.
402. Grippo L, Lampariello F, Lucidi S. A nonmonotone line search technique for Newton's method. SIAM Journal on Numerical Analysis. 1986; 23(4):707–716.
403. Press, WH.; Teukolsky, SA.; Vetterling, WT.; Flannery, BP. Numerical recipes in C: The art of scientific computing. Cambridge, U.K: Cambridge University Press;
404. Fletcher R, Reeves CM. Function minimization by conjugate gradients. The Computer Journal. 1964; 7(2):149–154.
405. Pollak E, Ribière G. Note sur la convergence de méthodes de directions conjuguées. Revue Française dInformatique et de Recherche Opérationnelle. 1969; 3(16):35–43.
406. Polyak BT. The conjugate gradient method in extremal problems. USSR Computational Mathematics and Mathematical Physics. 1969; 9(4):94–112.
407. Hestenes MR, Stiefel E. Methods of conjugate gradients for solving linear systems. Journal of Research of the National Bureau of Standards. 1952; 49(6):409–436.
408. Hager WW, Zhang H. A survey of nonlinear conjugate gradient methods. Pacific Journal of Optimization. 2006; 2(1):35–58.
409. Tustison NJ, Avants BB, Gee JC. Directly manipulated free-form deformation image registration. IEEE Transactions on Image Processing. 2009; 18(3):624–635. [PubMed: 19171516]
410. Powell MJD. How bad are the bfgs and dfp methods when the objective function is quadratic? Mathematical Programming. 1986; 34(1):34–47.
411. Byrd RH, Nocedal J, Yuan YX. Global convergence of a class of quasi-newton methods on convex problems. SIAM Journal on Numerical Analysis. 1987; 24(5):1171–1190.
412. Zikic D, Baust M, Kamen A, Navab N. A general preconditioning scheme for difference measures in deformable registration. International Conference on Computer Vision. 2011:49–56.
413. Thévenaz P, Unser M. Optimization of mutual information for multiresolution image registration. IEEE Transactions on Image Processing. 2000; 9(12):2083–2099. [PubMed: 18262946]
414. Klein S, Pluim JPW, Staring M, Viergever MA. Adaptive stochastic gradient descent optimisation for image registration. International Journal of Computer Vision. 2009; 81(3):227–239.
415. Bhagalia R, Fessler JA, Kim B. Accelerated nonrigid intensity-based image registration using importance sampling. IEEE Transactions on Medical Imaging. 2009; 28(8):1208–1216. [PubMed: 19211343]
416. Ford, LR.; Fulkerson, DR. Princeton, NJ: Princeton University Press.
417. Greig DM, Porteous BT, Seheult AH. Exact maximum a posteriori estimation for binary images. Journal of the Royal Statistical Society Series B (Methodological). 1989; 51(2):271–279.

418. Boykov Y, Veksler O, Zabih R. Fast approximate energy minimization via graph cuts. IEEE Transactions on Pattern Analysis and Machine Intelligence. 2001; 23(11):1222–1239.
419. Tang TWH, Chung ACS. Non-rigid image registration using graph-cuts. International Conference on Medical Image Computing and Computer-Assisted Intervention. 2007:916–924.
420. So RWK, Chung ACS. Multi-level non-rigid image registration using graph-cuts. International Conference on Acoustics, Speech and Signal Processing. 2009:397–400.
421. So RWK, Chung ACS. Non-rigid image registration by using graph-cuts with mutual information. International Conference on Image Processing. 2010:4429–4432.
422. So RWK, Tang TWH, Chung ACS. Non-rigid image registration of brain magnetic resonance images using graph-cuts. Pattern Recognition. 2011; 44(10):2450–2467.
423. Pearl, J. Probabilistic reasoning in intelligent systems: networks of plausible inference. Morgan Kaufmann; 1988.
424. Frey BJ, MacKay DJC. A revolution: Belief propagation in graphs with cycles. In Conference on Advances in Neural Information Processing Systems. 1997:479–485.
425. Murphy KP, Weiss Y, Jordan MI. Loopy belief propagation for approximate inference: An empirical study. Conference on Uncertainty in Artificial Intelligence. 1999:467–475.
426. Yang Q, Wang L, Ahuja N. A constant-space belief propagation algorithm for stereo matching. International Conference on Computer Vision and Pattern Recognition. 2010:1458–1465.
427. Heinrich MP, Jenkinson M, Brady SJM, Schnabel JA. Non-rigid image registration through efficient discrete optimization. Conference on Medical Image Analysis and Understanding. 2011:1–5.
428. Shekhovtsov A, Kovtun I, Hlaváč V. Efficient MRF deformation model for non-rigid image matching. Computer Vision and Image Understanding. 2008; 112(1):91–99.
429. Lee KJ, Kwon D, Yun ID, Lee SU. Deformable 3d volume registration using efficient mrfs model with decomposed nodes. British Machine Vision Conference. 2008:59.1–59.10.
430. Liu C, Yuen J, Torralba A. SIFT flow: Dense correspondence across scenes and its applications. IEEE Transactions on Pattern Analysis and Machine Intelligence. 2011; 33(5):978–994. [PubMed: 20714019]
431. Kwon D, Lee KJ, Yun ID, Lee SU. Nonrigid image registration using higher-order mrf model with dense local descriptor. Computer Vision and Pattern Recognition Workshop. 2011
432. Komodakis N, Tziritas G. Approximate labeling via graph cuts based on linear programming. IEEE Transactions on Pattern Analysis and Machine Intelligence. 2007; 29(8):1436–1453. [PubMed: 17568146]
433. Komodakis N, Tziritas G, Paragios N. Performance vs computational efficiency for optimizing single and dynamic MRFs: Setting the state of the art with primal-dual strategies. Computer Vision and Image Understanding. 2008; 112(1):14–29.
434. Glocker B, Komodakis N, Tziritas G, Navab N, Paragios N. Dense image registration through MRFs and efficient linear programming. Medical Image Analysis. 2008; 12(6):731–741. [PubMed: 18482858]
435. Glocker B, Sotiras A, Komodakis N, Paragios N. Deformable medical image registration: setting the state of the art with discrete methods. Annual Review of Biomedical Engineering. 2011; 13:219–244.
436. Glocker B, Komodakis N, Paragios N, Glaser C, Tziritas G, Navab N. Primal/dual linear programming and statistical atlases for cartilage segmentation. International Conference on Medical Image Computing and Computer-Assisted Intervention. 2007:536–543.
437. Sotiras A, Neji R, Deux J-F, Komodakis N, Fleury G, Paragios N. A Kernel-based graphical model for diffusion tensor registration. International Symposium on Biomedical Imaging. 2010:524–527.
438. Sotiras A, Komodakis N, Glocker B, Deux J-F, Paragios N. Graphical models and deformable diffeomorphic population registration using global and local metrics. International Conference on Medical Image Computing and Computer-Assisted Intervention. 2009:672–679.
439. Sotiras A, Komodakis N, Langs G, Paragios N. Atlas-based deformable mutual population segmentation. International Symposium on Biomedical Imaging. 2009:5–8.

440. Savinaud M, Sotiras A, Maitrejean S, Paragios N. Bioluminescence enhancement through fusion of optical imaging and cinematic video flow. International Symposium on Biomedical Imaging. 2010:688–691.

441. Zikic D, Glocker B, Kutter O, Groher M, Komodakis N, Kamen A, Paragios N, Navab N. Linear intensity-based image registration by Markov random fields and discrete optimization. Medical Image Analysis. 2010; 14(4):550–562. [PubMed: 20537936]

442. Kwon D, Lee K, Yun I, Lee S. Nonrigid image registration using dynamic higher-order mrf model. European Conference on Computer Vision. 2008:373–386.

443. Lee KJ, Kwon D, Yun ID, Lee SU. Optical flow estimation with adaptive convolution kernel prior on discrete framework. International Conference on Computer Vision and Pattern Recognition. 2010:2504–2511.

444. Santamaría J, Cordón O, Damas S. A comparative study of state-of-the-art evolutionary image registration methods for 3D modeling. Computer Vision and Image Understanding. 2011; 115(9): 1340–1354.

445. Hansen N, Ostermeier A. Completely derandomized self-adaptation in evolution strategies. Evolutionary Computation. 2001; 9(2):159–195. [PubMed: 11382355]

446. Crum WR, Griffin LD, Hill DLG, Hawkes DJ. Zen and the art of medical image registration: correspondence, homology, and quality. NeuroImage. 2003; 20(3):1425–1437. [PubMed: 14642457]

447. Shattuck DW, Mirza M, Adisetiyo V, Hojatkashani C, Salamon G, Narr KL, Poldrack RA, Bilder RM, Toga AW. Construction of a 3d probabilistic atlas of human cortical structures. NeuroImage. 2008; 39(3):1064–1080. [PubMed: 18037310]

448. Massachusetts General Hospital Center for Morphometric Analysis. Internet Brain Segmentation Repository. [Online]. Available: http://www.cma.mgh.harvard.edu/ibsr/

449. Klein A, Andersson J, Ardekani BA, Ashburner J, Avants B, Chiang MC, Christensen GE, Collins DL, Gee J, Hellier P, Song JH, Jenkinson M, Lepage C, Rueckert D, Thompson P, Vercauteren T, Woods RP, Mann JJ, Parsey RV. Evaluation of 14 nonlinear deformation algorithms applied to human brain mri registration. NeuroImage. 2009; 46(3):786–802. [PubMed: 19195496]

450. Christensen G, Geng X, Kuhl J, Bruss J, Grabowski T, Pirwani I, Vannier M, Allen J, Damasio H. Introduction to the non-rigid image registration evaluation project (nirep). International Workshop on Biomedical Image Registration. 2006:128–135.

451. Rohlfing T. Image similarity and tissue overlaps as surrogates for image registration accuracy: widely used but unreliable. IEEE Transactions on Medical Imaging. 2012; 31(2):153–163. [PubMed: 21827972]

452. Vandemeulebroucke, J.; Sarrut, D.; Clarysse, P. The popi-model, a point-validated pixel-based breathing thorax model; International Conference on the Use of Computers in Radiation Therapy. 2007. p. 195-199.[Online]. Available: http://www.creatis.insa-lyon.fr/rio/popi-model

453. Castillo R, Castillo E, Guerra R, Johnson VE, McPhail T, Garg AK, Guerrero T. A framework for evaluation of deformable image registration spatial accuracy using large landmark point sets. Physics in Medicine and Biology. 2009; 54(7):1849–1870. [PubMed: 19265208]

454. Murphy K, van Ginneken B, Klein S, Staring M, de Hoop BJ, Viergever MA, Pluim JPW. Semi-automatic construction of reference standards for evaluation of image registration. Medical Image Analysis. 2011; 15(1):71–84. [PubMed: 20709592]

455. Murphy K, van Ginneken B, Reinhardt J, Kabus S, Ding K, Deng X, Cao K, Du K, Christensen G, Garcia V, Vercauteren T, Ayache N, Commowick O, Malandain G, Glocker B, Paragios N, Navab N, Gorbunova V, Sporring J, de Bruijne M, Han X, Heinrich M, Schnabel J, Jenkinson M, Lorenz C, Modat M, McClelland J, Ourselin S, Muenzing S, Viergever M, De Nigris D, Collins D, Arbel T, Peroni M, Li R, Sharp G, Schmidt-Richberg A, Ehrhardt J, Werner R, Smeets D, Loeckx D, Song G, Tustison N, Avants B, Gee J, Staring M, Klein S, Stoel B, Urschler M, Werlberger M, Vandemeulebroucke J, Rit S, Sarrut D, Pluim J. Evaluation of registration methods on thoracic ct: The empire 10 challenge. IEEE Transactions on Medical Imaging. 2011; 30(11):1901–1920. [PubMed: 21632295]

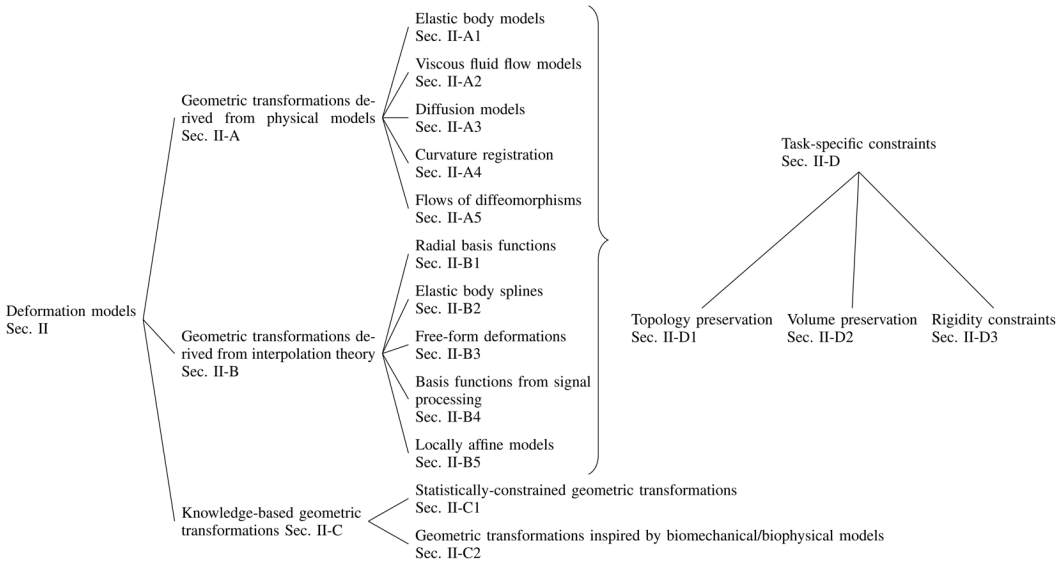

Fig. 1.

Classification of deformation models. Models that satisfy task-specific constraints are not shown as a branch of the tree because they are, in general, used in conjunction with physics-based and interpolation-based models.

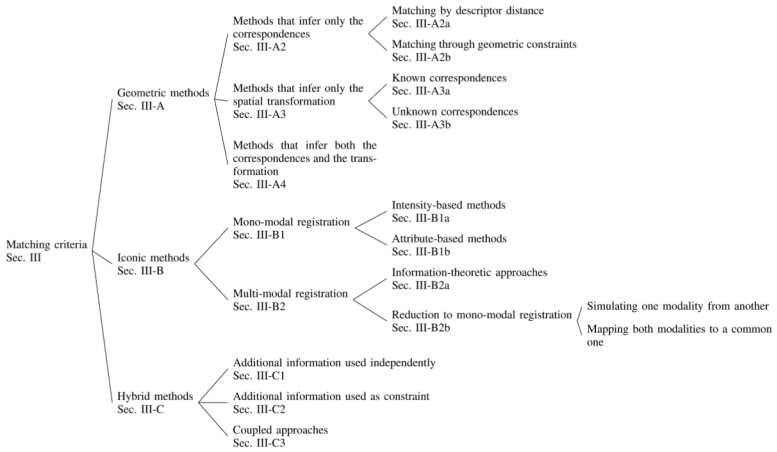

Fig. 2.
Classification of matching criteria.

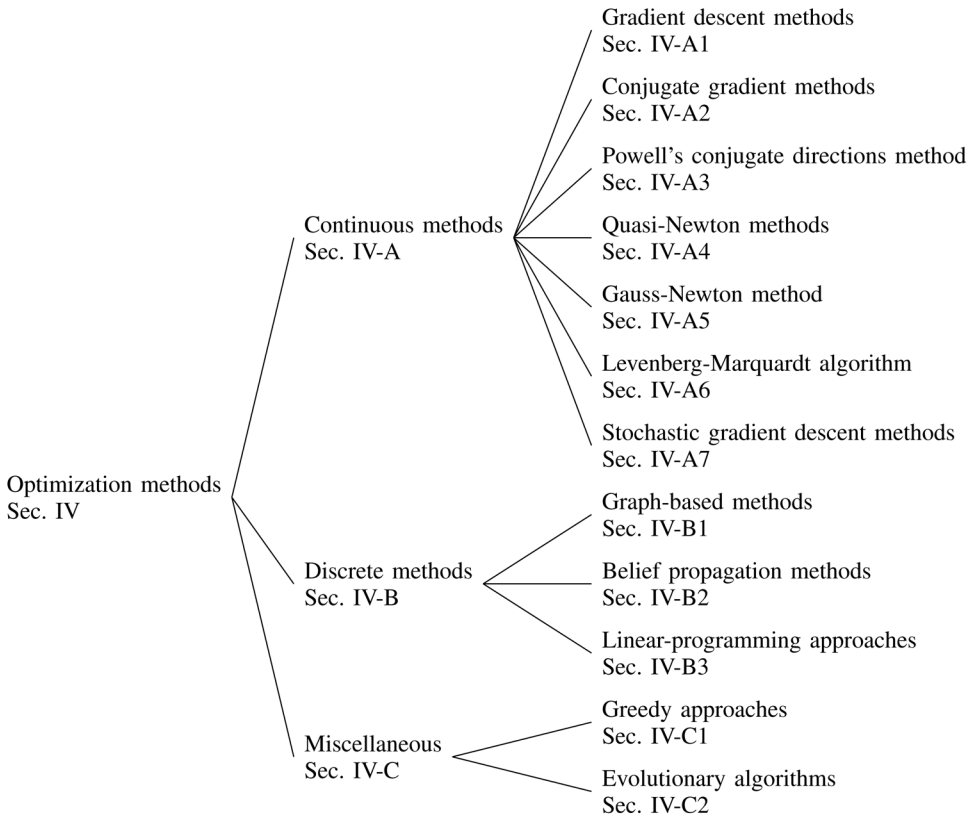

Fig. 3.
Classification of optimization methods.